

**Discovery of the first small molecules targeting the mRNA
binding protein IGF2BP2/IMP2 as potential target in cancer
therapy**

**Dissertation
zur Erlangung des Grades
des Doktors der Naturwissenschaften
der Naturwissenschaftlich-Technischen Fakultät
der Universität des Saarlandes**

von

Ali M. H. Abuhaliema

Saarbrücken

2020



Tag des Kolloquiums: 15. September 2020

Dekan: Prof. Dr. Guido Kickelbick

Berichterstatter: Prof. Dr. Alexandra K. Kiemer
Prof. Dr. Christian Ducho

Akad. Mitglied: Dr. Matthias Engel

Vorsitz: Prof. Dr. Alexander Titz



To my parents, wife, and little angel

Contents

Table of figures.....	VI
Table of tables.....	VIII
Appendix.....	IX
Abbreviations.....	X
Abstract	XVII
Zusammenfassung	XVIII
Chapter I: IMP2 is a promising target in cancer therapy.....	XIX
1 Introduction	1
1.1 Cancer incidence and mortality rates worldwide	1
1.1.1 Mode-of-action of chemotherapeutic agents.....	2
1.1.2 Potential chemotherapy side effects	3
1.2 RNA-binding proteins as promising targets in cancer therapy.....	3
1.2.1 Insulin like growth factor 2 mRNA binding proteins family	5
1.2.1.1 IMP2 role in cancer initiation and progression	6
1.2.1.2 IMP2 signaling pathways	8
1.2.1.3 Reported RNA target sequences of IMP.....	9
1.3 Biophysical methods used in drug discovery.....	9
1.3.1 Fluorescence polarization assay.....	10
1.3.2 Differential screening fluorometry / thermal shift assay.....	11
1.3.3 Microscale thermophoresis	12
1.3.4 Saturation transfer difference - nuclear magnetic resonance.....	13
1.4 Aim of the present study.....	14
2 Results	15
2.1.1 <i>In vitro</i> validation of IMP2 as a promising target in cancer therapy.....	16
2.1.2 Effect of IMP2 knockdown/knockout on cell viability and proliferation....	16
2.1.2.1 IMP2 knockdown impact on cell proliferation.....	16
2.1.2.2 IMP2 knockout impact on cell proliferation <i>via</i> MTT.....	18

Contents

2.1.2.3 IMP2 knockout impact on proliferation <i>via</i> ECIS.....	20
2.1.3 Influence of IMP2 reduction on IMP1 and IMP3 expression	21
2.1.3.1 Potential inter IMP interactions in colon cancer cells	21
2.1.3.2 Potential inter IMP interactions in liver cancer cells after IMP2 knockout	23
2.1.3.3 Potential inter IMP interactions in liver cancer cells after IMP2 knockdown.....	24
2.2 IMP2 isolation, characterization, and primary screening for inhibitors.....	26
2.2.1 Recombinant IMP2 isolation and characterization	26
2.2.2 IMP2 amino acid sequence confirmation	28
2.2.3 FP primary screening.....	29
2.2.3.1 Establishment of FP assay	29
2.2.3.2 FP-based primary screening.....	34
2.2.3.3 Pluronic® F-127 effect on FP assay findings.....	34
2.2.3.4 Dose response studies of hit compounds	35
2.2.3.5 Correlation of the half inhibitory concentration with competitive inhibitory constant.....	37
2.3 Secondary confirmation of IMP2-hit compound interactions	38
2.3.1 Confirmation of IMP2-hit compound interaction with thermal shift assay	38
2.3.2 Confirmation of IMP2-hit compound interaction with microscale thermophoresis	39
2.3.3 Confirmation and characterization of IMP2-hit compound interaction with STD–NMR.....	41
2.3.3.1 Establishment and optimization of STD-NMR experiment.....	41
2.3.3.2 Mode of interaction of compound # 4 with IMP2.....	41
2.3.3.3 Overall summary of IMP2-hit compound mode-of-interaction.....	42
2.3.4 <i>In silico</i> confirmation and characterization of IMP2-hit compound interaction.....	44

Contents

2.3.4.1	Molecular docking of compound # 4 in the RRM1 binding domains ...	45
2.3.4.1.1	Compound # 4 and inhibition of IMP2-RNA (ACAC) complex	45
2.3.4.1.2	Compound # 4 and inhibition of IMP2-RNA (CGGA) complex.....	45
2.4	Biological activity assessment of final hit compounds (potency, specificity, and safety)	47
2.4.1	Biological activity of final hit compounds.....	47
2.4.1.1	IMP2 expression in different cancer cell lines.....	47
2.4.1.2	Effect of hit compounds on cancer cell viability	48
2.4.1.3	Assessment of hit compound on-target activity <i>via</i> MTT.....	49
2.4.1.4	2.4.1.3 Assessment of hit compound on-target activity <i>via</i> ECIS.....	50
2.4.2	Cytotoxicity of hit compounds on human cells	52
2.4.2.1	Effect of hit compounds on HUVEC cells.....	52
2.4.2.2	Cytotoxicity of hit compounds on differentiated Huh7 cells.....	53
2.4.2.3	Influence of Huh7/7.5 cells differentiation on IMP expressions.....	54
2.4.2.3.1	Impact of HS differentiation on <i>IMP</i> RNA levels	54
2.4.2.3.2	Impact of HS differentiation on IMP protein levels	56
2.4.3	<i>In vivo</i> biological activity of hit compounds.....	57
3	Discussion	58
Chapter II: Methodology		63
4	Chemicals and reagents.....	64
5	Methods	64
5.1	Cell culture	64
5.2	IMP2 siRNA knockdown.....	64
5.3	IMP2 CRISPR mediated knockout	65
5.4	Western blot.....	66
5.4.1	SDS-polyacrylamide gel electrophoresis	66
5.4.2	Blotting.....	66
5.4.3	Near infrared immunodetection.....	67

Contents

5.5 Cytotoxicity and anti-proliferative measurement.....	68
5.6 Gene expression analysis	68
5.7 Bacterial culture	70
5.7.1 Generation to competent cells	70
5.7.2 Plasmid transformation	70
5.7.3 Plasmid isolation.....	71
5.8 Protein purification	71
5.8.1 IMP2 expression	71
5.8.2 Immobilized metal affinity chromatography.....	71
5.8.3 Recombinant IMP2 visualization.....	72
5.8.4 RNA electrophoresis	72
5.8.5 Liquid chromatography – tandem mass spectrometry	73
5.9 Fluorescence polarization-based screening assay.....	73
5.9.1 Probe design.....	73
5.9.2 Compound libraries.....	74
5.9.3 FP assay optimization and validation.....	74
5.9.4 FP-based screening.....	75
5.9.5 FP-based dose-response measurement.....	76
5.9.5.1 Compound solubility test.....	76
5.10 Thermal shift assay	76
5.11 Microscale thermophoresis technique	76
5.12 Saturation transfer difference – NMR.....	77
5.13 Molecular docking	78
5.14 Biological activity of hit compounds on cell viability and proliferation	78
5.15 Electric cell-substrate impedance sensing	78
5.16 Proliferation of primary human umbilical vein endothelial cell	79
5.17 Differentiation of Huh7 cells	79
5.18 <i>In vivo</i> xenograft zebrafish embryo model.....	79

Contents

5.19 Statistics.....	80
Summary and conclusion	81
supplementary data.....	82
References	88
Publications	99
Acknowledgment	100

Table of figures

Figure 1: Estimated number of the newly diagnosed cancer cases and deaths	1
Figure 2: Chemotherapeutic agents and their mode-of-action.....	2
Figure 3 : RBPs role in the post-transcriptional regulation.....	4
Figure 4: IMP's amino acid sequence and binding domains.....	5
Figure 5 : Structure of IMP2 and its variant p62	6
Figure 6: Association of IMP2 expression with survival rate	7
Figure 7: Descriptive sketch of IMP2 regulation network.....	8
Figure 8 : Concept of fluorescence polarization assay	10
Figure 9 : Principle of thermal shift assay.....	11
Figure 10: Principle of microscale thermophoresis technique.....	12
Figure 11 : Principle of STD-NMR in characterization of binding mode.....	13
Figure 12: Hypothesis to be tested	14
Figure 13 : Impact of IMP2 knockdown on cell viability	17
Figure 14 : Impact of IMP2 knockout on cell viability	19
Figure 15 : Effect of IMP2 knockout on cell proliferation.....	20
Figure 16 :Impact of IMP2 knockout on IMP1 and IMP3 expression in colon cancer cells	22
Figure 17: Impact of IMP2 knockout on IMP1 and IMP3 expression in liver cancer cells	23
Figure 18 : Impact of IMP2 knockdown on IMP1 and IMP3 expression in liver cancer cells	25
Figure 19 : Isolation and characterization of recombinant IMP2 protein	27
Figure 20 : IMP2 amino acid sequence confirmation.....	28
Figure 21 : Fluorescence polarization assay development and optimization	30
Figure 22 : The robustness of FP assay	31
Figure 23 : Characterization of IMP1 lead compound interaction with IMP2 RNAs ...	32
Figure 24 : Characterization of IMP2 functional binding to different RNA targets by FP assay	33
Figure 25 : FP primary screening and characterization of hit compounds	34
Figure 26 : Effect of Pluronic® on FP assay findings	35
Figure 27 : FP primary screening and characterization of hit compounds	36
Figure 28 : Chemical classification and IC ₅₀ S of hit compounds	36
Figure 29 : Thermal shift assay confirmation of hit compounds.....	38

Table of figures

Figure 30: Comparison of IC ₅₀ values for compound # 9 with MST and FP assays ..	40
Figure 31 : Interaction mode of compound # 4 predicted by STD-NMR	42
Figure 32 : Colored epitopes of hit compounds based on STD-NMR data	43
Figure 33 : Homology models for the molecular docking studies.....	44
Figure 34 : Molecular docking of compound # 4 in IMP2 binding domains.....	46
Figure 35 : IMP2/p62 expression in different cancer cell lines.....	47
Figure 36 : Biological activity of final screening hits.....	48
Figure 37 : Target specificity of hit compounds	49
Figure 38 : Impact of hit compounds on cell proliferation in the absence of IMP2	51
Figure 39 : Effect of hit compounds on HUVEC cells.	52
Figure 40 : Effect of hit compounds on differentiated Huh7 cells.....	53
Figure 41: Influence of Huh7.5 differentiation on IMPs expression.....	55
Figure 42 : Influence of Huh7 differentiation on IMPs expression.....	56

Table of tables

Table 1: Reported RNA target sequences of IMP.....	9
Table 2 : Summary of probe sequences used in FP assay validation	29
Table 3: Summary of Ki values of hit compounds.....	37
Table 4: siRNA oligonucleotide used in IMP2 knockdown.....	65
Table 5: Antibody dilutions used for immunodetection.	67
Table 6 : Conditions used in set up of qPCR reaction.	69

Appendix

Supplementary tables

Table 1. Descriptive data of class A	82
Table 2. Descriptive data of class B	83

Supplementary figures

Figure 1. STD-NMR IMP2 complex analysis	84
Figure 2. DMSO concentration vs mean cell viability.....	85
Figure 3. DMSO concentration vs median cell viability.....	86
Figure 4. Effect of hit compounds on cell proliferation in the absence of the target...87	

Abbreviations

Abbreviation	Meaning
ΔT_m	melting temperature shift
$^{\circ}\text{C}$	grad Celsius
μM	micro molar
^{13}C NMR	carbon NMR
^1H	proton spectrum
^1H NMR	proton NMR
2-ME	2-mercaptoethanol
aa	amino acid
ANOVA	analysis of variance
ARE	AU rich element
AU	adenylate-uridylate
BSA	bovine serum albumin
CaCl_2	calcium chloride
cDNA	complementary DNA
CDS	circular dichroism spectroscopy
Co	control
CO_2	carbon dioxide
CRISPR/Cas9	clustered regularly interspaced short palindromic repeats / associated cas9 protein.
d	doublet peak
D_2O	deteriorated water
DEPC	diethyl pyrocarbonate
DMEM	Dulbecco's Modified Eagle's Medium

Abbreviations

DMSO	dimethyl sulfoxide
DMSO D ₆	deteriorated DMSO
DNA	deoxyribonucleic acid
dpi	diploid
DTT	dithiothreitol
<i>E. coli</i>	Escherichia coli
EC ₅₀	half maximal effective concentration
ECIS	electric cell-substrate impedance sensing
eCLIP	enhanced crosslinking and immunoprecipitation
EDTA	ethylene diamine tetra acetic acid
ELAVL1	embryonic lethal abnormal vision Drosophila like 1
EMSA	electrophoretic mobility shift assay
FCS	fetal calf serum
FDA	American Food and Drug Administration
FI	fluorescence intensity
FLC	fluorescein
FP	fluorescence polarization
FPcomp	FP competition assay
FPKM	fragments per kilo base per million mapped reads
FPsat	FP saturation assay
FRET	fluorescence resonance energy transfer
GBC	gallbladder carcinoma
h	hour
HC	high control

Abbreviations

HCC	hepatocellular carcinoma
HCT116	human colon cancer cell line
HCV	hepatitis C virus
Hep3B	human liver cancer cell line
HepG2	human liver cancer cell line
HIPS	Helmholtz Institute for Pharmaceutical Research Saarland
His	histidine
HMGA2	high-mobility group AT-hook 2
hnRNPLL	heterogeneous nuclear ribonucleoprotein L-like
HPLC	high performance liquid chromatography
HS	human serum
HSQC	heteronuclear single quantum correlation
Huh7	human liver cancer cell line
HuR	human antigen R
HUVEC	human umbilical vein endothelial cell
I_0	intensity of one signal in the off-resonance or reference spectrum
IC ₅₀	half maximal inhibitory concentration
IGF2	insulin-like growth factor 2
IGF2BP1-3/IMP1-3	insulin-like growth factor 2 mRNA binding proteins 1-3
IgG	immunoglobulin G
IMAC	immobilized metal affinity chromatography
IPTG	isopropyl- β -d-thiogalactopyranosid
I_{sat}	intensity of a signal in the on-resonance spectrum

Abbreviations

J	coupling constant
kb	kilo base
KCl	potassium chloride
KD	constant of dissociation
kD	kilo Dalton
KH	K homology
LC	low control
LC-MS/MS	liquid chromatography - tandem mass spectrometry
m	multiple peak
MCF7	human breast cancer cell line
mg	milligram
MgCl ₂	magnesium sulphate
MgCl ₂	magnesium chloride
MgSo ₄	Magnesium sulfate
ml	milliliter
mM	millimolar
MOPS	3-(N-morpholino) propane sulfonic acid
mP	millipolarization
mp	melting point
mRNA	messenger RNA
MST	microscale thermophoresis
mTOR	the mammalian target of rapamycin
MTT	3-(4,5-dimethylthiazol-2-yl)-2,5-diphenyltetrazolium bromide

Abbreviations

MW	molecular weight
MWCO	molecular weight cut-off
NaCl	sodium chloride
NF- κ B	nuclear factor 'kappa-light-chain-enhancer' of activated b-cells
ng	nano gram
nM	nano molar
NMR	nuclear magnetic resonance
NS5A	nonstructural protein 5A
ON	overnight
<i>P</i> value	probability value
p62	splice variant of IMP2
PAR-CLIP	photoactivatable ribonucleotide – enhanced crosslinking and immunoprecipitation
PBS	phosphate buffered saline
PCR	polymerase chain reaction
pET-28a	bacterial expression vector in <i>E. coli</i>
pH	potential hydrogen
ppm	parts per million
PqsD	Pseudomonas quinolone signal biosynthetic enzyme
q	quartet peak
RAC1	Ras-related C3 botulinum toxin substrate 1
RBP	RNA binding protein
RNA	ribonucleic acid
RNAP	RNA-polymerase enzyme

Abbreviations

RNase	ribonuclease
ROS	reactive oxygen species
RPMI	Roswell Park Memorial Institute Medium
RRM	RNA recognition motif
RT	room temperature
RT-qPCR	real-time quantitative polymerase chain reaction
s	singlet peak
Sat	saturation
SD	standard deviation
SDS-PAGE	sodium dodecyl sulfate polyacrylamide gel electrophoresis
SELEX	systematic evolution of ligands by exponential enrichment
SEM	standard deviation of the mean
siRNA	small interfering RNA
STD	saturation transfer difference
SW480	human colon cancer cell line
t	triplet peak
T _m	melting temperature
tR	retention time
Tris-HCl	(hydroxymethyl)aminomethane-hydrochloride
TSA	thermal shift assay
UCP1	uncoupling protein 1
UV	ultraviolet
WB	Western blot

Abbreviations

WHO	World Health Organization
Z'	robustness value
ZBP1	zipcode binding protein 1

Abstract

The mRNA binding protein IGF2BP2/IMP2 is overexpressed in several cancer types, promotes tumorigenesis and tumor progression, and has been suggested to worsen disease outcome. Therefore, inhibition of IMP2 represents a promising approach in cancer therapy.

The hypothesis to be tested within this thesis was (I) validate the target, (II) set up a screening assay for small molecule inhibitors of IMP2, and (III) test the biological activity of the obtained hits *in vitro* and *in vivo*.

In vitro target validation using IMP2 siRNA knockdown and CRISPR/Cas9-mediated IMP2 inactivation showed a reduction in cell viability and proliferation, compared to control cells as determined by MTT assay, and electric cell-substrate impedance sensing (ECIS).

Different compound libraries were screened for IMP2 inhibitors using a fluorescence polarization assay, and results were confirmed by thermal shift assay, microscale thermophoresis and saturation transfer difference - NMR.

The biological activity of hit compounds was tested in cells expressing different IMP2 levels and confirmed specificity for cells expressing high levels of the target. Hit compounds significantly reduced tumor growth *in vivo*.

In conclusion, our findings support that IMP2 represents a druggable target to reduce tumor cell proliferation. The identified hits provide a basis for subsequent lead generation efforts.

Zusammenfassung

Das mRNA-bindende Protein IGF2BP2/IMP2 wird bei verschiedenen Krebserkrankungen überexprimiert. IMP2 fördert sowohl die Entstehung von Tumoren, als auch deren Progression, sodass es mit einer schlechten Krankheitsprognose in Verbindung gebracht wird. Daher stellt die Hemmung dieses Proteins einen vielversprechenden Ansatz in der Krebstherapie dar.

Die im Rahmen dieser Arbeit zu testende Hypothese bestand darin, (I) das IMP2 als Ziel zu validieren, (II) robuste Testverfahren für niedermolekulare IMP2-Inhibitoren zu etablieren und (III) die biologische Aktivität der erhaltenen Trefferverbindungen *in vitro* und *in vivo* zu testen.

Um IMP2 *in vitro* als Ziel validieren zu können, wurde dieses einerseits unter Verwendung von siRNA herunterreguliert und andererseits mittels CRISPR/Cas9 inaktiviert. Dabei konnte Sowohl im MTT-Test, als auch mit dem Verfahren der elektrischen Zellsubstrat-Impedanzmessung (ECIS) eine Verringerung der Lebensfähigkeit und Proliferation von Krebszellen im Vergleich zu Kontrollzellen gezeigt werden.

Fluoreszenzpolarisationsassays wurden benutzt, um verschiedene Substanzbibliotheken auf IMP2-Inhibitoren zu durchsuchen. Positive Ergebnisse konnten unter Verwendung der folgenden Verfahren bestätigt werden: Thermische Verschiebung Assay, Mikroskalige Thermophorese und Sättigungs-Transfer-Differenz - NMR bestätigt.

Die biologische Aktivität der Trefferverbindungen wurde in Zellen getestet, die unterschiedliche IMP2 – Spiegel exprimierten; in Zellen mit hoher IMP2-Expression konnte dadurch ebenfalls die Spezifität dieser Verbindungen untermauert werden. Des Weiteren reduzierten die Trefferverbindungen das Tumorwachstum *in vivo* signifikant.

Zusammenfassend zeigen unsere Ergebnisse, dass IMP2 als therapeutisches Ziel die Tumorzellproliferation reduzieren kann. Dabei bilden die identifizierten Trefferverbindungen eine Grundlage bei nachfolgenden Bemühungen Leitstrukturen zu generieren.

Chapter I: IMP2 is a promising target in cancer therapy

1 Introduction

1.1 Cancer incidence and mortality rates worldwide

Cancer is a global health burden, it ranks the first or second most leading cause of death in more than 90 countries worldwide (Bray et al., 2018). In 2018, more than eighteen million cases were newly diagnosed with different types of cancer worldwide (Figure 1 Bray et al., 2018). In 2040, according to the World Health Organization (WHO) estimates, the number of yearly diagnosed cancer cases will be increased by 2 folds (World Health Organization, 2020). Cancer incidence rate is increased progressively regardless to the demographic factors (Bray et al., 2018).

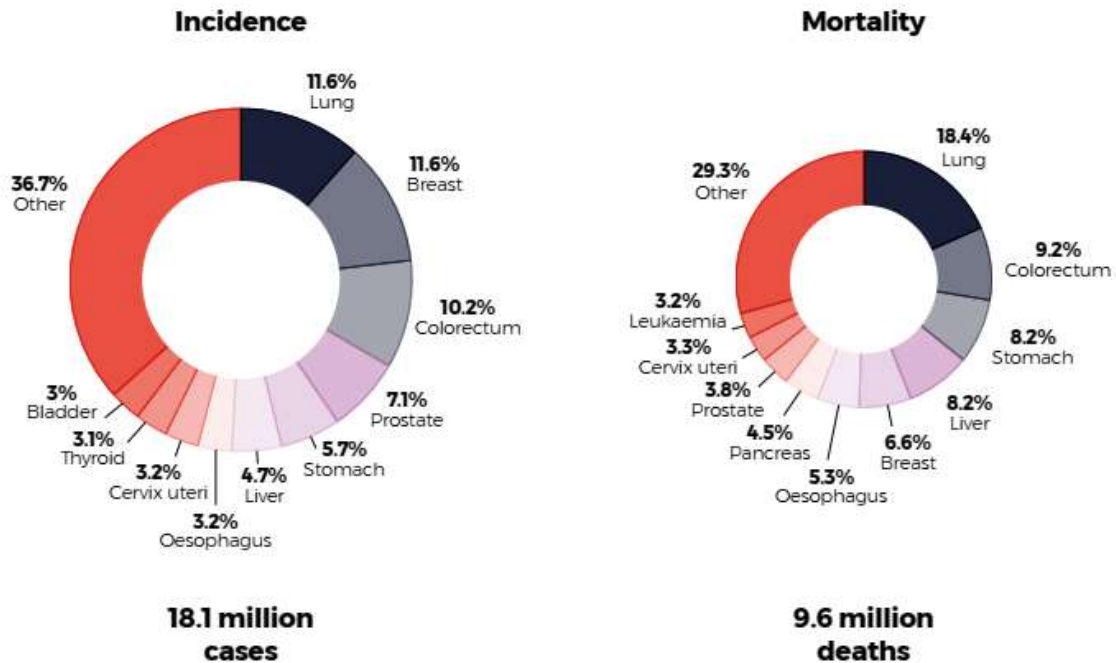


Figure 1: Estimated number of the newly diagnosed cancer cases and deaths in 2018 from both gender at all ages. Figure was adapted from Bray et al. (2018).

According to WHO statistics, the number of cancer deaths in 2018 exceeded nine millions worldwide (Figure 1 Bray et al., 2018). One out of six death cases is caused by one of cancer types (World Health Organization, 2020). In 2008, the overall economic impact of death and disability caused by cancer was \$895 billion worldwide (Armer et al., 2013). Adopting new policies by global health organizations for fighting against cancer burden will save millions of human lives, as well billions of dollars.

1.1.1 Mode-of-action of chemotherapeutic agents

Chemotherapy uses one or more chemotherapeutic agents as part of an identical chemotherapy regimen. Chemotherapeutic agents exert their actions in different mechanisms (Figure 2 Hoffman et al., 2012), some of them targeting specifically the cycling cells and others act on cycling and resting cells (cycling cells more sensitive) (Alimbetov et al., 2018; Mills et al., 2018).

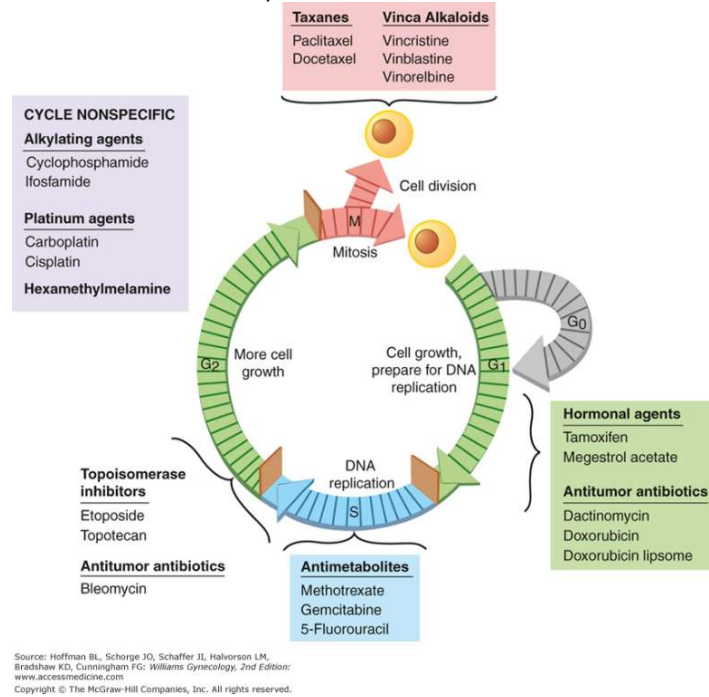


Figure 2: Chemotherapeutic agents and their mode-of-action. Figure was adapted from (Hoffman et al., 2012).

Folic acid analogues interfere with DNA and RNA synthesis by inhibiting their precursor products (Hagner and Joerger, 2010). Anthracycline antibiotics intercalate into DNA and inhibit its replication, and ergot alkaloids restricts the microtubules functions and inhibit formation of mitotic spindles (Booser and Hortobagyi, 1994). Alkylating agents lead to addition of an alkyl group to the guanine base of the DNA molecule, prevent double strand cross linkage, and induce breakage of the DNA strands (Ralhan and Kaur, 2007). Topoisomerase inhibitors as topotecan interfere with DNA transcription and replication by inhibition of the topoisomerase I and II enzymes. Topoisomerase

enzymes control the 3D structures of DNA *via* interfering of the phosphodiester backbone of DNA (Jain et al., 2017; Pommier, 2013).

Chemotherapy based on cancer type in the early stages could be curative and prevent cancer relapse (Berger, 1986). In moderate to advanced stages, chemotherapy could increase the survival time from months to few years based on cancer type and its sensitivity to chemotherapy (Neugut and Prigerson, 2017). In advanced and late stages, palliative chemotherapy is used to relieve symptoms, and improve the quality of life of the cancer patients (Neugut and Prigerson, 2017).

1.1.2 Potential chemotherapy side effects

Beside the desired biological activity of chemotherapeutic agents, they have also serious side effects. Most of chemotherapeutic agents lack the specificity and affecting the normal cells beside the cancerous cells (Pearce et al., 2017).

The side effects of chemotherapy range could be mild as nausea, vomiting, and skin sensitivity. Weight loss and hair loss are reported with most of the chemotherapeutic agents (Nurgali et al., 2018; Pearce et al., 2017).

Cardiotoxicity is a serious adverse effect caused by certain commonly used chemotherapeutic agents as doxorubicin, leading to increase in morbidity and mortality rates (Volkova and Russell, 2011). Chemo brain is a reported neurological side effect of chemotherapy concerning to foggy thinking, memory problems, and anxiety (Kovalchuk and Kolb, 2017).

Furthermore, serious drug-drug interactions were reported with a wide range of commonly used chemotherapeutic agents that limit their uses (Monteiro et al., 2019).

1.2 RNA-binding proteins role in cell biology

RNA-binding proteins (RBPs) are proteins that interact with RNA and make complex over one or multiple RNA-binding domains (Hentze et al., 2018). Binding of these proteins to RNA modify the fate and / or function of targeted RNAs (Idler and Yan, 2012). Numerous RBPs have been discovered and investigated, they play an important role in diverse physiological functions. They are involved in mRNA maturity,

stability, localization, and translation of mRNA targets (Figure 3 Glisovic et al., 2008). Several RBPs as hnRNPLL are splicing factors involved in exons recognition (Ergun et al., 2013). RBPs interact with several miRNAs and regulate their biogenesis and function (Newman et al., 2008; Taylor et al., 2013). Furthermore, RBPs play a role in the immune system responses by modulating the development and activation of B and T cells (Alkhatib et al., 2012; DeMicco et al., 2015).

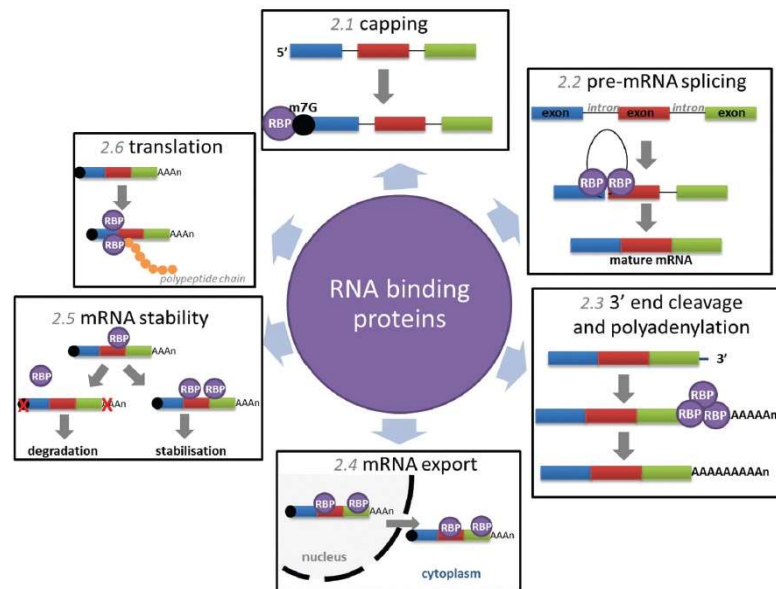


Figure 3 : RBPs role in the post-transcriptional regulation. Figure was adapted from Zhou et al. (2015).

RBPs are overexpressed in several diseases particularly in cancer, they serve as promising targets in disease treatment (Ascher et al., 2014; Hong, 2017).

1.2.1 Insulin like growth factor 2 mRNA binding proteins family

Insulin like growth factor 2 mRNA binding proteins (IGF2BPs/IMPs/VICKZs) are belong to RBPs, they bind to IGF2 RNA and other several targets RNAs and control their expression, translocation, maturity and translation (Cao et al., 2018). IMPs have high structure and function similarity (Figure 4 Degrauwe et al., 2016). They have two RNA recognition motifs (RRM1-2) in the N- terminal and four KH homology domains (KH1-4) in the C-terminal (Nielsen et al., 1999). *In vitro* investigations have revealed that the KH binding domains are responsible for RNA binding (Amarasinghe et al., 2001; Farina et al., 2003; Nielsen et al., 2002). In addition, RRM motifs play an essential role in the stability of IMP2-RNA complexes and regulate the interactions between IMP2-RNA complex and other RBPs (Bell et al., 2013; Nielsen et al., 2004). The linker region between RRM2 and KH1 mediates the interaction with mTOR mRNA by heterodimerization of IMP1 and IMP3, or homodimerization of IMP2 (Dai et al., 2013; Dai et al., 2011).

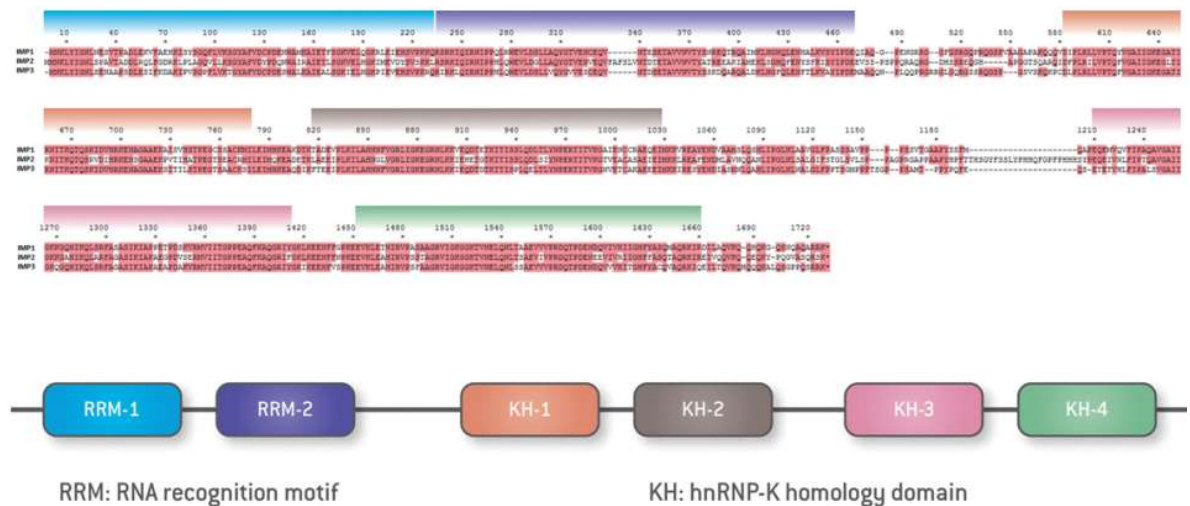


Figure 4: IMP's amino acid sequence and binding domains. (A) Alignment of IMPs amino acid sequence represent conserved similarity in RNA binding domains. (B) Schematic presentation of IMP RNA binding domains. Figure was adapted from Degrauwe et al. (2016).

IMPs are expressed extensively during fetal development and maturation in different tissues. IMP expression decreases in most tissues after birth (Czepukojc et al., 2019; Degrauwe et al., 2016). Overexpression of IMPs has been reported in several diseases as diabetes mellites, neural disorder, heart diseases and cancer. Expression of IMPs

in adult tissues has been described to be oncogenic in different types of tumors, including hepatocellular carcinoma (HCC), colon, and lung cancer (Dimitriadis et al., 2007; Kessler et al., 2016). IMPs regulate the mRNAs of several oncogenes that are involved in cancer initiation and progression, leading to aggressive tumors (Degrauwe et al., 2016).

1.2.1.1 IMP2 role in cancer initiation and progression

IMP2 gene is located on chromosome 3 locus 3q27.2 and contains 16 exons (Christiansen et al., 2009), encodes a 66.1 kDa IMP2 protein (Nielsen et al., 1999). IMP2 has six variants, p62 is a splicing variant lacks exon 10 encoding a 62 kDa IMP2 isoform (Figure 5 Cao et al., 2018). p62 has a 43 amino acids loss between KH23 binding domains (Cao et al., 2018).

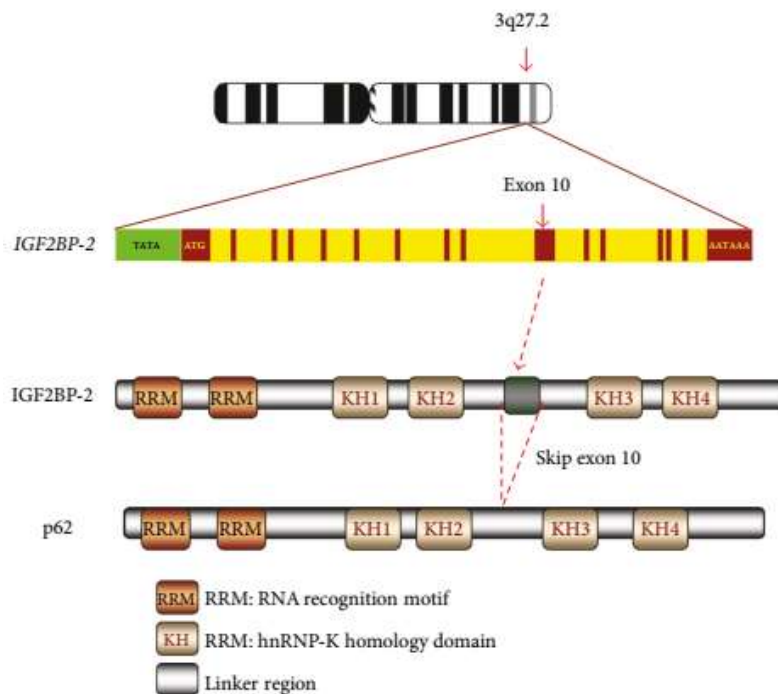


Figure 5 : Structure of IMP2 and its variant p62. Figure was adapted from Cao et al. (2018).

IMP2 protein has a distinct role in cancer progression and responsiveness to chemotherapy (Kessler et al., 2017). IMP2 was highly expressed in different cancers compared to IMP1 and IMP3 (Dai et al., 2017; Kessler et al., 2017). The expression and translation of different oncogenes is controlled directly or indirectly by IMP2. IMP2 oncogenes interaction increases cellular proliferation, growth rate, cell migration (Cao

et al., 2018). Furthermore, the metabolic activity and energy expenditure were improved after IMP2 was knocked out, lack of IMP2 reduces the development of fatty liver diseases and malignancy (Dai et al., 2015). IMP2 and its variant p62 are involved in elevation of RAC1 expression and generation of reactive oxygen species (Kessler et al., 2015). Furthermore, IMP2 knockdown in adherent Glioblastoma cells decreases their oxygen consumption rate and inhibit glycolysis (Janiszewska et al., 2012).

P62 transgenic mice model reflected higher rates of tumor initiation and progression compared to the wild type. Also, IMP2 knockout mice model showed reduction in size, total weight, and linear growth compared to the wide type (Kessler et al., 2015).

The correlation of IMP2/p62 overexpression with survival rate among cancer patients was investigated using Kaplan-Meier analysis. Results showed that the survival rate is significantly reduced with IMP2/p62 overexpression (Figure 6; Alajez et al., 2012; Barghash et al., 2016; Dahlem et al., 2019; Davidson et al., 2014; Kessler et al., 2015; Zhang et al., 2011).

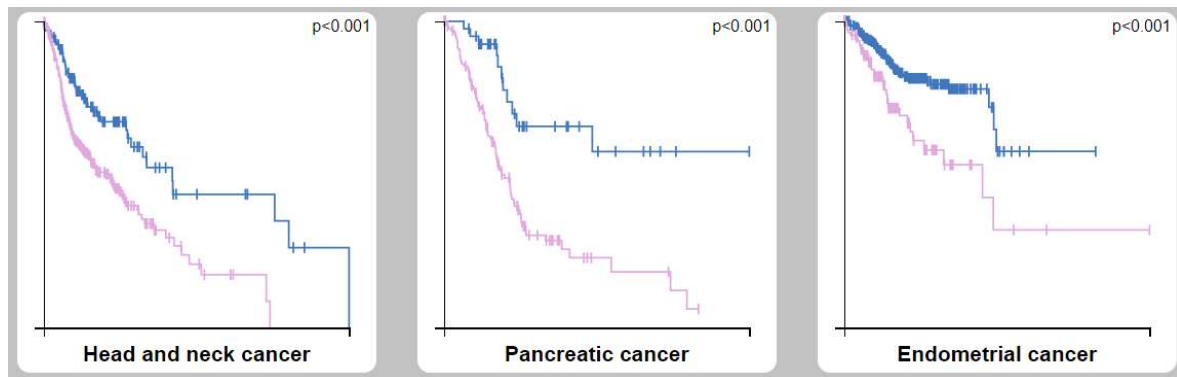


Figure 6: Association of IMP2 expression with survival rate. Based on the fragments per kilo base per million mapped read (FPKM) values of *IMP2* expression, patients were classified into high and low expression groups. Blue represents low *IMP2* expression and red represents high *IMP2* expression. Association between *IMP2* expression and patient survival rate was examined using Kaplan-Meier analysis. Figure was adapted from the Human Protein Atlas; available from www.proteinatlas.org (Uhlen et al., 2017).

1.2.1.2 IMP2 signaling pathways

All IMPs are reported to interact with IGF2 RNA, but each IMP protein displays a unique RNA interaction properties and interact with variable targets (Bell et al., 2013). Several studies have been reported that high mobility group proteins 2 (HMGA2) in assistance of nuclear factor κ B (NF- κ B) binds to the AT-rich region of the first intron of IMP2 gene and promote its transcription (Cleynen et al., 2007; Henriksen et al., 2010). This enhance cancer cells proliferation and increase their growth rate.

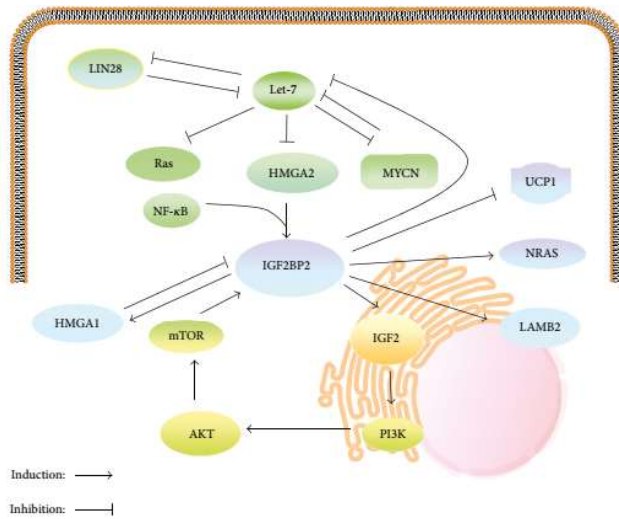


Figure 7: Descriptive sketch of IMP2 regulation network. Figure was adapted from Cao et al. (2018).

Several IMP2/p62 mRNA targets have been revealed associated with cancer initiation and progression, as IGF2, UCP1, C-Myc, and Let-7 miRNA (Figure 7 Cao et al., 2018). High expression levels of IMP2 activates IGF2/PI3K/Akt/mTOR pathway, and stimulate cancer cells proliferation, migration, and invasion (Dai et al., 2017; Mu et al., 2015; Waly et al., 2019). Furthermore, it has been reported that mRNAs of LIMS2, TRIM54, and LAMB2 are targeted by IMP2, increasing the migration ability of cancerous cells, cytoskeleton, and stimulating their metastatic behavior (Boudoukha et al., 2010; Manieri et al., 2012; Schaeffer et al., 2012). Also, wnt/ β -catenin pathway is targeted by IMP2, and enhances cell migration and reduces cellular adhesion (Xing et al., 2019).

1.2.1.3 Reported RNA target sequences of IMP

The clear identification and characterization of IMP targets are still not completely clear and needs more investigations (Biswas et al., 2019). The development in RNA-protein interaction detection methods revealed many target nucleotide sequences of RBPs (see Table 1; Biswas et al., 2019; Jia et al., 2018; Popova et al., 2015).

Table 1: Reported RNA target sequences of IMP.

RNA sequence	Reference	Sequence detection method	Domain	Site detection method	Specificity	Specificity validation
(A/U)-GG-(A/U)	(Biswas et al., 2019)	SELEX	KH3	site-directed mutagenesis	IMP2	EMSA N-HSQC
(C/A)-CA-(C/U)	(Biswas et al., 2019)	SELEX	KH4	site-directed mutagenesis	IMP2	EMSA N-HSQC
CGG-(A/U)	(Biswas et al., 2019)	SELEX	KH4	site-directed mutagenesis	IMP1 ^a	EMSA N-HSQC
(A/C)-CA	(Biswas et al., 2019)	SELEX	KH3	site-directed mutagenesis	IMP1 ^a	EMSA N-HSQC
CCCC	(Jia et al., 2018)	SELEX	RRM1	crystallography	IMP3 ^a	
ACAC	(Jia et al., 2018)	SELEX	RRM1	crystallography	IMP3 ^a	
(A/U)(U/C) ACA	(Conway et al., 2016)	eCLIP			IMP1	repetition
A(C/U)ACA(A/U)	(Conway et al., 2016)	eCLIP			IMP2	repetition
CAUC	(Hafner et al., 2010)	PAR-CLIP			IMPs ^b	repetition

^a: tested on either IMP1 or IMP3, and due to the high structure similarity might bind to both; ^b: the repetition number of each nucleotide sequence differ based on IMP target. Abbreviations: electrophoretic mobility shift assay (EMSA), photoactivatable ribonucleotide - enhanced crosslinking and immunoprecipitation (PAR-CLIP), enhanced-CLIP (eCLIP), heteronuclear single quantum correlation (HSQC), and systematic evolution of ligands by exponential enrichment (SELEX).

1.3 Biophysical methods used in drug discovery

Several biophysical and structural techniques are commonly used for small-molecule ligand detection and screening for binders / inhibitors (Renaud et al., 2016). These methods detect minimal changes in fluorescence, temperature, electrophoresis and refractive index, etc (Ciulli, 2013).

1.3.1 Fluorescence polarization assay

Fluorescence polarization (FP) assay is widely used to investigate molecular interactions, and enzymatic activity through direct and competitive binding assays (Burke et al., 2003). FP assay have been used widely in direct screening for enormous range of targets, and they are adopted for high-throughput screening (HTS) (Hall et al., 2016). Furthermore, FP assay are valuable, reliable, and low-cost screening approach for inhibitors for protein-nucleic acid and protein-protein interactions (Hall et al., 2016).

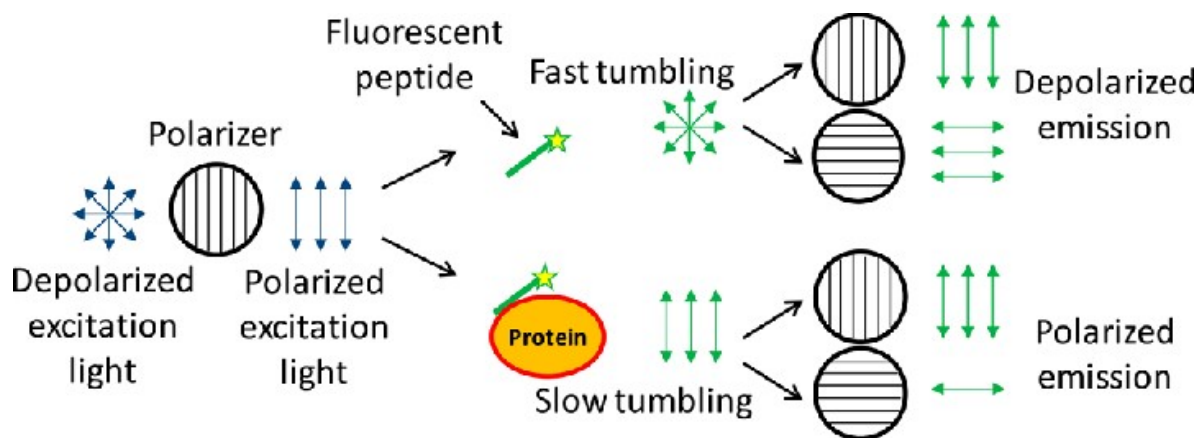


Figure 8 : Concept of fluorescence polarization assay in detection of protein interactions. Figure was adapted from Cheow et al. (2014).

When a fluorescently labeled molecule is exposed to a polarized light at certain wavelength, it is excited and then emits light with a certain degree of polarization which is inversely correlated with the molecular rotation rate (Moerke, 2009). Small fluorescently labeled molecules rotate fast, and the received light by perpendicular or / and parallel filters disappears rapidly and then the polarization value becomes low (Cheow et al., 2014). After binding to a macromolecule, the rotation becomes slower and then the polarization values become higher (Figure 8 Cheow et al., 2014).

1.3.2 Differential screening fluorometry / thermal shift assay

The concept of the thermal shift assay (TSA) based on the observation that when the protein is gradually heated, it denatures and loses the 3-dimensional structure. The temperature at which the denatured protein fraction is equal to the renatured fraction is called melting temperature (T_m) (Huynh and Partch, 2015). The denaturation is no longer reversible at temperature higher than T_m (Huynh and Partch, 2015). Addition of a fluorescent dye as Sypro Orange incorporated to the protein, as the denaturation is increased, the dye-protein fraction increases, and the measured fluorescence signal is increased (Figure 9 Bruce et al., 2019). At higher temperatures, the denatured protein is aggregated together, and Sypro Orange dye is liberated (Bruce et al., 2019). Several factors may interfere with protein melting point as pH, salts, drugs, and mutations (Crowther et al., 2009). The binding of low molecular weight molecules may stabilize the protein complex and increase the melting temperature or may destabilize the protein complex and decrease the melting temperature (Senisterra et al., 2012).

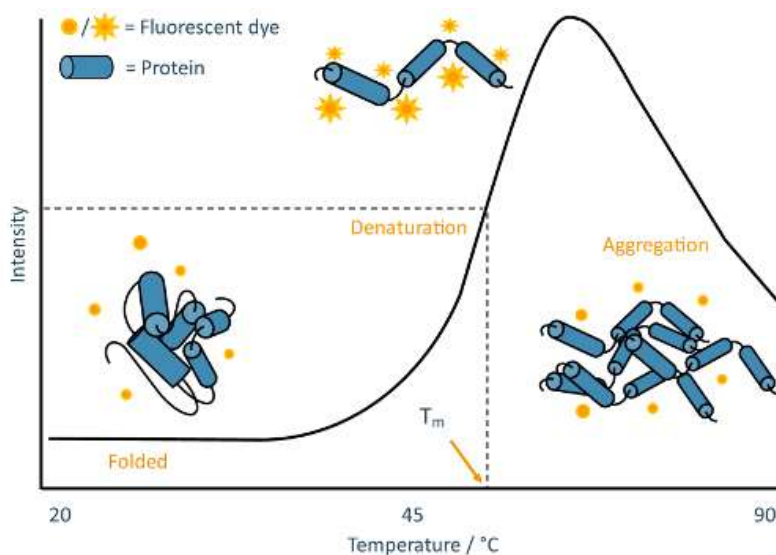


Figure 9 : Principle of thermal shift assay in detection of protein interaction. Figure was adapted from Bruce et al. (2019).

1.3.3 Microscale thermophoresis

The concept of microscale thermophoresis (MST) is based on detection of minimal changes in thermophoresis (Figure 10 Liu et al., 2015). The movement of molecules inside the solution under a temperature gradient, relies on a diversity of molecular properties as charge, size, polarity and hydration shell size (Jerabek-Willemsen et al., 2011). The binding of a small molecule to protein change its molecular properties and decrease the velocity of movement under the thermophoresis gradient (Jerabek-Willemsen et al., 2011). MST technique is extremely sensitive and detect any alteration in the molecular properties, permitting for an accurate quantification of molecular measures (Rainard et al., 2018). MST quantify high-affinity interactions with dissociation constants in picomolar range (Rainard et al., 2018). Furthermore, MST assay detect protein–protein interactions in pure mammalian cell lysates under semi natural environment (Seidel et al., 2013).

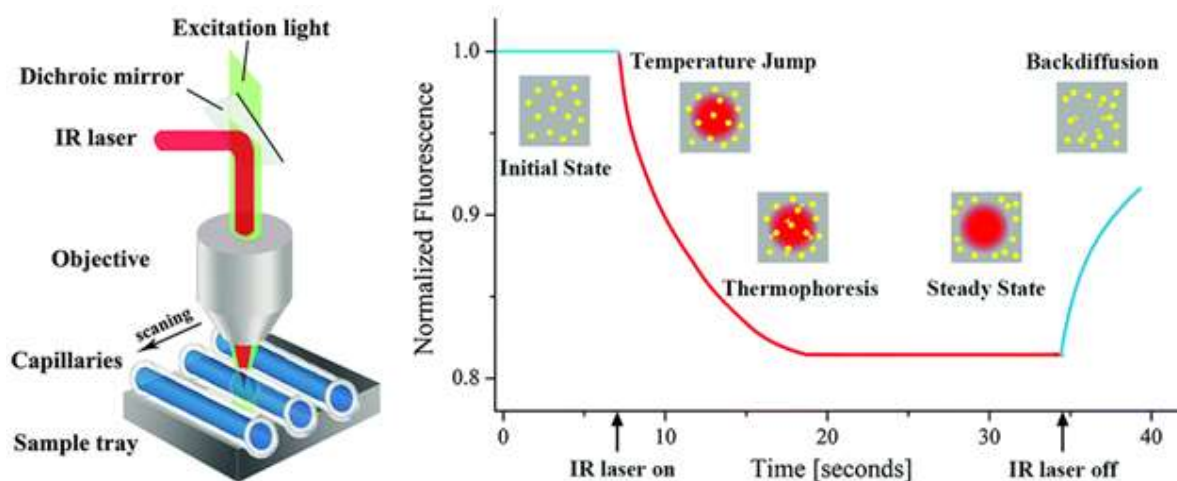


Figure 10: Principle of microscale thermophoresis technique in detection of protein interaction. Figure was adapted from Liu et al. (2015).

1.3.4 Saturation transfer difference - nuclear magnetic resonance

Saturation transfer difference (STD) nuclear magnetic resonance (NMR) spectroscopy is a robust and reliable fluorescence free orthogonal method (Figure 11 Viegas et al., 2011). STD-NMR used not only for investigating the protein–ligand interactions, but also predict the mode of binding pose (Haselhorst et al., 2009; Streiff et al., 2004). STD-NMR method identify the binding epitopes of a bound ligand to its target protein. The close protons of the ligand into the protein surface receive a higher degree of resonance saturation, and this strengthen STD spectrum signal (Haselhorst et al., 2009). Protons with less interaction or even protons that far from the protein surface and not involved in the ligand protein interactions, have low or no STD-NMR spectrum signal (Barile and Pellecchia, 2014). Therefore, the STD-NMR method gives an expectation about the ligand pharmacophore and it's an excellent tool for further optimization of the ligand structure (Barile and Pellecchia, 2014).

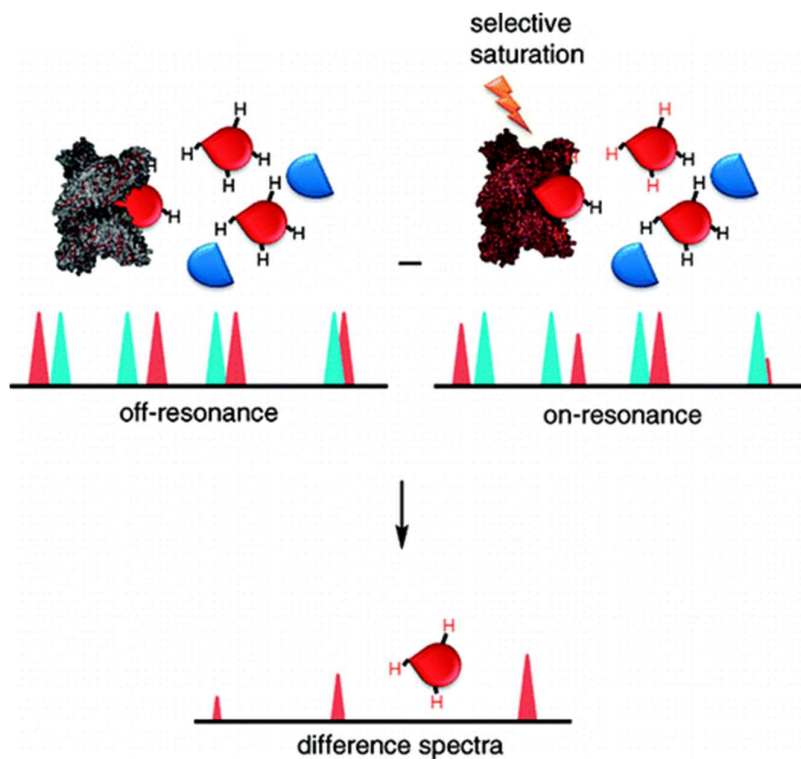


Figure 11 : Principle of STD-NMR in characterization of binding mode. Figure was adapted from Viegas et al. (2011).

1.4 Aim of the present study

We hypothesized that inhibition of the activity of IMP2 might be a novel and promising therapeutic approach for cancer therapy (Figure 12).

Therefore, we established *in vitro* studies for target validation, set up a screening assay for small molecule inhibitors of IMP2, and test the biological activity of the obtained hits *in vitro* and *in vivo*.

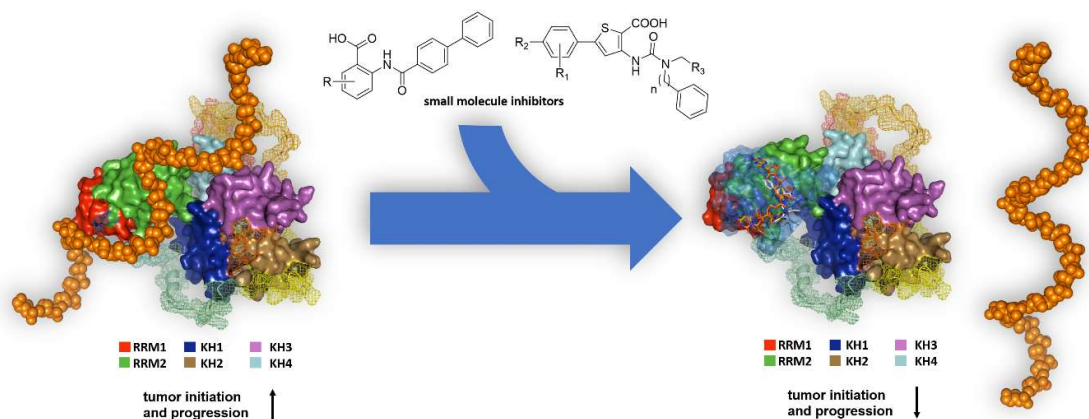


Figure 12: Hypothesis to be tested. Inhibition of IMP2 with small molecules might be a promising therapeutic approach in cancer therapy. Homologous IMP2 model was generated by Phyr 2 Protein Homology Recognition Engine (Kelley et al., 2015); graphical processing was done by PyMOL software (Molecular Graphics System, Version 2.0 Schrödinger, LLC.).

2 Results

2.1.1 *In vitro* validation of IMP2 as a promising target in cancer therapy

2.1.2 Effect of IMP2 knockdown/knockout on cell viability and proliferation

2.1.2.1 IMP2 knockdown impact on cell proliferation

siRNA knockdown approach was used to reduce IMP2 expression in SW480, and Hep3B cells. IMP2/p62 expression were knocked down with mixture of siRNAs in both SW480 and Hep3B cells, results were confirmed by Western blot (Figure 13A, B).

IMP2 knockdown cells were seeded in equal densities to their respective control cells (random siRNA treated cells) and treated under the same conditions. Cell viability was measured 72 h after siRNAs treatment and normalized to their respective controls. Cellular proliferation was reduced after IMP2 knockdown in SW480 and Hep3B cells (Figure 13C).

Results

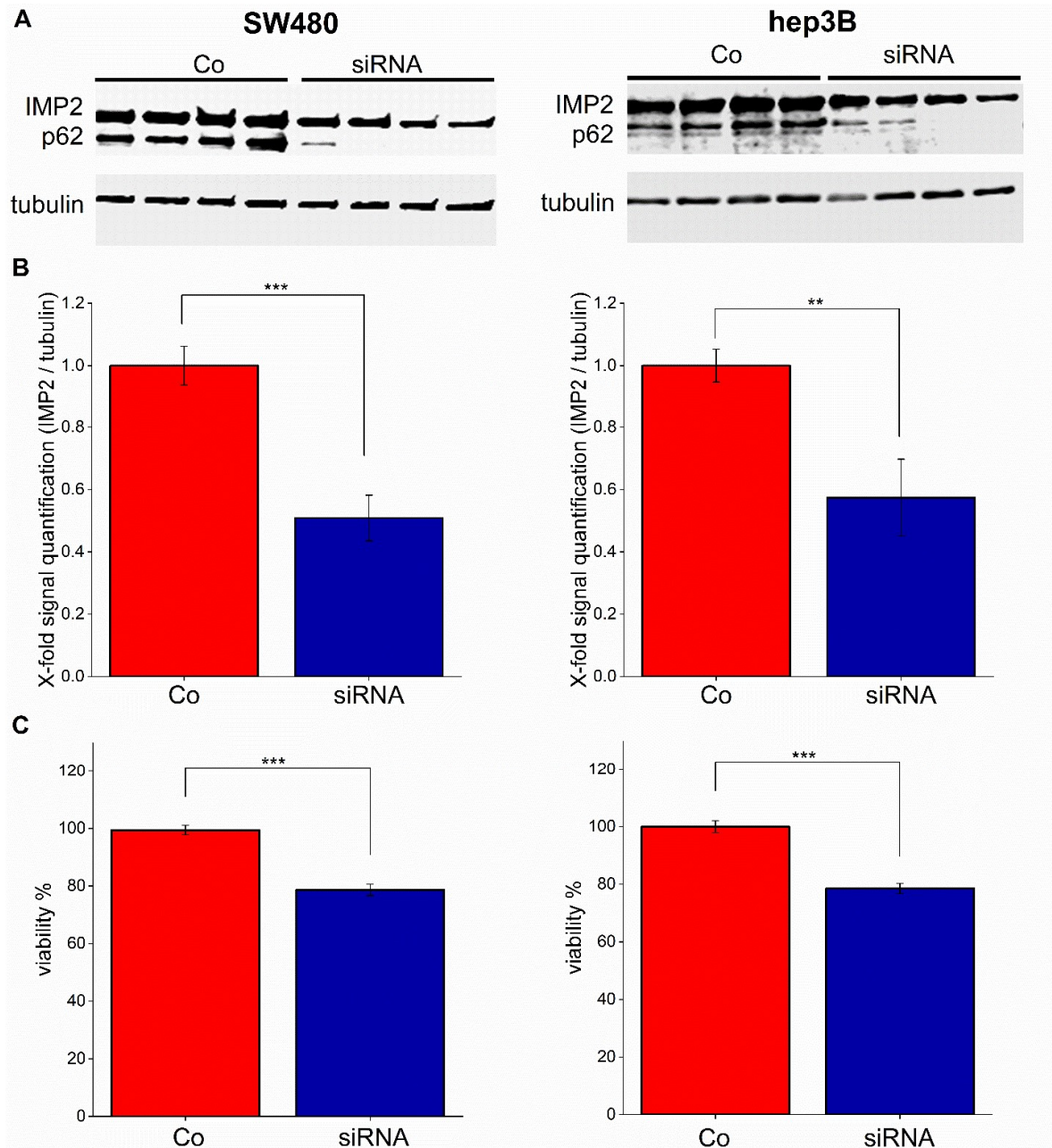


Figure 13 : Impact of IMP2 knockdown on cell viability. The siRNA knockdown approach was used to reduce IMP2 in SW480, Hep3B cells. Mixture of siRNAs were used to knockdown IMP2 expression, and control cells (Co) were transfected cells with random siRNA. (A), (B) Representative Western blots show reduction of IMP2/p62 expression after knockdown of IMP2. IMP2 signal intensities were normalized to the tubulin signal. Data represent mean \pm SEM; $n = 3$ (4,2,2 replicates). (C) Cell viability was measured with MTT 72 h after incubation with siRNA. Data were normalized to their respective controls. Data represent mean \pm SEM; $n = 5$ (9,9,3,3,3, replicates). P value was calculated either with ANOVA or Mann-Whitney test.

2.1.2.2 IMP2 knockout impact on cell proliferation *via* MTT

CRISPR/Cas9 approach was established in our lab to knockout IMP2. Multiple cycles of CRISPR/cas9 trials by Tarek Kröhler led to biallelic knockout of IMP2 in HCT116, and monoallelic knockout in SW480, and Huh7 cells. Western blot (WB) was done to confirm the complete knockout in HCT116, and partial knockout in SW480, and Huh7 cells (Figure 14A, B). The difficulty of growing cells from single cell colony in SW480, and Huh7, supports that IMP2 is essential for cell proliferation.

IMP2 knockout cells were seeded in equal densities to their respective parental control cells and treated under the same conditions. Cell viability was measured with MTT 96 h after seeding and normalized to their respective controls. Cellular proliferation was reduced significantly after IMP2 knockout in the tested cells (Figure 14C).

Results

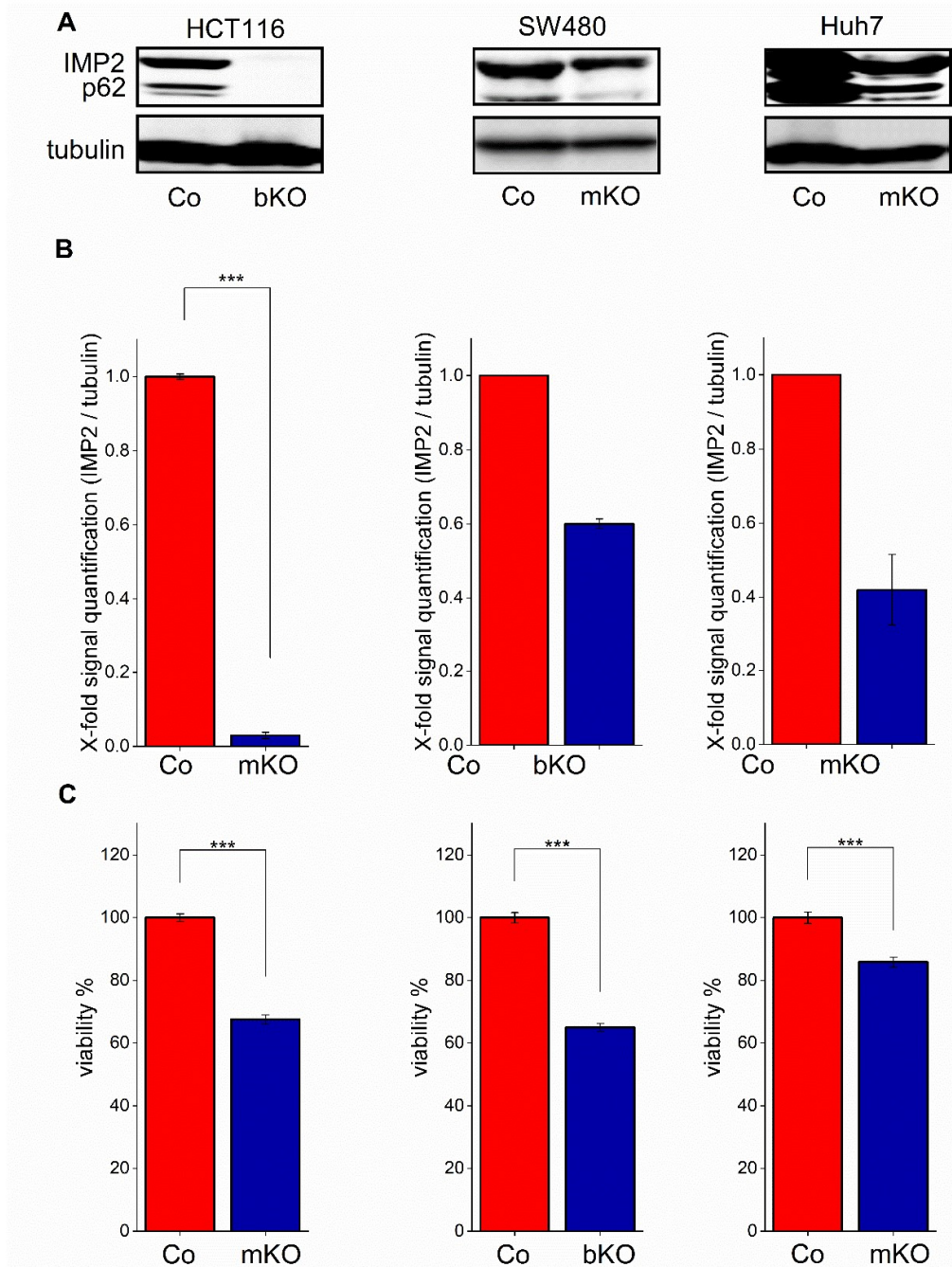


Figure 14 : Impact of IMP2 knockout on cell viability. IMP2/p62 expression was reduced in HCT116, SW480, and Huh7 cells by Tarek Kröhler using CRISPR/Cas9 approach. Control cells were the respective parental cells (Co). (A), (B) WB results show reduction of IMP2 expression after knockout of IMP2. IMP2 signal intensities were normalized to tubulin signal. Data represent mean \pm SD; $n = 2$ (one replicate), except in HCT116 $n = 3$ (1,1,3 replicates). (C) Cell viability was measured with MTT 96 h after cell seeding. Data were normalized to their respective controls. Data represent mean \pm SEM. For HCT116 $n = 5$ (30,6,6,9,9 replicates); SW480 $n = 4$ (30,3,3,6 replicates); Huh7 $n = 2$ (30,3 replicates). P value was calculated either with ANOVA or Mann-Whitney test.

2.1.2.3 IMP2 knockout impact on proliferation *via* ECIS

The MTT assay is able to predict cell proliferation based on the metabolic activity of cell mitochondria. The alteration in cell metabolism and mitochondrial content might affect cell viability (Rai et al., 2018).

Electric Cell-Substrate Impedance Sensor (ECIS) provides a real-time estimation of cell proliferation (Szulcek et al., 2014; Zudaire et al., 2008) by measuring the impedance of adherent cell layers to the well surface. In addition, altered impedance also allows assessment of changes in cellular behavior, such as, adhesion, which has been shown to be affected by IMP2 (Szulcek et al., 2014; Xing et al., 2019). HCT116 cells after plate coating with rat tail collagen were suitable to be used in ECIS method to evaluate the role of IMP2 knockout on proliferation rate.

Our findings showed IMP2 knockout cells have lower proliferation rate compared to the control cells (Figure 15). ECIS results further supported the role of IMP2 in cell proliferation.

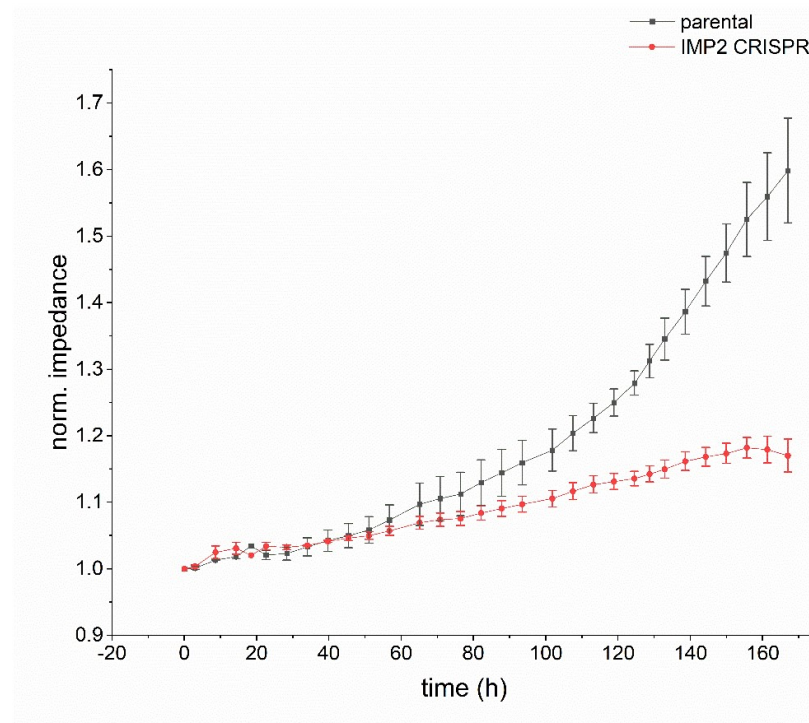


Figure 15 : Effect of IMP2 knockout on cell proliferation. Cell impedance was measured in real-time using ECIS method. HCT116 parental cells and IMP2 CRISPR/cas9 knockout cells were seeded in equal numbers and conditions. Cell impedance was normalized to the starting impedance point (0-4 h).

Data represent mean \pm SEM; n = 2 (triplicates). IMP2 knockout HCT116 cells were received from Tarek Kröhler.

2.1.3 Influence of IMP2 reduction on IMP1 and IMP3 expression

The mRNA of *IMP1* and *IMP3* may serve as potential targets for IMP2 regulation. For this purpose, the expression of IMP1 and IMP3 after IMP2 knockdown/knockout was investigated by WB and RT-qPCR. Duplicate samples of confirmed IMP2 knockout/knockdown were used to investigate IMP1 and IMP3 expression.

2.1.3.1 Potential inter IMP interactions in colon cancer cells

We observed that IMP1 expression was upregulated and IMP3 expression was down regulated in HCT116 cells (RNA and protein levels). In SW480 cells, the expression of IMP1 and IMP3 was down regulated (RNA and protein levels) (Figure 16A-C).

Results

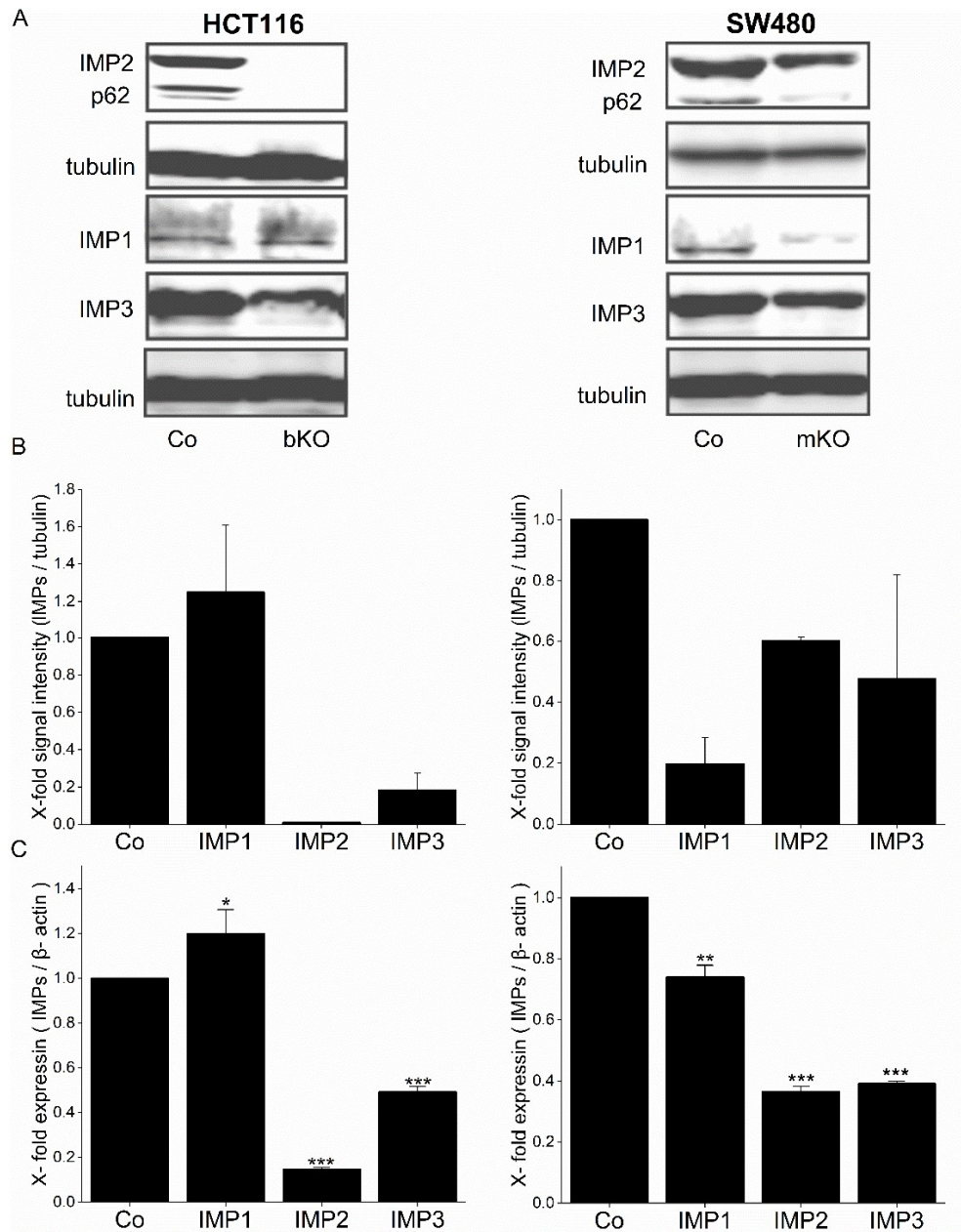


Figure 16 :Impact of IMP2 knockout on IMP1 and IMP3 expression in colon cancer cells. Western blot and RT-qPCR data show the expression of IMPs after IMP2 knockout. (A), (B) WB shows IMP2 biallelic (bKO) knockout in HCT116 cells, and monoallelic (mKO) knockout in SW480. WBs from duplicated samples show IMP1 and IMP3 expression after IMP2 knockout. Parental cells were used as controls (Co). IMPs signal quantification was normalized to tubulin control signal. Data represent mean \pm SD; n = 2 (one replicate). (C) represent *IMPs* mRNA expression measured with RT-qPCR. *IMPs* expression was normalized to the expression of β -actin housekeeping gene. Data represent mean \pm SEM; n = 2 (6,3 replicates). *P* value was calculated either with one-way ANOVA or Mann-Whitney test.

2.1.3.2 Potential inter IMP interactions in liver cancer cells after IMP2 knockout

In the protein levels, we observed that IMP1 was upregulated and IMP3 was down regulated in Huh7 cells (Figure 17A, B). Furthermore, the *IMPs* expression was unchanged in Huh7 cells (Figure 17C).

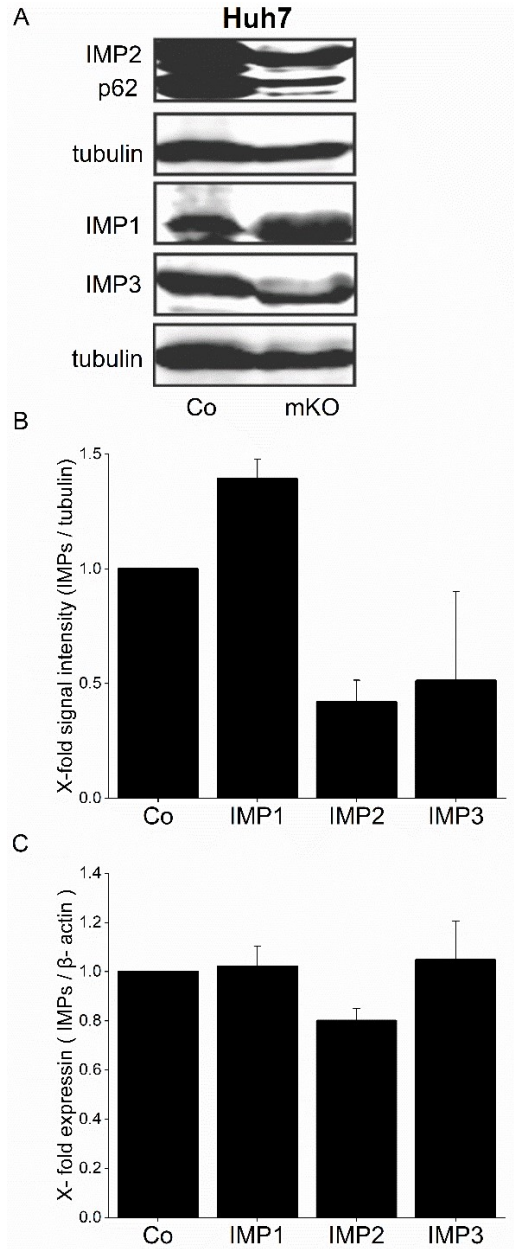


Figure 17: Impact of IMP2 knockout on IMP1 and IMP3 expression in liver cancer cells. Western blot and RT-qPCR data show the expression of IMPs after IMP2 knockout. (A), (B) WB shows IMP2 partial monoallelic (mKO) knockout in Huh7. WBs from duplicated samples show the expression of IMP1 and IMP3 after IMP2 knockout. Parental cells were used as controls (Co). IMPs signal quantification was

Results

normalized to tubulin control signal. Data represent mean \pm SD; n = 2 (one replicate). (C) represents *IMPs* mRNA expression measured with RT-qPCR. *IMPs* expression was normalized to the expression of β -*actin* housekeeping gene. Data represent mean \pm SEM; n = 2 (6,3 replicates). *P* value was calculated either with one-way ANOVA or Mann-Whitney test.

2.1.3.3 Potential inter IMP interactions in liver cancer cells after IMP2 knockdown

We observed that IMP1 and IMP3 expression were downregulated. The mRNA of *IMP1* in Hep3B cells was unchanged, and IMP3 expression was upregulated. In Plc/Prf/5 cells, *IMP1* expression was upregulated, and *IMP3* was unchanged (Figure 18A-C).

Our results might predict the potential inter IMP regulations and these findings need more experiments to draw a reliable conclusion.

Results

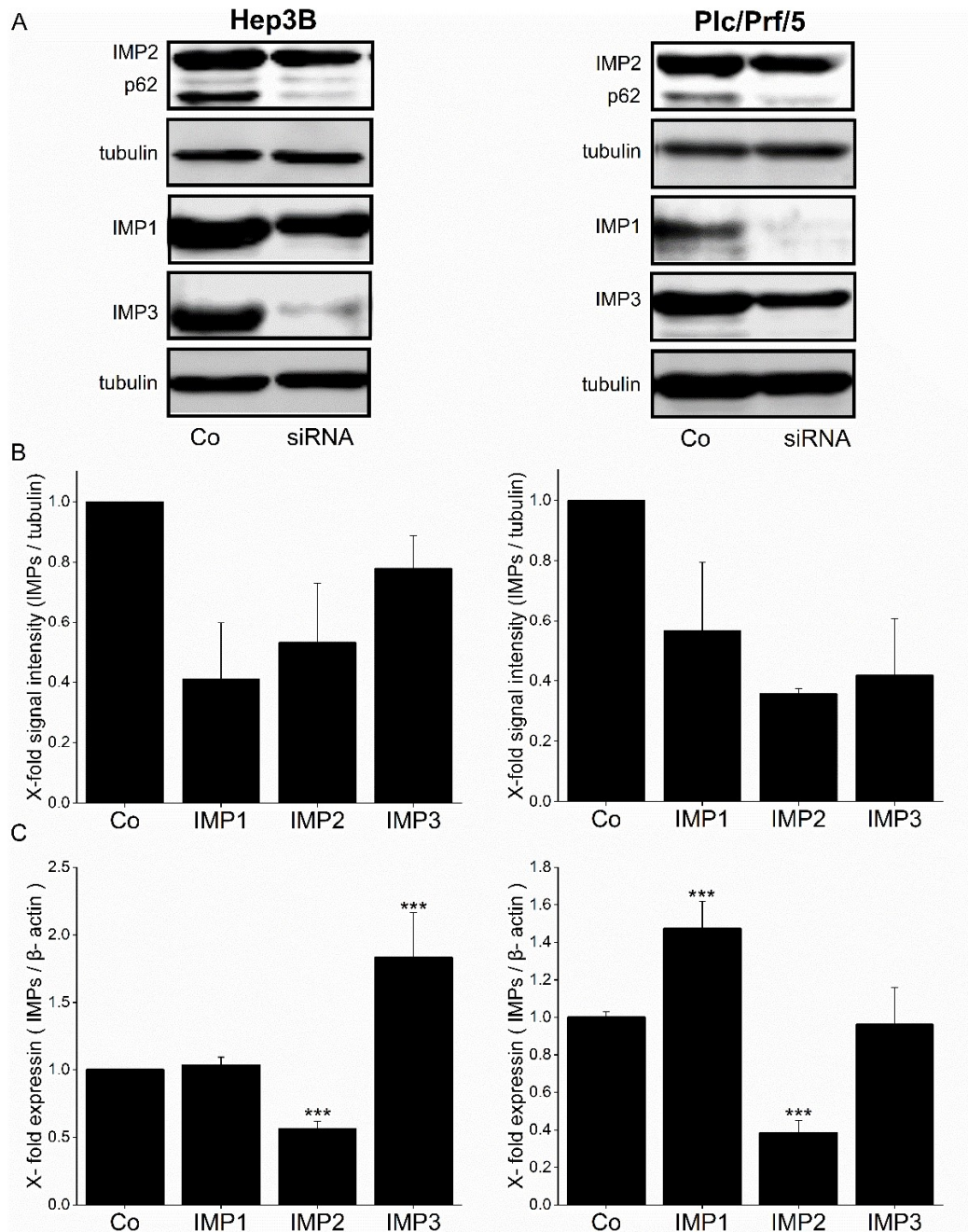


Figure 18 : Impact of IMP2 knockdown on IMP1 and IMP3 expression in liver cancer cells. Western blot and RT-qPCR data show IMPs expression after IMP2 knockdown. (A) WB shows IMP2/p62 expression after IMP2 siRNA knockdown in Hep3B and Plc/Prf/5 cells. IMP2 knockout affect the expression of IMP1 and IMP3. Cells treated with random siRNA were used as controls (Co). (B) IMPs signal quantification was normalized to tubulin control signal. Data represent mean \pm SD; n = 2 (1 replicate). (C) represent IMPs mRNA expression measured with RT-qPCR. IMPs expression was normalized to the expression of β -actin housekeeping gene. Data represent mean \pm SEM; n = 2 (6,3 replicates). P value was calculated either with one-way ANOVA or Mann-Whitney test.

2.2 IMP2 isolation, characterization, and primary screening for inhibitors

2.2.1 Recombinant IMP2 isolation and characterization

For the purpose of detection of inhibitors for IMP2 RNA interaction, production of large quantities of human IMP2 was required. Recombinant protein technology is an essential approach in the molecular biology that aimed to produce large quantities of proteins (Rosano and Ceccarelli, 2014). Recombinant IMP2 was isolated using immobilized-metal affinity chromatography (IMAC). Before starting the FP assay, the purity and integrity of IMP2 protein was confirmed by SDS-PAGE. Furthermore, Western blot confirmed the mass and identity of eluted IMP2 (Figure 19A, B). Since FP assays are based on the use of small labeled RNA sequences, we confirmed the absence of any RNase activity in the protein preparation under assay conditions (Figure 19C). Circular dichroism (CD) spectrometry confirmed the presence of α -helical and β -sheet secondary structure elements indicating correct folding of IMP2 (Figure 19D).

Results

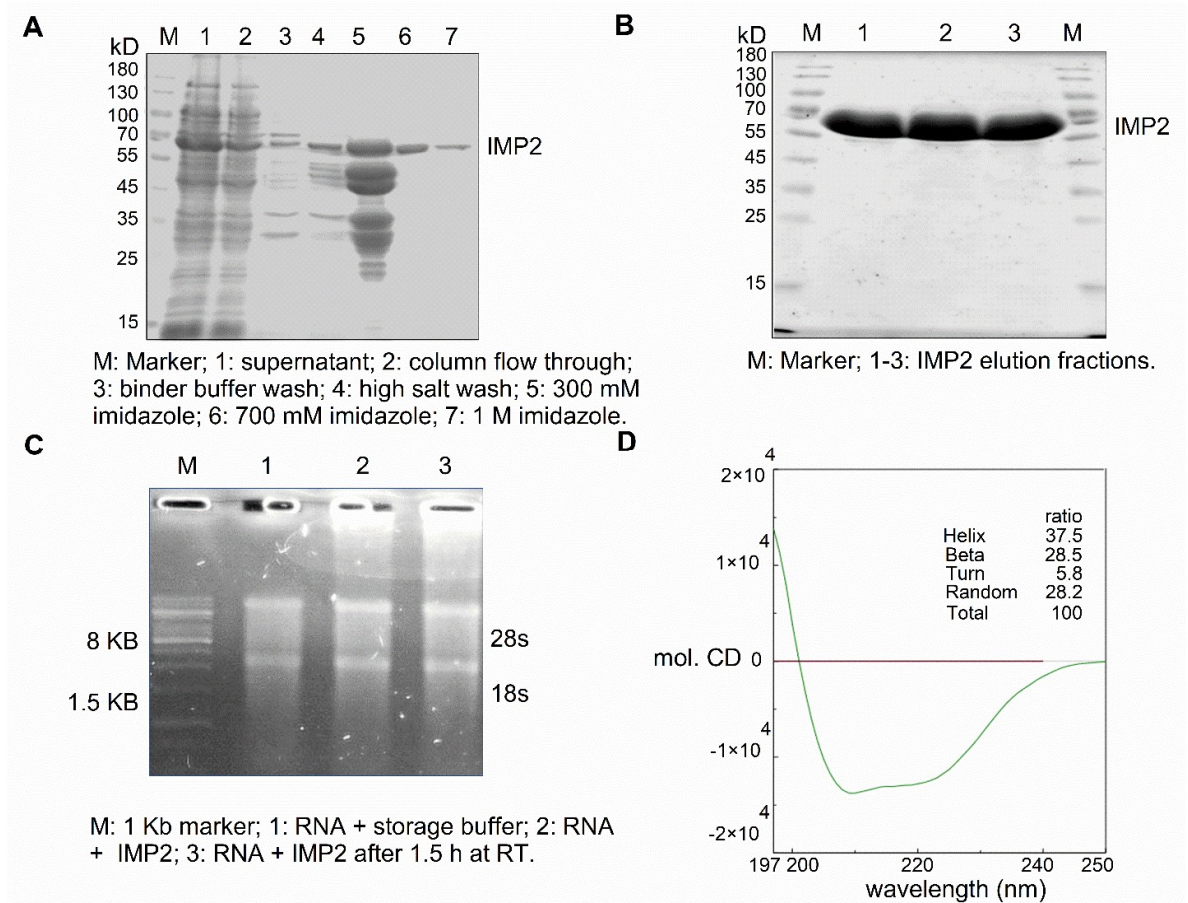


Figure 19 : Isolation and characterization of recombinant IMP2 protein. Histidine-tagged IMP2 was overexpressed in *E. coli* and isolated *via* affinity chromatography using a HisTrap HP Nickel–Sepharose column. Protein was eluted in an imidazole buffer with increasing imidazole concentrations. (A) Fractions were collected and run on an SDS-PAGE (lanes 5 – 7). A 10-180 kD protein ladder marker (M), the unpurified cell lysate (1), the column flow-through (2), and washing buffers (3 – 4) were also run on the gel. The gel was stained with Coomassie blue and revealed the pure IMP2 protein in the 300 mM and 700 mM imidazole fractions (lanes 6 and 7). IMP2 containing fractions were combined and concentrated. (B) The identity of the 67 kDa protein IMP2 was confirmed by Western blot analysis. (C) The absence of RNase activity was confirmed *via* RNA integrity measurement of MCF7 RNA in the presence of eluted protein, as visualized on an agarose gel. M: 1 kb marker, 1: RNA incubated with storage buffer for 1.5 h as a control, 2: RNA incubated with IMP2 for 1.5 h on ice, 3: RNA incubated with IMP2 for 1.5 h at room temperature (RT). (D) Circular dichroism (CD) spectroscopy was used to verify the correct protein folding of the purified protein. Prof. Alexandra Kiemer participated in writing this legend.

2.2.3 FP primary screening

2.2.3.1 Establishment of FP assay

For the purpose of functional inhibition of IMP2 RNA interaction, known IMP2 RNA binding sequences were involved in different RNA probes. Two RNA oligonucleotides were designed as IMP2 binding partners (RNA_A/B). A control RNA oligonucleotide was used as a control sequence (RNA_C). The sequences of RNA probe used in FP assay are summarized in Table 2.

Table 2 : Summary of probe sequences used in FP assay validation.

Code	Sequence (5'-3')
RNA_A	AUGCAUCCCCGCAGCUACACACACAACA
RNA_B	CCCCCUUUCACGUUCACUCUGUCU
RNA_C	GAAAAAAGAUUUUUUUUUUAAGA

The FP signal was tested at different DMSO concentrations between 0 and 10% (v/v), FP signal was stable up to 10% DMSO. A final concentration of 5% DMSO was selected for later screening experiments (Figure 21A, B). FP signals were measured at different time points, the FP signal was clearly stable after 1 h of incubation at room temperature until at least for 3 h, a 1.5 h of incubation was considered appropriate for the further screening experiments (Figure 21C, D).

Results

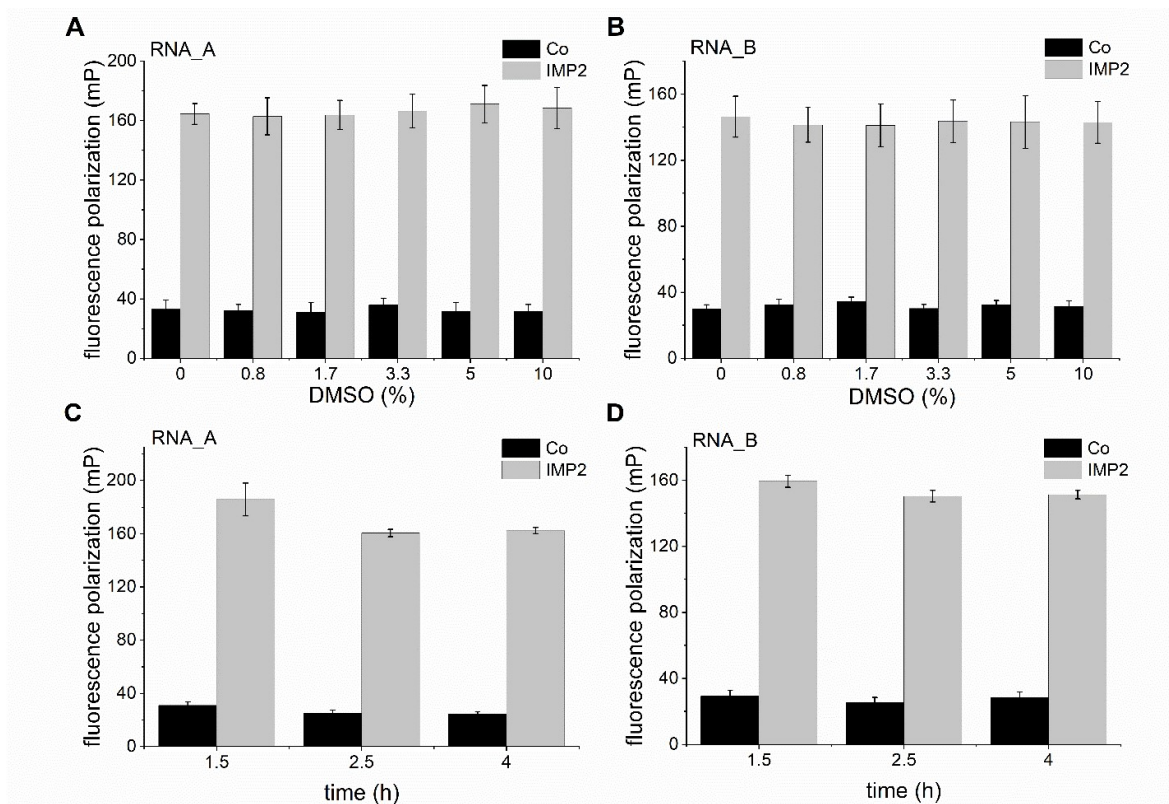


Figure 21 : Fluorescence polarization assay development and optimization. (A, B) The DMSO tolerance of the FP assay was determined by using 1 nM of either the (A) RNA_A or the (B) RNA_B probe, IMP2 (120 nM for RNA_A and 160 nM for RNA_B), and varying concentrations of DMSO (v/v). Unlabeled RNA was used as a control. (C, D) The stability of the protein-RNA complex was assessed for 5% DMSO at different time points. Data are represented as means \pm SD, n = 2 (triplicates).

The robustness of FP assay was investigated using low controls (fluorophore alone) and high controls (IMP2 and fluorophore). The Z' value was 0.9 for both RNAs and confirmed that the FP assay was robust and appropriate for further competitive screening (Figure 22A-C).

Results

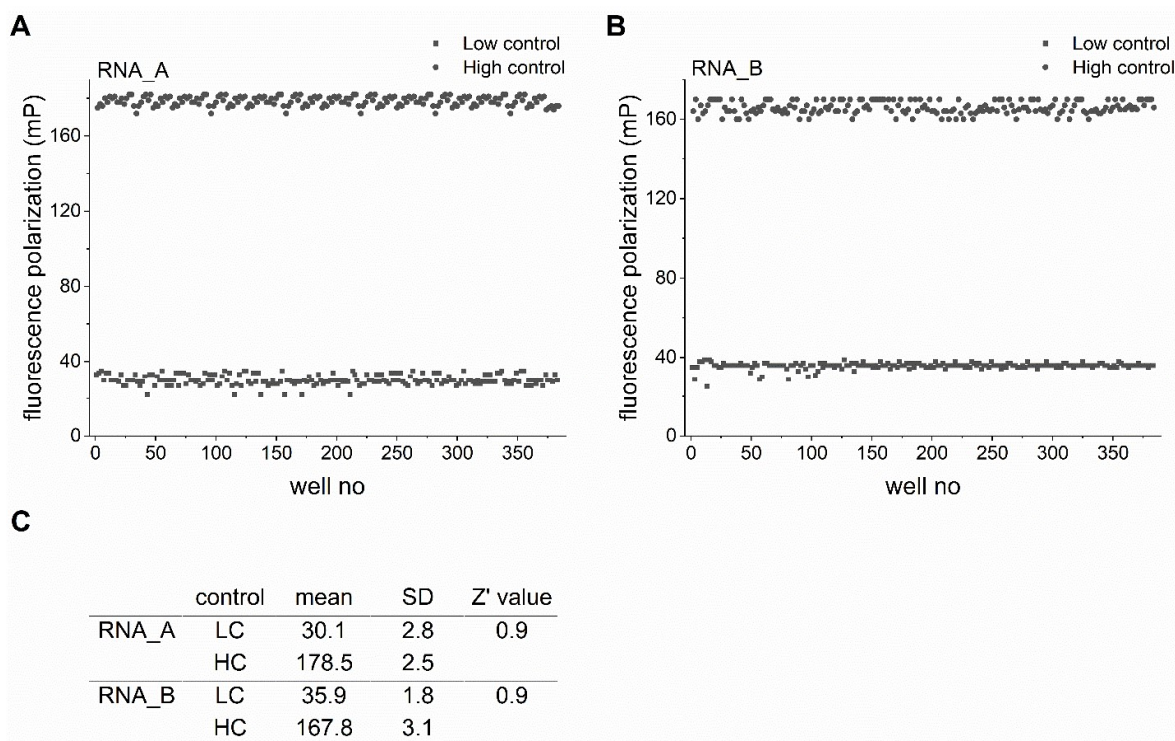


Figure 22 : The robustness of FP assay. (A, B) To determine the robustness of the FP assay, 192 samples of low controls (LC), containing 1 nM (A) RNA_A or (B) RNA_B without IMP2, and 192 samples of high controls (HC) containing additionally 120 nM and 160 nM IMP2 for RNA_A and RNA_B, respectively, were assessed at 5% DMSO in the FP assay after 1.5 h incubation. (C) Z'-factors were calculated based on the obtained data.

A lead inhibitor (2-((8-bromo-5-methyl-5H-[1,2,4]triazino[5,6-b]indol-3-yl)thio)-N-(1-phenylethyl)acetamide) was published by Mahapatra et al. (2014) for IMP1 RNA interaction. The used RNA probe (ACAGAACAA) in the FP screening assays share structure similarity with RNA_A (ACACAACA). A competition FP assay was done for IMP1 lead compound for its potential off target inhibition of IMP2 RNA_A / B interaction. The solubility limit of IMP1 lead compound was 62.5 μ M determined by measuring the change in absorbance at 620 nm. Different concentrations from IMP1 lead compound were tested against RNA_A and RNA_B. IMP1 lead compound did not inhibit IMP2 interaction either with RNA_A or RNA_B (Figure 23).

Results

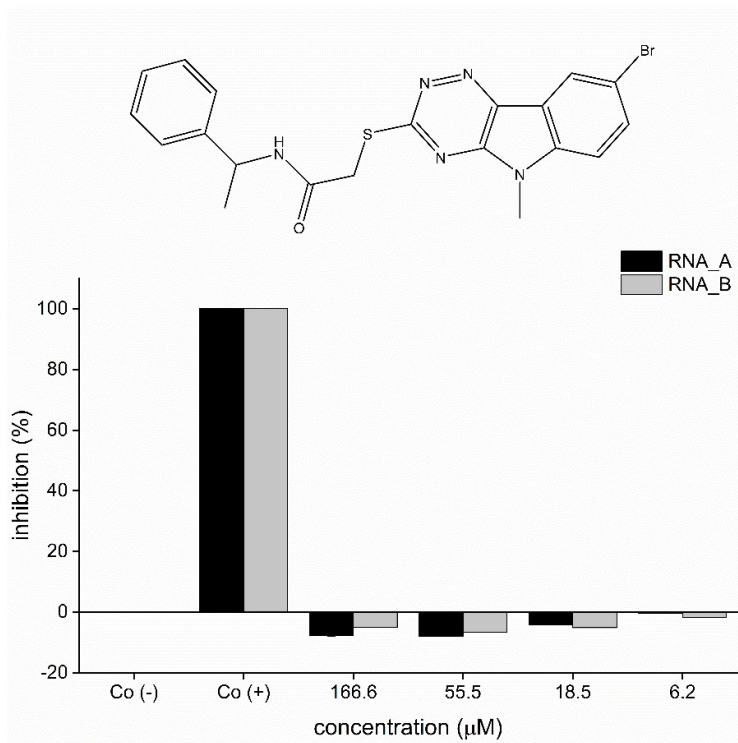


Figure 23 : Characterization of IMP1 lead compound interaction with IMP2 RNAs. Competition experiments were conducted using fixed concentrations of labeled RNA_A/B (1 nM), and IMP2 200 nM, and varying concentrations of IMP1 lead compound. Mixture of labeled RNA_A/B (1 nM), and IMP2 200 nM was used as a negative control, Co(-), and labeled RNA_A/B (1 nM) were used as a positive control, Co(+). Data represent means of FP values of duplicates \pm SD; n = 2.

We developed the fluorescence polarization assay for detecting potential hits capable to inhibit IMP2 RNA interactions. Serial dilutions of IMP2 were titrated against 1 nM of three different RNA sequences; IMP2 showed high affinity to RNA_A-B with EC_{50} values of 60.7 nM and 80.5 nM, respectively. No binding occurred with control RNA_C. BSA was used as a control protein and titrated against RNA_A/B, where no binding was detected (Figure 24A).

RNA_A and RNA_B are target RNAs and RNA_C serves as a control sequence. Saturation experiments were performed by titrating 1 nM of fluorescein labeled RNAs with a serial dilution of IMP2 protein or unrelated protein BSA.

Results

None labeled RNA_A and RNA_B used to test displacement of labeled RNAs in competitive FP assay, serial dilutions of their different RNA sequences titrated against 200 nM and 1 nM labeled RNAs. The IC₅₀ values for RNA_A and RNA_B were 5.3 and 4.7 μM, respectively (Figure 24B, C).

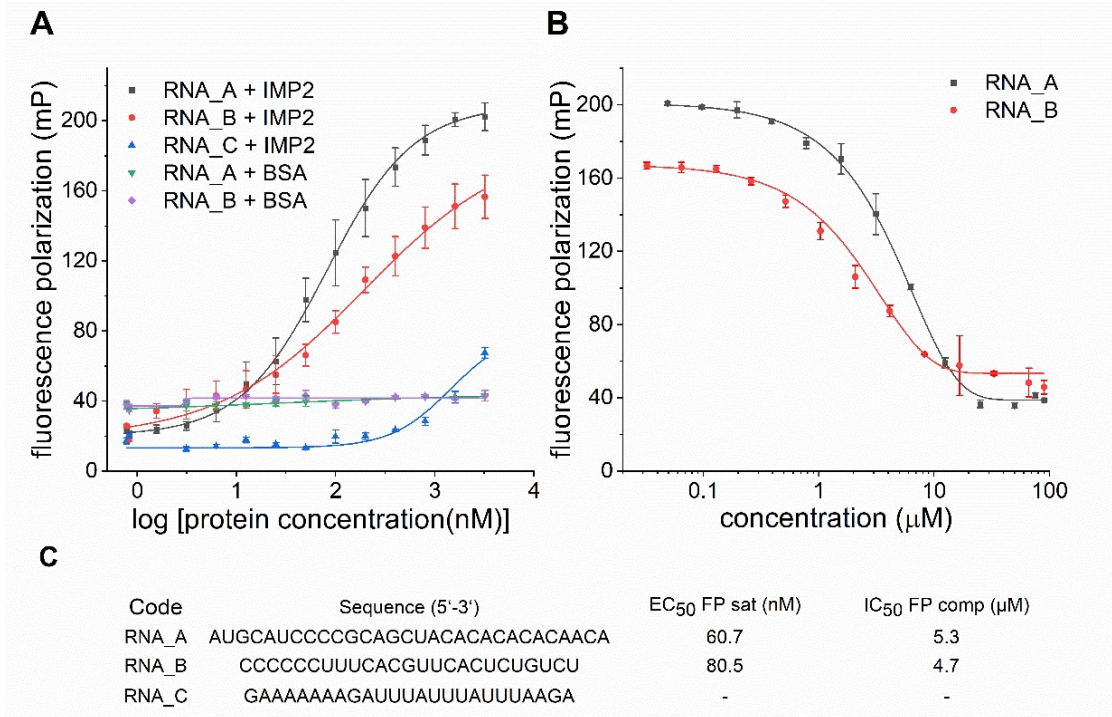


Figure 24 : Characterization of IMP2 functional binding to different RNA targets by FP assay. Direct and competition binding assays were performed by FP assay using full-length IMP2. Different RNAs and substrates were used to test the specificity of IMP2: RNA interactions. (A) Fluorescein-labeled target RNA sequences (RNA_A/B) and control sequence (RNA_C) were used in saturation experiments by titrating 1 nM RNA with a serial dilution of IMP2 protein or unrelated protein BSA. (B) Competition experiments were conducted using fixed concentrations of 1 nM RNA_A/B, 200 nM IMP2, and varying concentrations of the respective non-labeled RNA as a competitor. (C) Half maximal effective concentrations in saturation assay (EC₅₀ FP_{sat}) and half-maximal inhibitory concentrations in competition assay (IC₅₀ FP_{comp}) were calculated using non-linear regression analysis. Data are represented as means of FP values ± SD, n = 2 (duplicates).

2.2.3.2 FP-based primary screening

A total number of 46 and 38 compounds achieved more than 50% inhibition with IMP2 for RNA_A and RNA_B, respectively. Twenty-five and sixteen active compounds were excluded as a result of quenching the fluorescence intensity or the auto-fluorescent nature for RNA_A and RNA_B, respectively (Figure 25A, B).

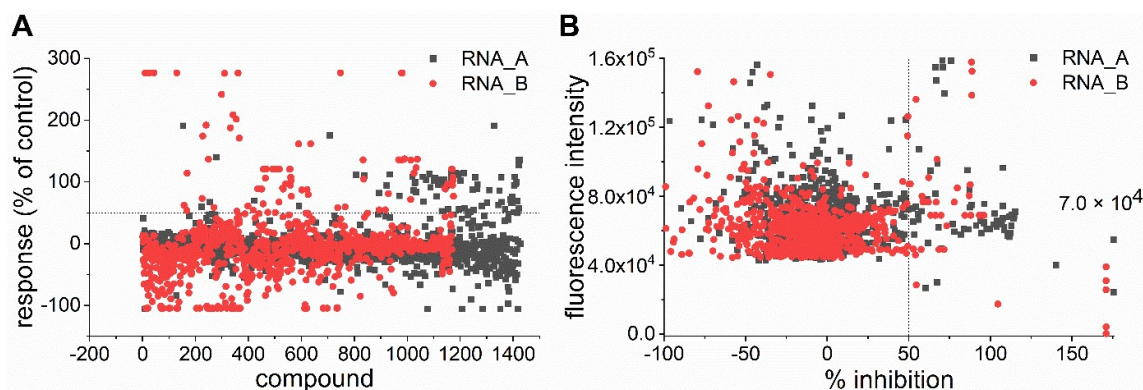


Figure 25 : FP primary screening and characterization of hit compounds. In a primary screening, 1,428 compounds were screened for RNA_A and 1,175 compounds for RNA_B in an FP assay at a final compound concentration of 150 μ M. (A) The scatter plot represents FP mean values of responses normalized to the response of non-labeled RNAs, used as a positive control. (B) Mean fluorescence intensities of screened compounds were plotted against % inhibition. Compounds achieving more than 50% inhibition without interfering with the fluorescence intensity were considered as a hit. The dashed lines indicate the hits threshold.

2.2.3.3 Pluronic® F-127 effect on FP assay findings

Pluronic® F-127 is a non-ionic polymer surfactant that have been used to facilitate solubilization of lipophilic probes. Pluronic® F127 has been used in broad range of therodiagnostic applications in biomedical and pharmaceutical sciences (Akash and Rehman, 2015; Maruyama et al., 1989). Pluronic® F-127 has been utilized to ease the dispersion of acetoxymethyl esters of fluorescent ion indicators such as indo-1, fura-2, fluo-3, fluo-4 and SBF1 (Fan et al., 2011; Maruyama et al., 1989; Qu et al., 2016). The use of Pluronic® F-127 in our study revealed some false positive hits that were excluded from further examinations. A total of 13 active compounds were excluded

Results

after addition of Pluronic® F-127 (Figure 26A). Only 16 and 12 compounds were considered as true hits for RNA_A and RNA_B, respectively. Ten compounds were common and able to inhibit IMP2 binding to both RNAs. Furthermore, the aggregated fraction of hit compounds was reduced after the addition of Pluronic® F-127 (Figure 26B).

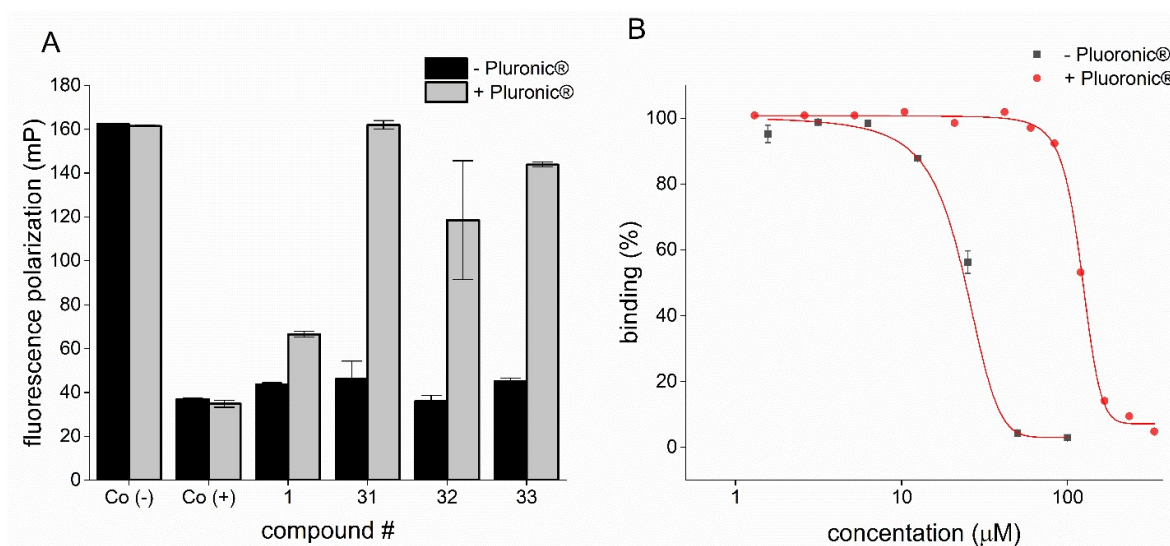


Figure 26 : Effect of Pluronic® F-127 on FP assay findings. The role of Pluronic® on FP assay was to rule out potential false positive results. (A) To minimize unspecific aggregation and, therefore, false-positive results, 0.013% Pluronic® F-127 were added to FP buffer. The inhibitory effect of compounds 31 – 33 was lost after addition of Pluronic® F-127, but not for compound 1. Data are represented as means \pm SD, n = 1 (duplicates). (B) The IC₅₀ value of compound 3 was increased from 26.7 to 123.2 μ M. Data represent mean \pm SD, n = 2 (duplicates).

2.2.3.4 Dose response studies of hit compounds

Hit compounds belong into either benzamidobenzoic acid compounds group (class A), and urea compounds group (class B). The IC₅₀s were measured by FP assay, results revealed IC₅₀ values in range of 65.3 to 120.9 μ M for RNA_A and 72.3 to 333.3 μ M for RNA_B (Figure 27A, B).

Results

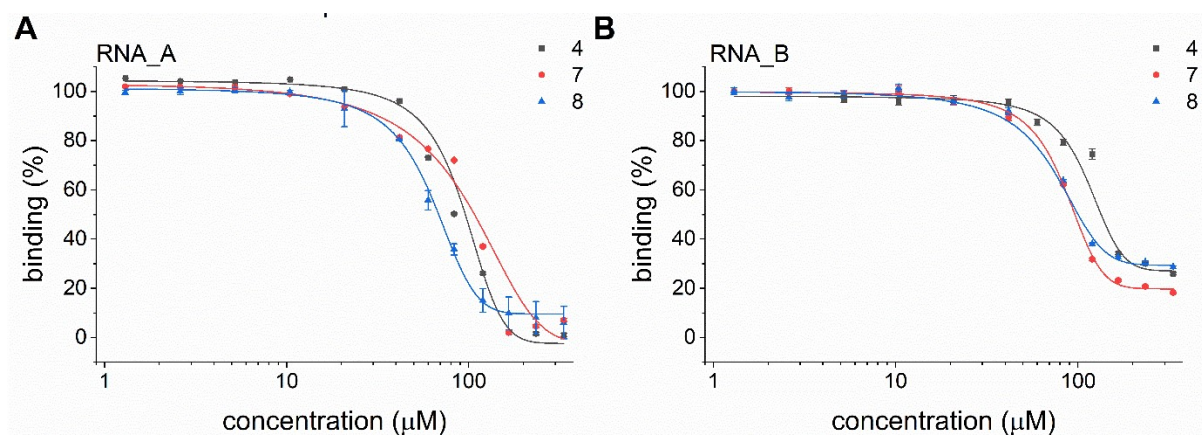


Figure 27 : FP primary screening and characterization of hit compounds. (A) and (B) Dose-response studies were performed with three representative hit compounds (compounds 4, 7, 8) against (C) RNA_A and (D) RNA_B in the FP-based competition assay. Competition assays were conducted using fixed concentrations of RNA_A/B (1 nM), and IMP2 (200 nM), and varying concentrations of hit compounds. Data are represented as means of FP values \pm SD, n = 2 (duplicates).

The 10 most promising hits belonged either to the benzamidobenzoic acid class (A) or the ureidothiophene class (B) (Figure 28A, B; Supplementary data: Table 1, 2).

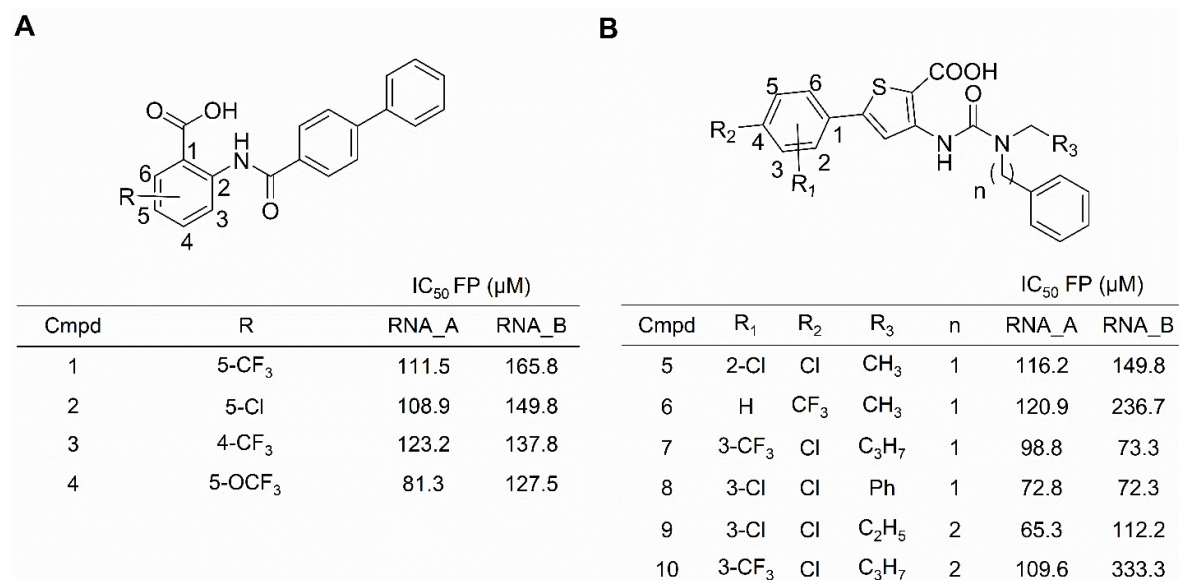


Figure 28 : Chemical classification and IC₅₀s of hit compounds. (A) and (B) The chemical structures and IC₅₀ values of hit compounds (cmpd) from class A (benzamidobenzoic acid group, A) and class B (ureidothiophene group, B) compounds. IC₅₀ values were calculated based on competition experiments, using the established FP assay (1 nM RNA_A/B, 200 nM IMP2, and varying concentrations of hit compounds). N = 2 (duplicates).

2.2.3.5 Correlation of the half inhibitory concentration with competitive inhibitory constant

The inhibition constant (K_i) is kinetically defined as the ratio of association rate constant over dissociation rate constant (k_{off}/k_{on}). The K_i value is an intrinsic indicator of the binding affinity, even though it may depend on the substrate concentration and affinity. The IC_{50} value additionally depends on the enzyme concentration.

The well-known Cheng-Prusoff equation is commonly used for the calculation of the competitive binding inhibitions (Cheng and Prusoff, 1973). The Cheng-Prusoff equation is not valid in FP competitive binding assays. For this purpose, a newly developed and validated mathematical equation that was generated by Nikolovska-Coleska et al. (2004). Accordingly, this equation is $K_i = [I]_{50} / ([L]_{50} / EC_{50} + [P]_0 / EC_{50} + 1)$. where $[I]_{50}$ represents the concentration of the free inhibitor at 50% inhibition (FP IC_{50} value), $[L]_{50}$ represents the concentration of the free labeled RNA probes (1 nM) at 50% inhibition, EC_{50} is half maximal effective concentrations (60.7 nM for RNA_A and 80.5 nM for RNA_B), and $F[P]_0$ is the free IMP2 concentration at 0% inhibition (200 nM). The K_i values of final hit compounds were summarized in Table 3.

Table 3: Summary of K_i values of hit compounds.

Class A			Class B		
	K _i (μM)			K _i (μM)	
cmpd #	RNA_A	RNA_B	cmpd #	RNA_A	RNA_B
1	25.9	47.5	5	27.0	43.0
2	25.3	43.0	6	28.1	67.9
3	28.7	39.5	7	23.0	21.0
4	18.9	36.6	8	16.9	20.7
			9	15.2	32.2
			10	25.5	95.6

2.3 Secondary confirmation of IMP2-hit compound interactions

2.3.1 Confirmation of IMP2-hit compound interaction with thermal shift assay

TSA was used to further confirm hit compounds IMP2 interaction. The T_m of IMP2 was 43°C and change in melting temperature after addition of hit compounds were calculated. All hit compounds showed shifts in IMP2 T_m by -5.5 to -1.2°C (Figure 29A, B).

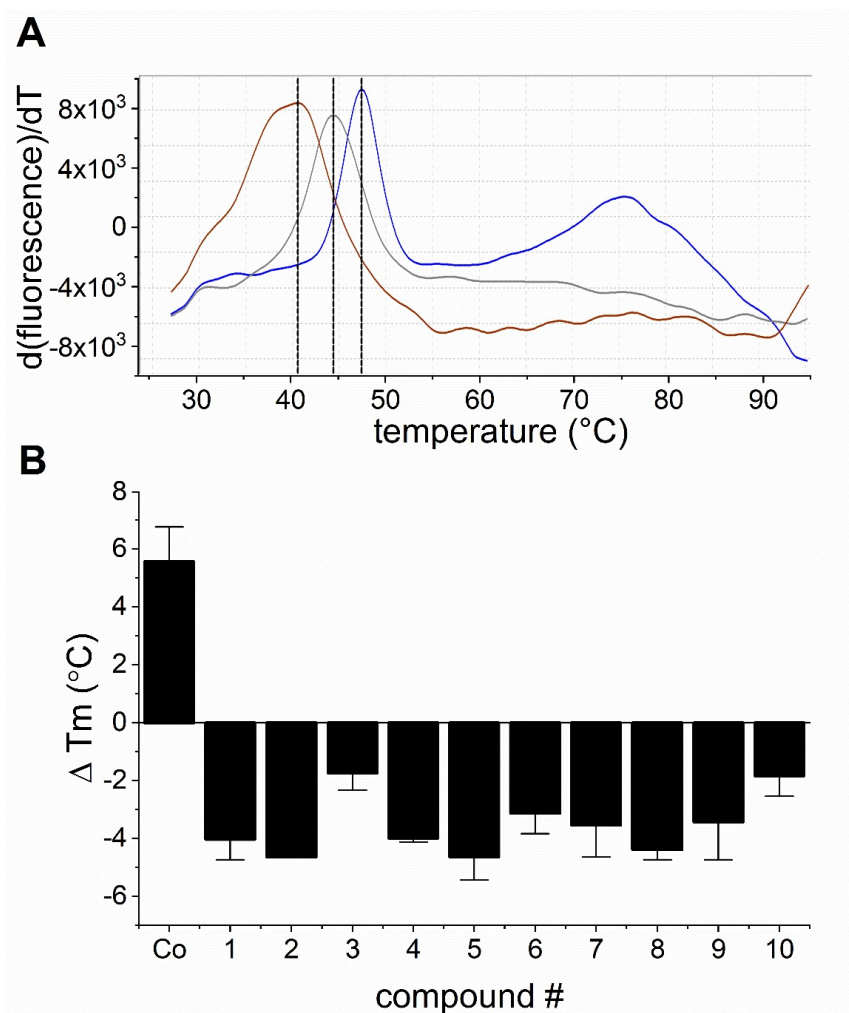


Figure 29 : Thermal shift assay confirmation of hit compounds. Thermal shift assays were performed to confirm IMP2-hit compound interaction at fixed concentrations of IMP2 (4.5 μM) and non-labeled RNA (100 μM) or hit compound (100 μM), respectively, measuring the fluorescence of Sypro Orange. (A) Representative melting curves demonstrate a shift in the IMP2 melting temperature (T_m) resulting from

the binding to either RNA (blue) or hit compound 8 (red) compared to the control (gray). (B) Melting temperature shifts (ΔT_m) resulting from compound interactions were quantified and compared to the non-labeled RNA control. Data are presented as means \pm SD, n = 2 (one replicate).

2.3.2 Confirmation of IMP2-hit compound interaction with microscale thermophoresis

The thermophoresis movement of a fluorescent NTA His tagged IMP2 was changed dependently to the increase of IMP2 bound fraction with compound # 9. IMP2 showed a stronger reduction in fluorescence in the bound state compared to the unbound state. The dissociation constant (K_d) is fitted to 43.2 ± 6.9 . The dose response titration of compound # 9 that was measured by FP and MST assays, showed similar range of IC_{50} values (Figure 30A-D).

Results

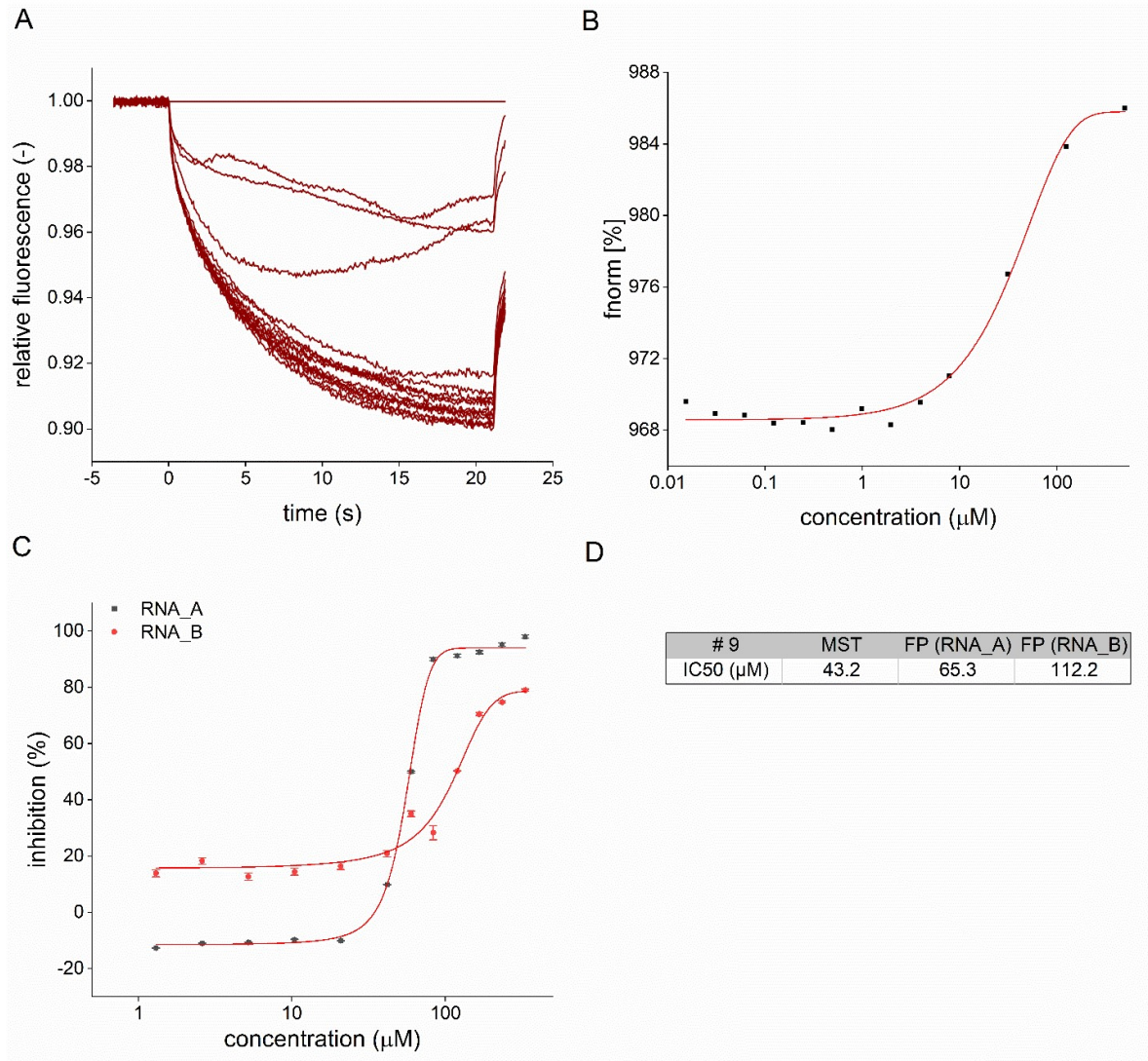


Figure 30: Comparison of IC₅₀ values for compound # 9 with MST and FP assays. A ligand titration experiment was done with MST technique to confirm the measured IC₅₀ results with FP assay (A) The thermophoresis movement of a fluorescent NTA His tagged IMP2 was changed dependently to the increase of IMP2 bound fraction with the compound # 9. (B) The normalized fluorescence difference [%] reflects the thermophoresis movement. A final concentration of 300 nM of IMP2 was titrated against different concentration of compound # 9. (C) FP-based competition experiments were conducted using 1 nM of RNA_A/B as probe, 200 nM of IMP2, and different concentrations of compound # 9. Data are represented as mean FP values of each duplicate \pm SD. IC₅₀ values were determined using non-linear regression analysis (D) The IC₅₀ values for MST and FP (RNA_A, and RNA_B) are represented in μM .

2.3.3 Confirmation and characterization of IMP2-hit compound interaction with STD – NMR

IMP2 has many flexible loops making the crystallization of full length IMP2 a huge burden. STD-NMR (orthogonal) method was applied as an alternative to have a closer look into the binding pose. Furthermore, STD-NMR was utilized to further confirm ligand-protein interaction by a fluorescence free method (Becker et al., 2018; Viegas et al., 2011). Typically, the proton with the strongest STD effect is used to normalize the signals of the other protons resulting in values between 0 - 100%.

2.3.3.1 Establishment and optimization of STD-NMR experiment

The STD-NMR buffer was optimized for protein stability and generation of clear spectra. STD-NMR experiments were performed at fixed concentrations of 2.5 or 5 μ M IMP2. Hit compounds were used either in concentrations of 250 μ M for compound 2 and 3 or 500 μ M for compounds 4 - 6 and 13 - 14. Concentrations were selected based on the solubility limit in 10% DMSO D6. A control spectrum was performed under the same conditions without a protein to test for artifacts. The theoretical chemical shifts range was predicted by Chemical Communications (ChemDraw) software and the area of each peak was calculated by integration.

2.3.3.2 Mode of interaction of compound # 4 with IMP2

The overlay of the off-resonance and STD spectra of compound # 4 in presence of IMP2 predicts the mode of interaction of IMP2 compound # 4 complex. A first observation was that protons H-1, H-2, and H-3 of the benzoic acid ring are interacting strongly with the protein (H-1 73.7%, H-2 100% observed together with H-11, H-3 75.7 % observed together with H-6/7; Figure 31).

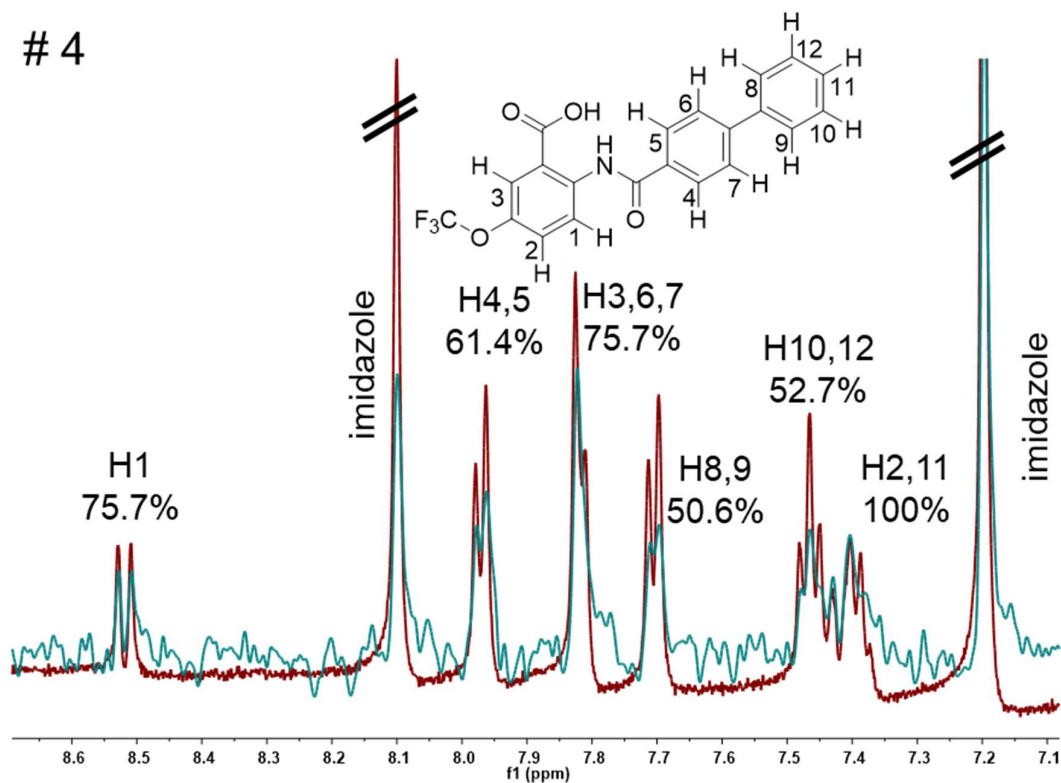


Figure 31 : Interaction mode of compound # 4 predicted by STD-NMR. STD-NMR experiment results of compound # 4 in complex with IMP2. The reference spectrum is shown in red, and the STD difference spectrum is shown in green. Overlaid STD off-resonance and STD effect spectra were normalized to the signal of H2, and 11.

Secondly, within the middle ring, chemically equivalent protons H-6 and H-7 (75.7%; observed together with proton H-3) presumably are in closer proximity to IMP2 than H-4 and H-5 (61.4%). Finally, the terminal phenyl moiety seems to interact less strongly overall (H-8/9 50.6%, H-10/12 52.7 %, H-11 100% observed together with proton H-2). Dr. Martin Empting participated in writing this result part.

2.3.3.3 Overall summary of IMP2-hit compound mode-of-interaction

STD-NMR was successfully performed with compounds 2-6 as well as 13 and 14. Among this set of STD-NMR-investigated compounds were three compounds belonging to class A (2-4) and four compounds belonging to class B (5, 6 and 13, 14). For the latter two compounds (13, 14), which inhibit only RNA_A. The overall STD effect was not very prominent and did not allow for a conclusive result. This might explain different affinities of hit compounds for multiple RNA binding domains. The

Results

overall STD-NMR results of all tested compounds were summarized in Figure 32 (STD-NMR data are shown in Supplementary data: Figure 1).

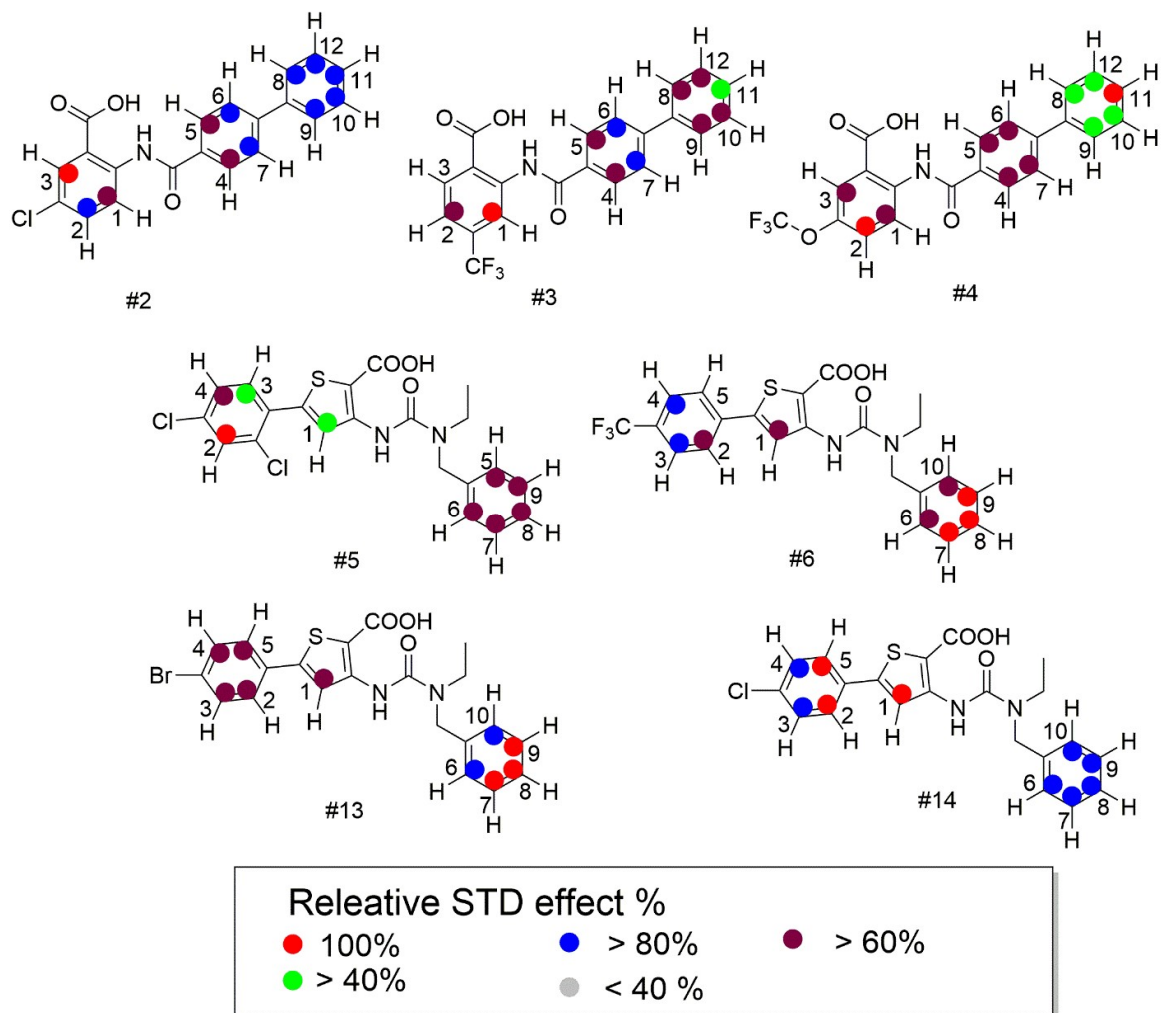


Figure 32 : Colored epitopes of hit compounds based on STD-NMR data. Colored epitopes of hit compounds display the interaction mode of IMP2 legend complex. Colored dots represent the percentage of relative STD effect and shown as: red dots represent of 100% relative STD; purple dots over 80%, violet dots over 60%, yellow dots over 40%, and blue dots below 40%.

2.3.4 *In silico* confirmation and characterization of IMP2-hit compound interaction

molecular docking is commonly used in drug optimization and validation such as pharmacophore modeling and quantitative SAR studies (Meng et al., 2011). We generated docking models for IMP2 that might be used later for structure optimization or virtual screening. The first generated model was a homology model of IMP2 RRM1 domain in complex with ACAC and CCCC RNA binding motifs using the homologous IMP3 RRM12 structure. A second model was a homology model of IMP2 KH34 domains in complex with CAC/CCC and CGGA RNA binding motifs using the homologous IMP3 KH34 structures (Figure 33).

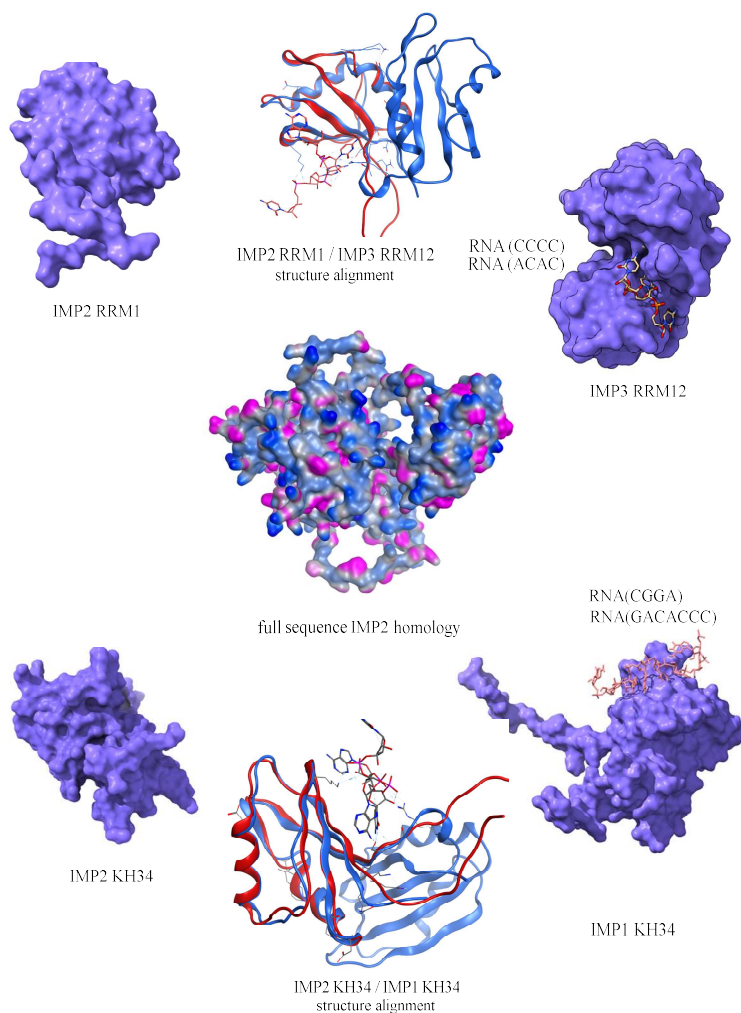


Figure 33 : Homology models for the molecular docking studies. A homology model for IMP2 RRM1 was generated using a reported NMR structure of IMP2 an X-ray structure of IMP3 in complex with RNAs

(ACAC and CCCC). Another homology model for IMP2 KH34 was generated using a reported X-ray structure for IMP2 and an X-ray structure for IMP1 in complex with RNAs (CAC/CCC, and CGGA).

2.3.4.1 Molecular docking of compound # 4 in the RRM1 binding domains

With the aim to derive a plausible binding pose for hit compounds and based on the assumption that our IMP2-RNA-interaction inhibitors act in an RNA-competitive manner, we docked compound 4 (representative for class A) to the RRM1 and KH34 RNA binding sites. The highest ranked docking pose reflected some key observations from the STD-NMR experiment.

2.3.4.1.1 Compound # 4 and inhibition of IMP2-RNA (ACAC) complex

In this hypothetical IMP2 RRM1 ACAC interaction complex, the benzoic acid head group interacts strongly with the protein, the carbonyl function being involved in a salt bridge with nearby Arg90 sidechain and H-3 being the most solvent exposed (less interacting) proton in this ring. Protons H-4 to H-7 showed a mixed solvent exposure profile, which is in agreement with the observed STD effect. Finally, in this docking pose the terminal phenyl ring is the part of the molecule, which is mostly exposed to the solvent although it is predicted to interact with Ser76 *via* a hydrophobic arene-H interaction with the proton at the α -carbon of the residue (Figure 34A, B). Dr. Martin Empting participated in writing this result part.

2.3.4.1.2 Compound # 4 and inhibition of IMP2-RNA (CGGA) complex

The RNA (CGGA) sequence was not involved either in RNA_A or RNA_B probes used in the competitive FP assays. In order to predict whether compound # 4 interact with RNA (CGGA) in IMP2 KH 4 domain, docking studies were performed. In the hypothetical IMP2 KH4 CGGA complex, the benzoic acid ring is predicted to interact with Gly529 *via* a hydrophobic arene-H interaction with the proton at the α -carbon of the residue. Protons H-4 to H-7 showed a mixed solvent exposure profile, which is in agreement with the observed STD effect. The proximal phenyl ring is predicted to interact with Arg547 *via* a hydrophobic arene-H interaction with the proton at the α -

carbon of the residue. Finally, in this docking pose the terminal phenyl ring is the part of the molecule, which is mostly exposed to the solvent although it is predicted to interact with Arg547 and Asp548 *via* a hydrophobic arene-H interaction with the proton at the α -carbon of the residue (Figure 34C, D).

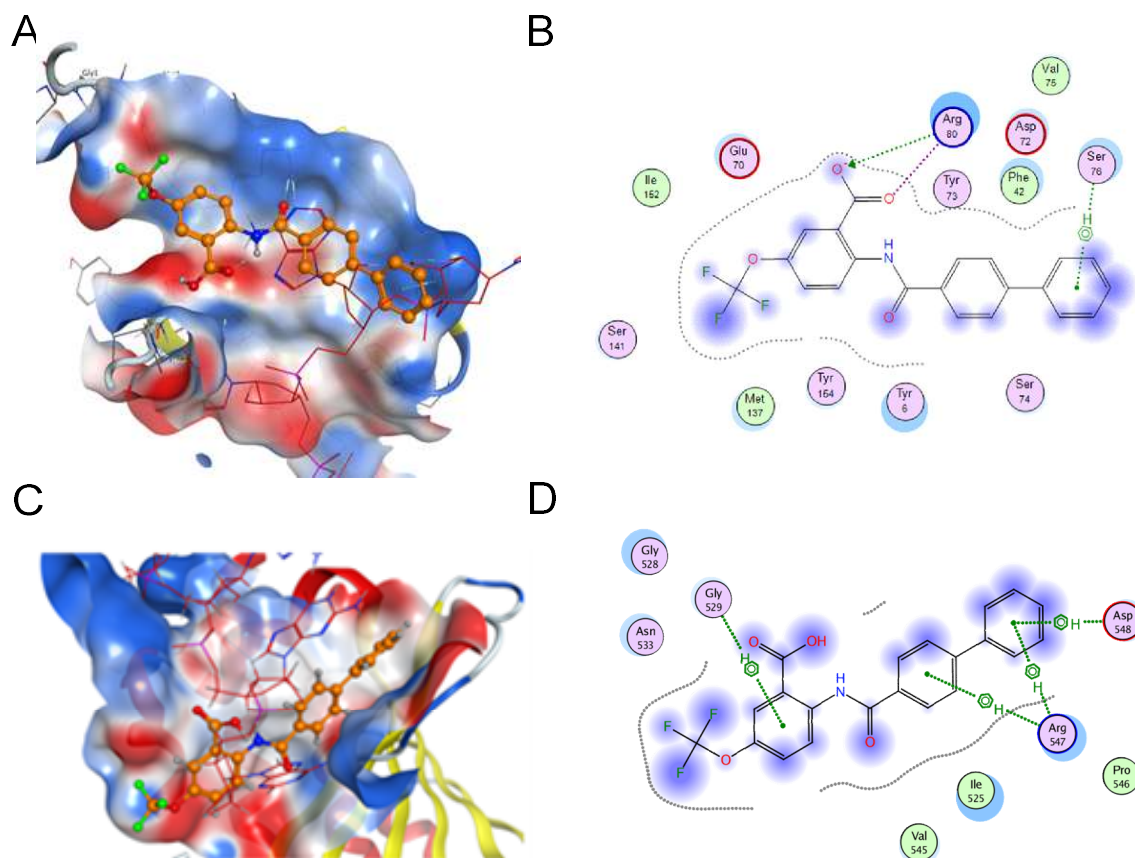


Figure 34 : Molecular docking of compound # 4 in IMP2 binding domains. (A) and (B) show the 3D and 2D interactions of compound 4 with RNA (ACAC) in IMP2 RRM1. (C) and (D) show the 3D and 2D interactions of compound 4 with RNA (CGGA) in IMP2 KH4.

2.4 Biological activity assessment of final hit compounds (potency, specificity, and safety)

2.4.1 Biological activity of final hit compounds

2.4.1.1 IMP2 expression in different cancer cell lines

Different cell lines were used to estimate the biological activity of hit compounds. Colon cancer cells (HCT116, and SW480) and liver cancer cells (HepG2, Hep3B, and Huh7) expressing high IMP2 levels. MCF7 cells are not expressing IMP2 and were used as a control cell lines (see Figure 35 and Cancer Cell Encyclopedia (Ghandi et al., 2019)). Since hit compounds are dissolved in DMSO solvent, cell tolerance to different concentrations of DMSO was tested in different cell lines (Supplementary data: Figure 2, 3).

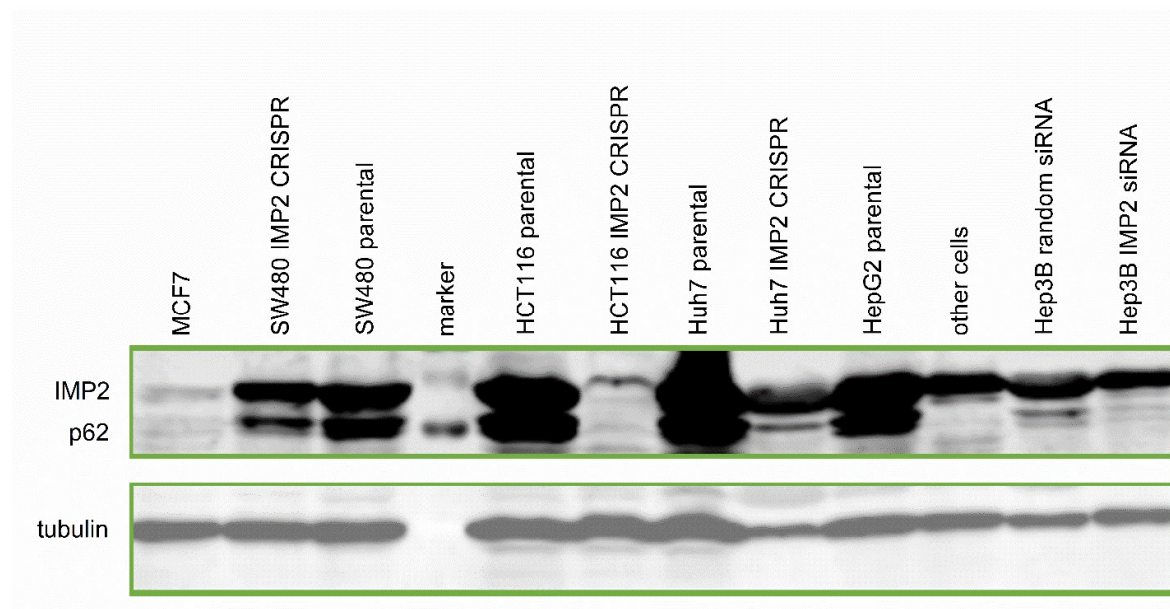


Figure 35 : IMP2/p62 expression in different cancer cell lines. IMP2/p62 expression were assessed before biological experiments in parental MCF7, SW480, HCT116, Huh7, HepG2, and Hep3B cells and compared to their respective IMP2 knockout/knockdown cells. MCF7 cells served as control cells in the biological assessment of hit compounds. IMP2 knockout was performed by CRISPR/Cas9 in HCT116, SW480, HepG2 and Huh7 cells. IMP2 knockdown was done with siRNA transfection in Hep3B cells. The immunodetection of tubulin served as a loading control. N = 3 (1-2 replicates).

Results

2.4.1.2 Effect of hit compounds on cancer cell viability

Dose-response studies were performed for hit compounds. The cell viability was measured *via* MTT 96 h after treatment with hit compounds. The lowest biological activity was observed in MCF7 representing higher affinity of hit compounds on target. SW480 cells were the most sensitive among IMP2 expressing cells. Compound # 3 from class A, and compound # 5 from class B have the weakest potency (Figure 36A, B).

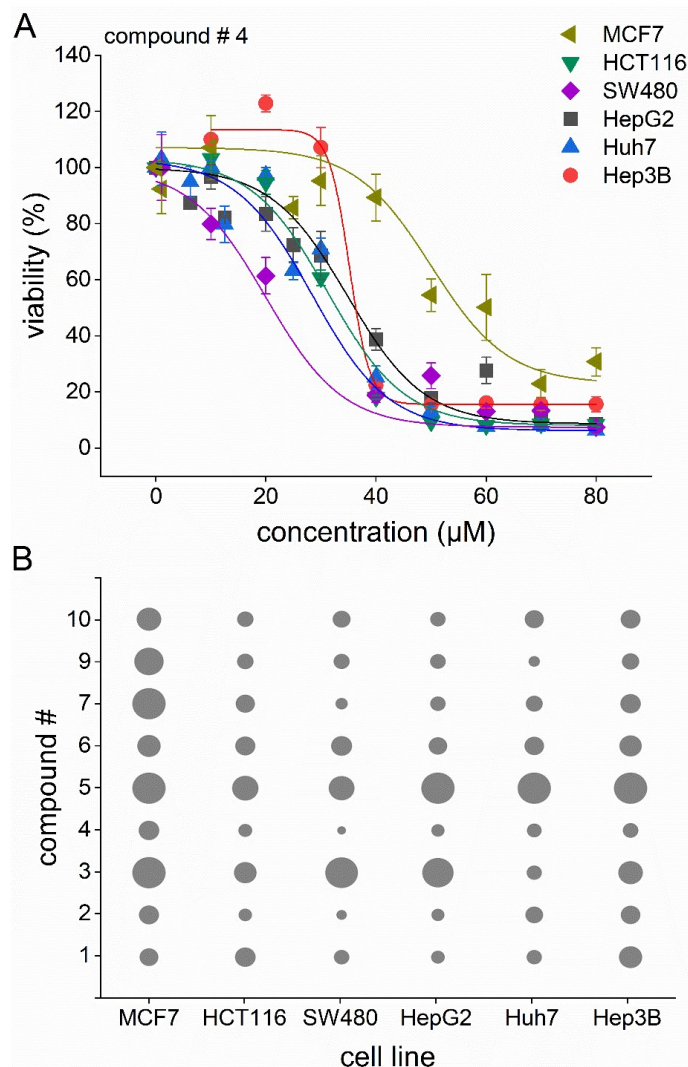


Figure 36 : Biological activity of final screening hits. The biological activity of hit compounds was assessed using MTT assay in cancer cell lines expressing high IMP2 levels (HCT116, SW480, HepG2, Huh7, Hep3B) or low IMP2 levels (MCF7). (A) represents a dose-response studies of a representative hit compound. Cell viability was measured 96 h after treatment with hit compounds (1-80 μM) or DMSO solvent control. (B) IC₅₀ values were calculated using non-linear regression analysis. Dots represent

Results

IC₅₀ values of hit compounds (largest circle $\geq 80 \mu\text{M}$, smallest circle $18.2 \mu\text{M}$). The dot plot was generated with Python 3.8.1 software. $n = 5$ except in HCT116 and Hep3B; $n = 2$ (triplicates).

2.4.1.3 Assessment of hit compound on-target activity *via* MTT

HCT116, and SW480 cells were selected based on target validation and IC₅₀ values to test the potency of hit compounds on parental cells compared to IMP2 reduced cells. Cellular proliferation was measured with MTT 96 h after treatment of hit compounds at different concentrations.

Hit compounds showed more potent effect on all cells expressing higher levels of IMP2 confirming target specificity (Figure 37A-B).

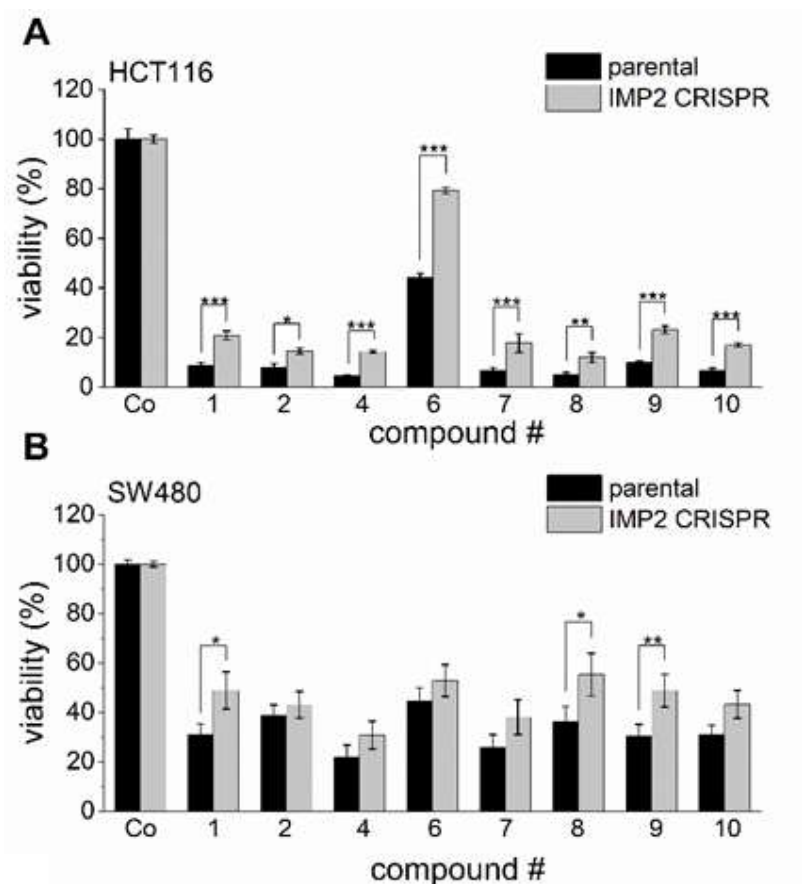


Figure 37 : Target specificity of hit compounds. The cell viability was measured with MTT in parental and IMP2 knockout cells to assess hit compounds affinity on target. IMP2 knockout cells were treated with either hit compounds or the respective DMSO solvent control (Co). (A) and (B) Hit compounds were employed at $80 \mu\text{M}$ for HCT116 and HepG2 cells, (C) Hit compounds were employed at $40 \mu\text{M}$ for

Results

SW480 cells. Cell viability was normalized to the respective control cells. Data are represented as means \pm SEM, n = 2 in HCT116 and HepG2 and n = 5 in SW480 (triplicates).

Furthermore, the target specificity of hit compounds was assessed in dose dependent manner (5, 10, 20, 40, 80 μ M) 96 h after treatment with hit compounds. Also, 72 h time point was investigated at concentrations of 40 μ M and 20 μ M (Data not shown).

2.4.1.4 Assessment of hit compound on-target activity *via* ECIS

The measured viability *via* MTT after hit compounds treatment represents mixed cytotoxic and anti-proliferative effects. ECIS estimated the proliferation of HCT116 cells after hit compounds treatment *via* readout parameter of cell spread and migration. Non-toxic concentrations (25 μ M) were used to treat HCT116 parental and IMP2 knockout cells. All hit compounds showed more potent inhibitory effect on parental cells compared to IMP2 knocked out cells (Figure 38A, B; Supplementary data: Figure 4).

Results

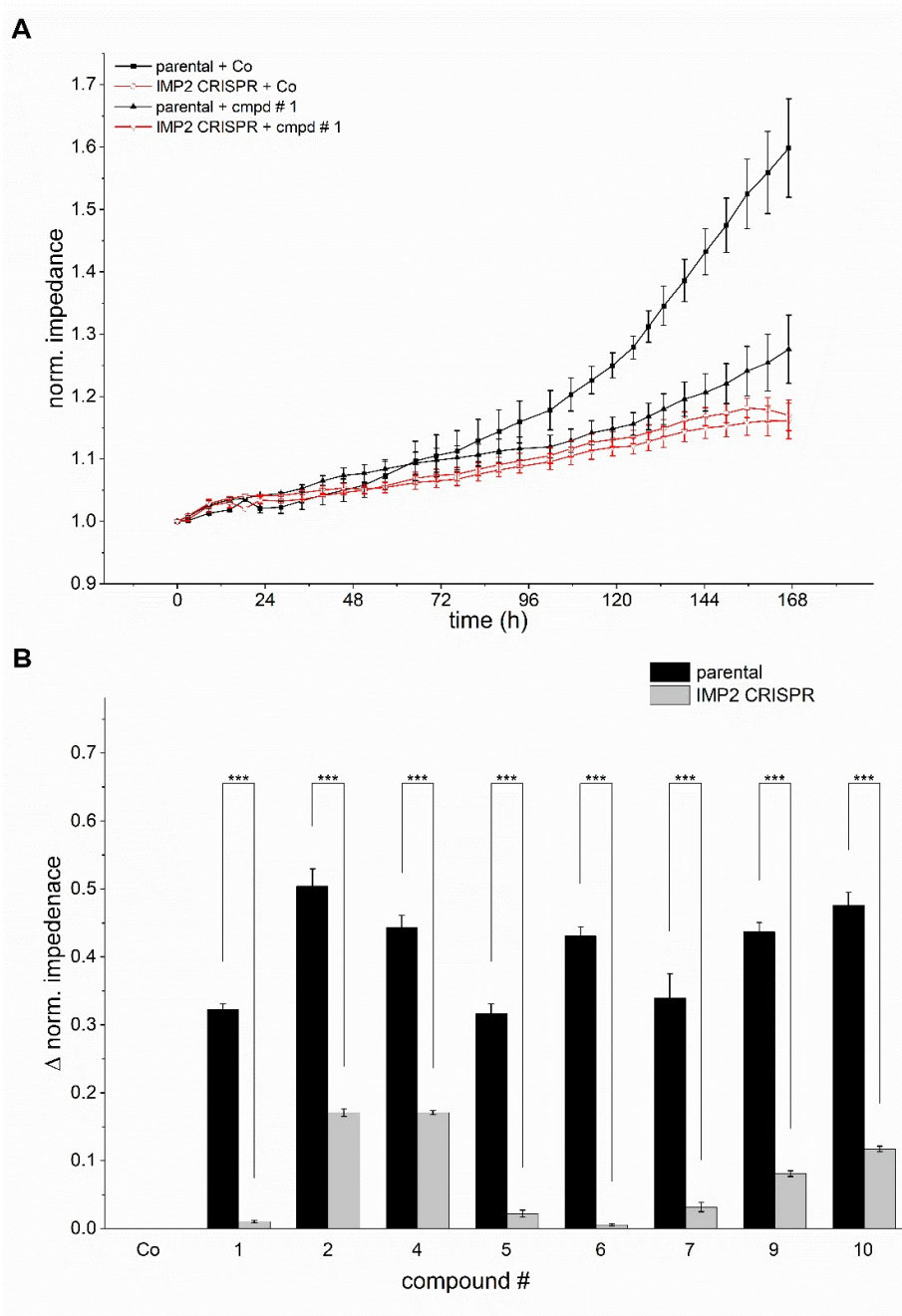


Figure 38 : Impact of hit compounds on cell proliferation in the absence of IMP2. Cell impedance of HCT116 was assessed by ECIS as a readout parameter for cell density and adhesion. (A) Both parental and IMP2 CRISPR/Cas9 knockout cells were seeded in equal numbers and treated with 25 μ M compound 1 or DMSO solvent control (Co), respectively. (B) Bars indicate impedance differences between compound and control treatment for parental and IMP2 knockout cells, calculated for the timepoint 163-168 h. Data are represented as means \pm SEM; n = 2 (triplicates).

2.4.2 Cytotoxicity of hit compounds on human cells

2.4.2.1 Effect of hit compounds on HUVEC cells

HUVEC cells, a normal human cell line, are a commonly used cells to evaluate compounds safety profile. Since HUVEC cells are embryonic cells, they are expressing IMP2 (see The Human Protein Atlas). IMP2 is important for HUVEC cells proliferation, and growth and they might be targeted by hit compounds.

Treatment of HUVEC cells with hit compounds after 72 h showed that class A hit compounds has above 50% viability even at 50 μ M. Class B has more potent effect on HUVEC cells at 25 and 50 μ M compared to class A (Figure 39).

Our findings showed that the proliferation of HUVEC cells was reduced after treatment with hit compounds. The same findings were reported by Charlotte Dahlem after treatment HUVEC cells with compounds # 1 and # 9.

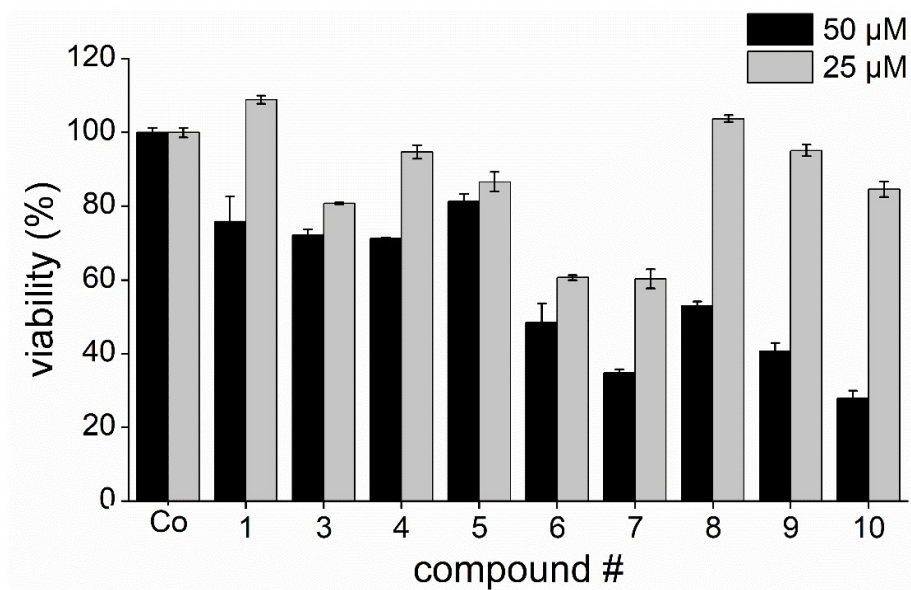


Figure 39 : Effect of hit compounds on HUVEC cells. The cytotoxicity assessment of hit compounds was performed using normal human cells (HUVEC). Cell viability was measured with MTT 72 h treatment after hit compounds. Cell viability was normalized to their respective control. Data represent mean \pm SEM; n = 1 (triplicates).

2.4.2.2 Cytotoxicity of hit compounds on differentiated Huh7 cells

Since HUVEC cells are expressing IMP2, it might not be the best model for safety profile assessment. Another approach has adapted for cytotoxicity assessment of hit compounds using differentiated Huh7. The replacement of the fetal calf serum (FCS) in culture medium of Huh7/7.5 cells with their native adult human serum (HS), differentiate cells toward the normal behavior and alter several cancerous properties (Steenbergen et al., 2018). After differentiation of Huh7.5 cell, the growth is arrested, cells are polarized and have epithelial, cuboid morphology (Steenbergen et al., 2018).

Cell viability was measured *via* MTT 96 h after treatment of differentiated and normal Huh7 with hit compounds. Compounds # 6, 7, 8, 9 and 10 affected the viability of normal Huh7, but not the differentiated cells. Compound # 4 significantly reduced the viability of both differentiated and non-differentiated Huh7 cells compared to the relative controls. Compound # 3 was highly toxic for differentiated Huh7 (Figure 40).

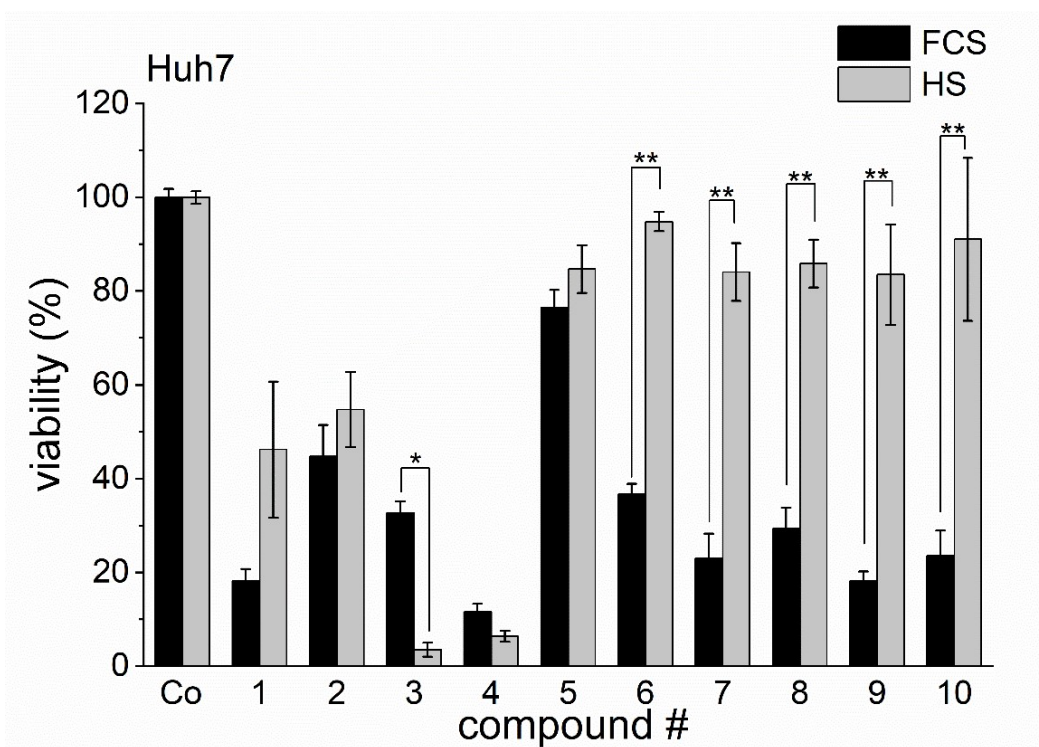


Figure 40 : Effect of hit compounds on differentiated Huh7 cells. Huh7 cells were differentiated in human serum (HS) for 21 days. Huh7 and HS-differentiated Huh7 were treated either with 50 μ M hit compounds or DMSO solvent control. Cell viability was determined by MTT 96 h after treatment with hit compounds. The cell viability was normalized to their respective control. Data are represented as means \pm SEM; n = 2 (triplicates).

2.4.2.3 Influence of Huh7/7.5 cells differentiation on IMP expressions

2.4.2.3.1 Impact of HS differentiation on *IMP* RNA levels

To investigate whether the expression of IMPs was involved in Huh7 cells differentiation, IMPs expression was investigated on RNA and protein levels. Huh7.5 cells were harvested at different time points (24h, W1, W2, W3) by Charlotte Dahlem. Then, *IMPs* expression was investigated by RT-qPCR. A total of two housekeeping genes were used as control genes. The results of geNORM tool showed the expression of *18S* is more stable compared to β -*actin* housekeeping gene. The expression of *IMPs* was downregulated over the (21 day) incubation time (Figure 41A-C). However, the expression of both housekeeping genes was altered after huh7.5 differentiation. As a result, we cannot draw a conclusion based on qPCR data, since the cellular content of both cells are variable. This might indicate that the noticed down regulation in *IMPs* was caused by upregulation in the *18S* housekeeping gene.

Results

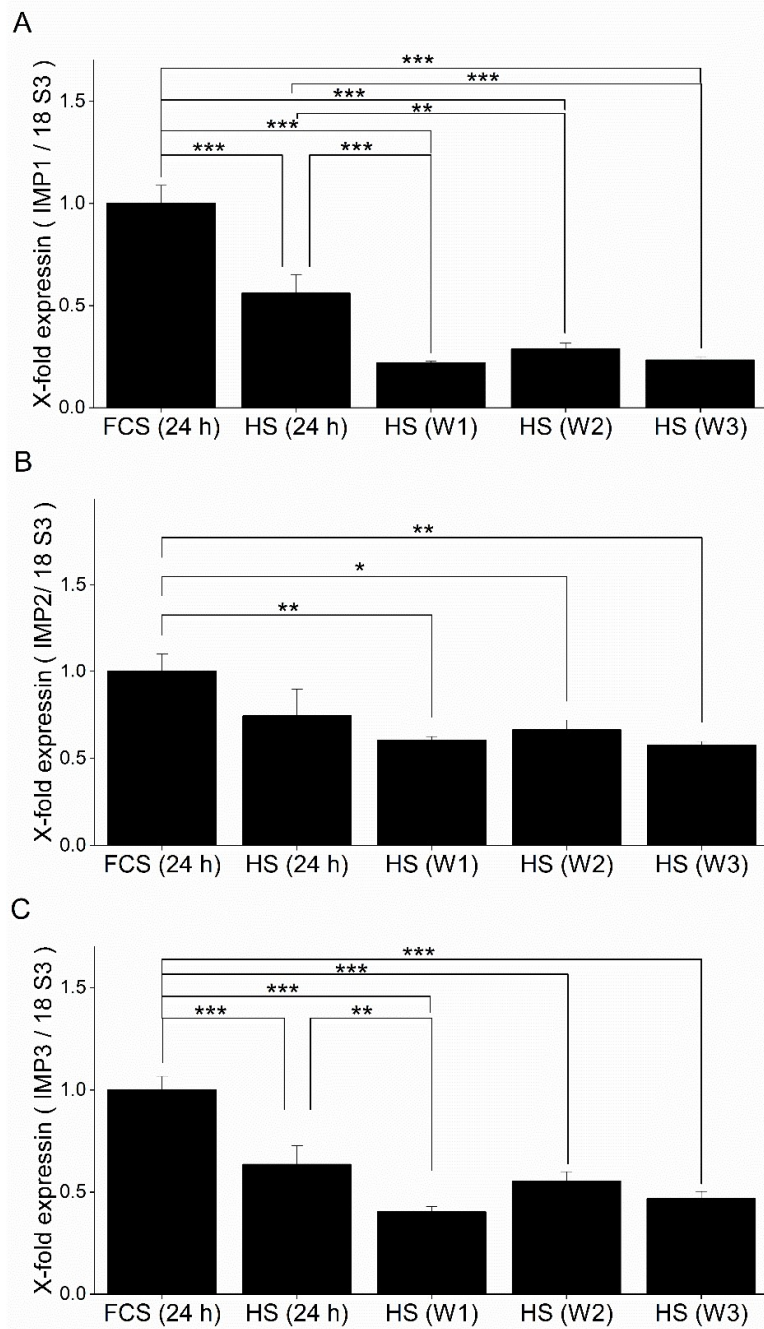


Figure 41: Influence of Huh7.5 differentiation on *IMPs* expression. The expression of *IMPs* was investigated over the period of HS treatment using RT-qPCR. *IMPs* expression in the differentiated Huh7.5 cells were normalized to *18S* housekeeping gene. The expression of *IMPs* after HS treatment (24 h, W1, W2, W3) were normalized to the control FCS treated Huh7.5 cells. *P* value was calculated either with ANOVA or Mann-Whitney. Data represent mean \pm SEM; n = 2 (triplicates).

2.4.2.3.2 Impact of HS differentiation on IMP protein levels

Furthermore, the influence of HS differentiated Huh7 cells on IMPs expression was assessed on the protein levels. Samples were collected from Huh7 cells at different time points during HS treatment (W1, W2, W3), Huh7 cells treated with FCS for 24 h was used as a control cell. Western blot shows IMP1 expression was down regulated but neither IMP2 nor IMP3 were affected during Huh7 differentiation over 3 weeks (Figure 42A, B).

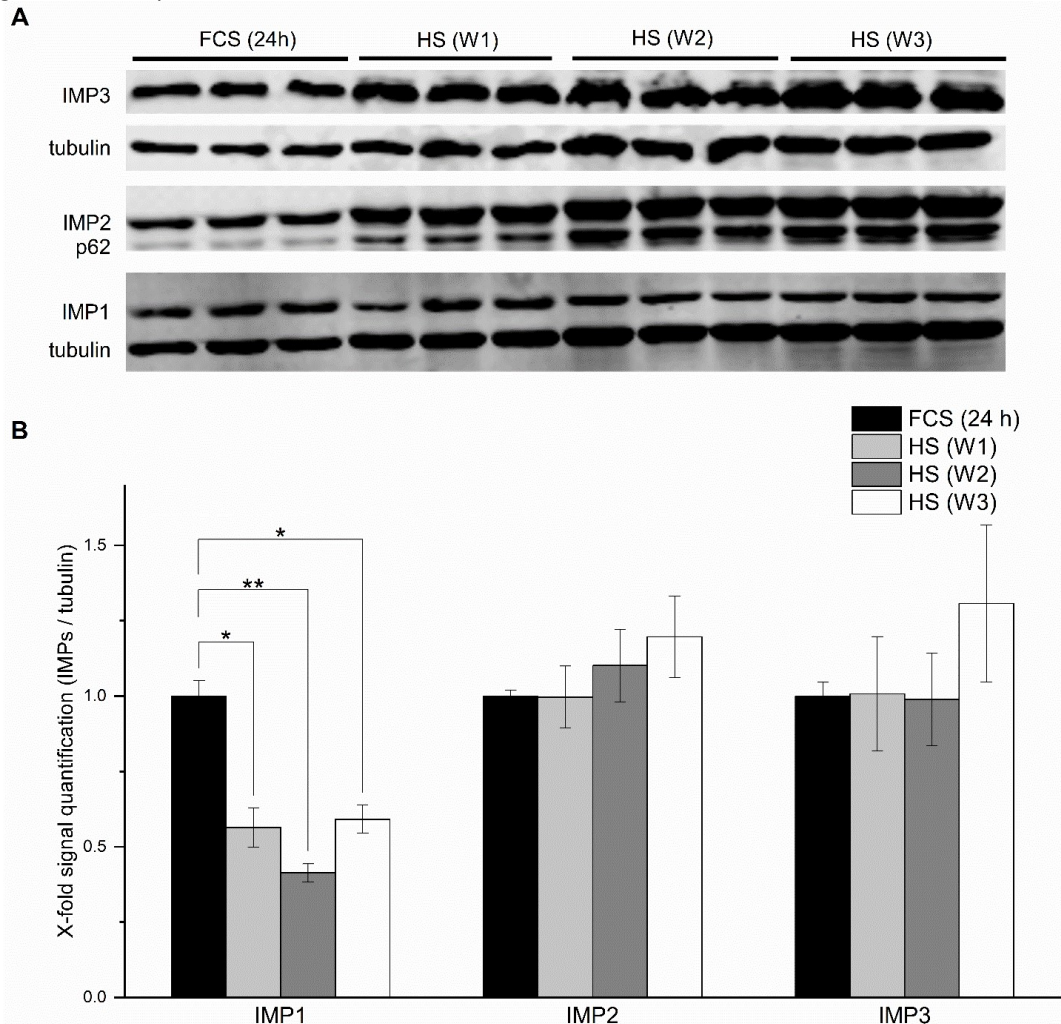


Figure 42 : Influence of Huh7 differentiation on IMPs expression. Long term treatment (21 day) of Huh7 with HS differentiate Huh7 toward the normal hepatocytes. Representative Western blot shows IMPs expression in Huh7 cells during HS treatment. The signal quantification of IMPs expression was normalized to the tubulin signal. The expression of IMPs after HS treatment (W1, W2, W3) was normalized to the control FCS treated Huh7 cells. *P* value was calculated either with ANOVA or Mann-Whitney. Data represent mean \pm SEM. N = 2 (triplicates).

2.4.3 *In vivo* biological activity of hit compounds

A xenograft Zebrafish experiment was performed to investigate the potential *in vivo* biological activity for final hit compounds. Based on the collected data from the biophysical assays, biological assessment, on-target activity, and cytotoxicity to differentiated Huh7 cells, three compounds were selected for further *in vivo* assessment. Compound # 4, # 6 and # 9 were used in concentrations of 20 μ M and 50 μ M. Zebrafish experiment was done by Charlotte Dahlem, the quantification of fluorescence signal with ImageJ software showed that compound # 4 and # 6 at 50 μ M reduced tumor progression in HCT116 xenograft (Data not shown).

3 Discussion

Expression of IMPs in adult tissues has been described to be oncogenic in different types of tumors, including hepatocellular carcinoma (HCC), colon, and lung cancer (Dimitriadis et al., 2007; Kessler et al., 2016). IMP2 is highly expressed in different cancers compared to IMP1 and IMP3 (Dai et al., 2017; Kessler et al., 2017). Also, it has been reported that elevated IMP2 expression is associated with poor survival rate while that of IMP1 and IMP3, is not (Davidson et al., 2014; Kessler et al., 2017). IMP2 and its variant p62 are involved in a higher extent compared to IMP1 and IMP3 with elevated RAC1 expression and generation of reactive oxygen species (Kessler et al., 2017). Depletion of IMP1 reduced the migration of cancer cells, but did not affect cellular proliferation (Hsieh et al., 2013), data not available regarding to IMP3 knockout model.

IMP2 knockout mediated by CRISPR/Cas9 approach reduced the proliferation rate in different cancer lines (Dai et al., 2017; Degrauwe et al., 2016). The overexpression of IMP2 enhanced the proliferation of cancer cells in a dose dependent pattern to IGF2 (Dai et al., 2017). P62 knockdown by RNAi decreased tumor growth and autophagy activation in the *in vitro* and xenograft model experiments (Ren et al., 2014). Our findings were in the same direction, the proliferation rate was reduced significantly after IMP2 knockdown/knockout.

IMPs structure and function similarities might predict inter IMP family regulation (Conway et al., 2016; Nielsen et al., 1999). The reported mRNA binding sequences of IMP2 have been noticed frequently in IMP1 and IMP3 mRNAs. However, Dai and his colleges revealed that IMP2 knockout in mouse embryo fibroblasts did not alter both IMP1 and IMP3 expressions (Dai et al., 2017). Our findings predicted potential inter IMP regulation in cell type dependent pattern, even though the available literature regarding to inter IMP regulation is not sufficient to draw a consistent conclusion.

Targeting RNA binding proteins is a promising approach in the treatment of different diseases (Ascher et al., 2014; Hong, 2017). NS5A is an RNA binding protein which is expressed in the HCV infected cells, and it is crucial for genome replication (Bell et al., 2016). Daclatasvir and Elbasvir are FDA approved medications targeting NS5A, and

could successfully limit the growth of HCV and improved the therapy outcome (Bell et al., 2016). This information together with the knowledge on IMP2 oncofetal nature are important aspects interpreting why IMP2 represents a promising therapeutic target in cancer therapy.

FP assay is a method that permit rapid, reliable and quantitative detection of protein ligand interactions and compound screening for the purpose of small molecule drug discovery (Burke et al., 2003; Lea and Simeonov, 2011). FP assay has been utilized in direct screening for enormous range of targets as DNA, RNA, protein (Bridges and Jennison, 1984).

For IMP1 small molecule inhibitors were suggested using FP assay to inhibit IMP1 RNA (AGAACAA) interaction (Mahapatra et al., 2017; Mahapatra et al., 2014). IMP1 lead compound did not show any inhibitory effect on IMP2 interactions with either RNA_A or RNA_B. Hafner and colleges showed that RNA (ACACAA) is specific binding sequence for IMP2 (Hafner et al., 2010). FP assay results revealed some potential inhibitors for HuR/ELAVL1(RBP) interaction with adenine- and uridine-rich elements (ARE) in 3'UTR of target mRNAs, (Wu et al., 2015). Another RBP, MSI-1, has been shown *via* FP assay to be targeted by (-)-gossypol (Lan et al., 2015). LIN28, an RBP, interaction with Let-7 was inhibited with potential inhibitor discovered with protein/RNA-FRET approach (Roos et al., 2016).

Our identified hit compounds with FP assay were initially synthesized as antibacterial agents and both compounds classes reported in Hinsberger et al. (2013) and Sahner et al. (2013), they were designed as inhibitors of bacterial RNA polymerase enzyme (RNAP). The amino acid sequences and the architecture of bacterial RNAP differs fundamentally from the eukaryotic RNAP. No amino acid sequence similarities were found between either RNAP or IMP2. Furthermore, the Benzamidobenzoic acid derivatives (class A) are potent inhibitors for bacterial cell to cell communication system (Hinsberger et al., 2014). Pseudomonas quinolone signal communication system (PqsD) is a substrate for class A hit compounds.

FP assay is a robust method that has low hit rate (0.1%) and minimal chance of false positive hits (Hall et al., 2016). However, false positive results reported in FP assay due aggregation and formation of missile like particles (Seidler et al., 2003; Shoichet,

2006). As a result, further confirmation assays for the primary screening results generated by FP assay was recommended using different detection concepts (Bibette, 2012; Sink et al., 2010). IMP2-hit compound interactions were confirmed by TSA, MST, STD-MNR, and molecular docking.

In TSA, the increase in protein thermal stability is proportional to the affinity and concentration of ligand (Bai et al., 2019; Cimperman et al., 2008). However, several studies reported that the bound ligands might destabilize proteins (Bernetti et al., 2017; Cimperman et al., 2008). Some ligands destabilize the protein complex by enhancing protein refolding and this might reduce the fluorescence signal (Bai et al., 2019). Another explanation, ligand might bind selectively to the unfolded state of the protein, destabilize and reduce protein melting temperature (Cimperman et al., 2008). Our TSA results showed that class A and B hit compounds destabilize IMP2 and reduce its melting temperature. In concordance to our findings, similar hits for LANA protein were reported to destabilize LANA complex and lead to reduction of melting temperature. (Kirsch et al., 2019).

The IC₅₀ value of compound # 9 measured by MST is relatively lower than what is reported in FP assays. MST assay performed in semi natural environment, and the protein itself is labeled instead of RNA as in FP assay (Seidel et al., 2013). This might be interpreted by the competitive interaction mode in FP assay but not in MST (Lea and Simeonov, 2011). Furthermore, recently Biswas and colleges revealed that the RNA (CGGA) interacts with IMP2 KH4 binding domain (Biswas et al., 2019). The reported RNA sequence was not included in either RNA_A or RNA_B.

Several studies reported uses of STD-NMR in detection and confirmation of small molecules interaction with RNA / DNA binding proteins (Della Volpe et al., 2019; Kirsch et al., 2019). Furthermore, STD-NMR could provide a crucial insight into the ligand protein interactions and reveal the ligand active pharmacophores (Harris et al., 2013; Mayer and James, 2004; Vasile et al., 2018). Our STD-NMR findings showed that most of ligand epitopes are involved in the interaction with IMP2. This suggest the surface interaction that might require to inhibit IMP2 interactions with macromolecules as RNA. Our findings were in concordance with Kirsch and colleges findings for similar hits (Kirsch et al., 2019). Furthermore, STD-NMR produced a conclusive interaction pattern of optimized hits for LANA, and provided a robust approach for further structure

optimization and improvement (Kirsch et al., 2019). Our STD-NMR findings revealed inconsistent mode-of-interaction of hit compounds. This might result from different binding affinities of hit compounds to IMP2 RRM and KH binding domains. Furthermore, further STD-NMR experiments for other compounds optimized for IMP2 might lead to provide a consistent mode-of-interaction.

Virtual screening techniques have been used for identification of small molecule and lead optimization (Gohlke and Klebe, 2002). Usually, virtual screening is a preliminary screening approach, before starting with the traditional experimental screening assays (Bailey and Brown, 2001; Moitessier et al., 2008). In the opposite direction, our molecular docking approach was set up to validate hit compounds binding and predict their interaction pose in the light of STD-NMR findings. In the same direction, STD-NMR and docking studies revealed the interaction mode of HuR/ELAVL1 with small molecule inhibitors (Della Volpe et al., 2019; Vasile et al., 2018). Our findings revealed that all hit compounds *in silico* can inhibit different RNAs interaction (ACAC/CAC, CCCC, CGGA) with IMP2 (RRM1 and KH34 domains) in different affinities based on RNA and binding domain (data are not shown).

The process of classical drug discovery relies on interactive cycles gathering medicinal chemistry and biological evaluation (Sliwoski et al., 2013). The challenge in cancer therapy is to develop therapeutic agents targeting specifically the oncogenic factors responsible for the initiation and progression of cancers (Bhullar et al., 2018; Hoelder et al., 2012).

Validation of target specificity for a hit compound can be investigated based on lead potency on target expressing cells compared to target non-expressing cells (Hughes et al., 2011). The anti-proliferative activity of small molecule inhibitors targeting IMP1 c-myc interaction was investigated using IMP1 expressing cells (IGROV-1) compared to IMP1 non-expressing cells (PC-3) (Mahapatra et al., 2017; Mahapatra et al., 2014). The natural product (-)-gossypol has been reported to inhibit MSI-1 and showed anti-proliferative effect on colon cancerous cells compared to normal colon cells (Lan et al., 2015). Our findings showed most of final hit compounds were biologically active against different cancer cell lines. Furthermore, hit compounds showed the lowest potency on MCF7 cells compared to IMP2 expressing cells.

Assessment of compounds specificity *via* target gene knockout model is a robust approach compared to different cells comparison (Smith, 2003; Wyatt et al., 2011). The current study findings showed on-target biological activity of hit compounds compared to IMP2 knockout/knockdown cells.

Differentiated Huh7/7.5 cells might serve as suitable model for the cytotoxicity assessment of IMP2 inhibitors (Steenbergen et al., 2018). Class A compounds has affected the viability of differentiated and non-differentiated Huh7 cells. In addition to RNAP enzyme, class A hit compounds have broader spectrum as antibacterial compared to class B, since they interact with bacterial PqsR enzyme (Hinsberger et al., 2014; Hinsberger et al., 2013; Sahner et al., 2013). The multi-target activity of class A compounds might explain the reported higher toxicity in comparison to class B compounds.

During Huh7/7.5 differentiation, 32% of genes were upregulated or downregulated indicating process of cell reprogramming. The expression of genes encode CYP450 enzymes is upregulated, cells resorted their secretory process (Petersen et al., 2017; Steenbergen et al., 2018). The noticed nontoxic effect in class B compounds might be associated with the elevated cell metabolism after upregulation of CYP450 enzymes (Petersen et al., 2017; Steenbergen et al., 2018).

Recently, the use of the *in vivo* zebrafish model in drug discovery and drug toxicity assessment became a prominent model since zebrafish embryos are transparent and develop rapidly (Chakraborty et al., 2009). Our hit compounds showed *in vivo* inhibition of tumor growth in xenograft zebrafish model.

Our findings regarding the generated hit compounds serve as a promising starting point for further optimization *via* structure activity relationship studies aiming to generate more potent and target-specific compounds. Furthermore, screening of additional libraries through the established biophysical methods and molecular docking in order to identify structure-divergent compound series. Screening for small molecules *via* IMP2 mediated CRISPR/cas9 HCT116 might serve as a robust biological screening approach.

Chapter II: Methodology

4 Chemicals and reagents

Kanamycin sulfate, cOmplete® protease inhibitor cocktail tablets, diethylpyrocarbonate (DEPC), isopropyl-β-D-thiogalactoside (IPTG), Pluronic®, lysozyme, bovine serum albumin (BSA), and salts were purchased from Sigma Aldrich (Darmstadt, Germany). Water was treated with 0.1% (v/v) DEPC in all experiments handling with RNA. Secondary antibodies utilized in immunodetection IRDye® 680RD goat anti-rabbit (#926-68071), and IRDye® 800 CW goat anti-mouse (#926-32210) were purchased from LI-COR Biosciences (Bad Homburg, Germany). The InstantBlue® Ultrafast Protein Stain solution was purchased from Sigma-Aldrich (# ISB1L, Darmstadt, Germany). The High Capacity cDNA Reverse Transcription Kit (#4368813), and RNase inhibitor RNaseOUT® (#10777019), were purchased from Thermo Fisher Scientific (Darmstadt, Germany).

5 Methods

5.1 Cell culture

SW480, HCT116, and MCF7 cells were maintained in DMEM, HepG2, Hep3B, Huh7, and Plc/Prf/5 cells in RPMI 1640 medium. Media were supplemented with 10% fetal bovine serum (FBS), 1 mM glutamine, 100 U/mL penicillin, and 100 µg/mL streptomycin. Cells were cultured at 37°C and 5% CO₂.

5.2 IMP2 siRNA knockdown

A mixture of 4 different HPLC-purified double-stranded RNA oligonucleotides were used for IMP2 knockdown. Random siRNA was used as a control, the RNA oligonucleotides were purchased from Qiagen (Hilden, Germany). RNA oligo sequences are shown in Table 4.

Table 4: siRNA oligonucleotide used in IMP2 knockdown.

siRNA oligonucleotide	Catalog no	Sequence (5' - 3')
oligo 1	SIO4367020	CCCGGGTAGATATCCATAGAA
oligo 2	SIO4138820	CAGCGAAAGGATGGTCATCAT
oligo 3	SIO3232481	TCCGCTAGCCAAGAACCTATA
oligo 4	SIO3176593	CAGGGCGTTAAATTCACAGAT
random	4390771	AACACGTCTATACGC

IMP2 knockdown in Hep3B cells was performed in 96-well plates. Forward transfection was done for SW480 (5,000 cells / well) and Hep3B cells (12,750 cells / well), and reverse transfection was used for Plc/Prf/5 cells (7,500 cells/ well). The siRNA concentration per well was 0.25 nM for SW480 and 1 nM for Hep3B and Plc/Prf/5 using INTERFERin® Polyplus-Transfection (Illkirch, France) transfection reagent to 0.75 µl / well as recommended by the manufacturer. Cell viability was measured *via* MTT assay 72 h after transfection.

5.3 IMP2 CRISPR mediated knockout

CRISPR/Cas9 experiments were done by Tarek Kröhler. The CRISPR/Cas9 technique was adapted to disrupt the gene of human IMP2 in mammalian colon (SW480, HCT116) and liver cancer cell lines (HepG2, Huh7). The cells were transfected with a validated single guide (sg) RNA (TrueGuide® synthetic guide RNA, Thermo Fisher Scientific, Munich, Germany) targeting IMP2 (5'-GATGGACTTTTGGCTCAATA-3') and a recombinant Cas9 protein (TrueCut®Cas9 Protein v2, #A36496, Thermo Fisher Scientific, Munich, Germany) using Lipofectamine® CRISPRMAX® Cas9 transfection reagent (#CMAX00001, Thermo Fisher Scientific, Munich, Germany) according to the manufacturer's instructions. 80,000 cells were seeded in RPMI or DMEM media as described above, without antibiotics into a 12 well plate, incubated overnight, and transfected the next morning at a confluency of 30-70%. After 48 hours incubation time, the cells were detached, counted, and seeded into 96 well plates at a concentration of 0.8 cells/well for limiting dilution cloning. The residual cells were used for gDNA extraction and further verification of editing efficiency *via* T7E1 mismatch assay. Surviving clones were cultured in 24 well plates and harvested for downstream experiments until knockout of *IMP2* or at least reduced expression (monoallelic editing of the target region as assessed by Sanger sequencing) could be confirmed by

Western blot. Clones that showed reduced IMP2 expression in Western blots underwent the whole procedure again until knockout was achieved. At least two rounds of CRISPR/Cas9 editing did not induce a biallelic knockout in SW480 and Huh7 cells. Tarek kröhler participated in writing this part.

5.4 Western blot

Preparation of protein lysate was done in SB lysis buffer (50 mM Tris-HCl, 10% glycerol, 1% SDS, 5% β -mercaptoethanol, 0.004% bromophenol blue), in presence of a cOmplete[®] Mini protease inhibitor cocktail (#04693124001, Roche, Mannheim, Germany). Samples were stored overnight at -80°C to increase the efficacy of cell lysis, samples were aliquoted and stored at -20°C.

5.4.1 SDS-polyacrylamide gel electrophoresis

SDS-polyacrylamide gel electrophoresis (SDS-PAGE) was done using polyacrylamide gels (4% collection gel and 12% separation gel) and the Mini PROTEAN system (Bio-Rad, Munich, Germany). Samples were thawed on ice and denatured at 95°C for 5 min and gently centrifuged before loading into polyacrylamide gel. A pre-stained 10 to 180 kDa protein marker (#26616, Thermo Fisher Scientific, Mannheim, Germany) was run in parallel to the tested samples in each run to estimate protein masses. Equal amount of tested proteins and an appropriate protein ladder volume were loaded onto the polyacrylamide gel and separated in electrophoresis (running) buffer (25 mM Tris, 192 mM glycine, 0.1% SDS in final volume of 1 l distilled water) by electrophoresis at 80 V for 20 min, then at 120 V for 2.5 h using the Mini-PROTEAN[®] system (Bio-Rad, Richmond, CA, USA).

5.4.2 Blotting

The separated samples were transferred onto an Immobilon[®]-FL polyvinylidene fluoride (PVDF) membrane (#IPFL00010, Merck, Darmstadt, Germany) using a Mini TransBlot[®] cell (Bio-Rad, Munich, Germany). The stuff used in gel sandwich preparation were equilibrated in blotting (transfer) buffer (25 mM Tris, 192 mM glycine,

20% methanol, 0.05% SDS in final volume of 1 l distilled water). The PVDF membrane were activated prior to blotting for 30 seconds in methanol. Blotting was performed in cold transfer buffer at 80 mA overnight. The membrane was blocked in Rockland blocking buffer (RBB) (#MB-070, Rockland Immunochemicals, Limerick, PA, USA) for 1 h to render the antibodies unspecific binding.

5.4.3 Near infrared immunodetection

Different antibodies were used in the immunodetection, they were diluted in RBB according to Table 5.

Table 5: Antibody dilutions used for immunodetection.

Antibody	Dilution	Cat. Number	Supplier
anti-human IMP1, mouse IgG	1:200 in RBB	sc-166344	Santa Cruz, Heidelberg, Germany
anti-human IMP2/p62, rabbit IgG	1:1,000 in RBB	Lu et al. (2001)	in house
anti-human IMP3, rabbit IgG	1:1,000 in RBB	12750-1-AP	Proteintech, St. Leon-Rot, Germany
IRDye® 680RD goat anti rabbit IgG	1:10,000 in RBB	926-68071	Bioscience, Bad Homburg, Germany
IRDye® 800CW goat anti mouse IgG	1:10,000 in RBB	926-32210	Bioscience, Bad Homburg, Germany

The membranes were incubated with anti-human IMP2 or IMP3 antibodies for 3 h at RT, and with anti-human IMP1 antibody overnight at 4°C. After incubation, the membranes were washed 4 times with PBST (0.1% Tween-20 (v/v) in 1 x PBS (10 mM Na₂HPO₄, 1.8 mM KH₂PO₄, 137 mM NaCl, 2.7 mM KCl, pH 7.4)) (each time for 5 min on shaker), followed by incubation with anti- α -tubulin antibody for 1 - 1.5 h at RT. Afterward, the membranes were washed (4 x, 5 min) with PBST, followed by incubation with mixture of IRDye®680 and IRDye®800 conjugated secondary antibodies for 1-2 h at RT. The membranes were washed prior to detection with PBST (3 x, 5 min), and PBS (2 x, 5 min). Signal intensities were determined by using the Odyssey near-infrared imaging system from LI-COR Bioscience (Bad Homburg, Germany). Western

blot signal intensities were quantified by Studio lite software (LI-COR Bioscience, Bad Homburg, Germany).

5.5 Cytotoxicity and anti-proliferative measurement

The 3-(4,5-dimethylthiazol-2-yl)-2,5-diphenyltetrazolium bromide (MTT) assay was used to measure the cell viability after IMP2 knockdown/knockout or treatment with hit compounds. Cells were seeded at different densities in 96 well plates based on the cells type and incubation time. Control cells were either non-treated or treated cells with the respective vehicle concentration according to the experiment set up. At the time of measurement, the medium was aspirated, and cells were incubated with prewarmed MTT solution (0.5 mg/ml in suitable medium) for 0.15 - 1 h at 37°C. Then, MTT solution was aspirated and cells were lysed by 100 µl of DMSO (100%). The absorbance was measured at wavelength of 550 nm and reference wavelength at 690 nm in a microplate reader (XFluor4 Sunrise[®], TECAN, Promega, Madison, WI, USA).

5.6 Gene expression analysis

The human RNA from cultured cells was extracted with the High Pure RNA Isolation Kit

(#11828665001, Roche, Mannheim, Germany), according to the manufacturer's instructions. Total RNA concentration was measured at 260 nm and purity was controlled by 260/280 ratio with the Thermo Scientific[®] NanoDrop Lite Spectrophotometer (Wilmington, DE, USA).

Reverse transcription of RNA and cDNA synthesis was performed with 300 ng total RNA per sample using the High Capacity cDNA Reverse Transcription Kit (#4368813, Thermo Fisher Scientific, Darmstadt, Germany), and RNase inhibitor RNaseOUT[®] (#10777019, Thermo Fisher Scientific, Darmstadt, Germany), according to the manufacturer's instructions. Gene expression was analyzed using 5xHotFirePol EvaGreen qPCR Mix (#08-25-00020, Solis BioDyne, Tartu, Estonia) on a CFX96

Methodology

touch® Real-Time PCR detection system running the CFX Manager 2.1 software (Bio-Rad Laboratories, Munich, Germany).

RT-qPCR efficiency was checked for each run to be in an accepted range of 90 - 105%. In general, Ct values were normalized to the housekeeping gene *β-actin* (*ACTB*) or *18S*. Primers for *IMP1*, *IMP2*, and *IMP3* genes, as well as the reference genes (*ACTB* or *18S*) were purchased from Eurofins Genomics (Ebersberg, Germany). The used conditions in set up of qPCR reaction are summarized in Table 6.

Table 6 : Conditions used in set up of qPCR reaction.

Gene	Forward primer sequence 5'-3'	Reverse primer sequence 5'-3'	µl primer [10 µM] / reaction	Annealing T (°C)
<i>IMP1</i>	AGATAGACGTGCATAGGAAG	GTGTCCTTAGCCTCTTTATG	0.5	62
<i>IMP2</i>	CATATACAACCCGGAAAGAAC	CTCTGGATAAGAGTGATGATG	0.4	62
<i>IMP3</i>	GGAGGAGATCATGAAGAAAATC	TTTCTGATTGCTCAAACCTGC	0.4	62
<i>ACTB</i>	GACGACATGGAGAAAATCTG	ATGATCTGGGTCATCTTCTC	0.4	60
<i>18S</i>	AGGTCTGTGATGCCCTTAGA	GAATGGGGTTCAACGGGTTA	0.5	61

A total volume of 20 µl per PCR reaction was used, all samples were performed in biological duplicates and technical triplicates within the PCR runs using the following program:

denaturation	95°C	15 min	} 35 cycles
denaturation	95°C	0.15 min	
annealing	°C*	0.20 min	
elongation	72°C	0.20 min	
final elongation	72°C	10 min	
Melting curve			
	65°C	} 0.5°C / 5s	
	95°C		

* Annealing temperatures for each gene was adjusted based on Table 6.

5.7 Bacterial culture

Different *E. coli* strains were used either for plasmid amplification or protein expression. The *E. coli* DH5 α strain (Invitrogen, Carlsbad, CA, USA) was utilized as a host organism for plasmid amplification. The BI-21 and Rosetta[®] (DE3) *E. coli* strains (Invitrogen, Carlsbad, CA, USA) were utilized as host organisms for recombinant proteins expression. Bacteria were cultured and grown in lysogeny broth (LB) medium (10% NaCl, 10% tryptone, 5% yeast extract in dd water, pH 7.4), in presence or absence of kanamycin as a selection marker (50 μ g/ml, Sigma-Aldrich). Agar plates (LB_{kan}) were prepared by addition of 7.5 g agar-agar to 500 ml of the LB medium in presence of kanamycin.

5.7.1 Generation to competent cells

Calcium chloride (chemical) method was used in generation of competent *E. coli*. A total volume of 5 ml from overnight culture was used to inoculate 100 ml LB medium without kanamycin. The bacterial culture was grown at 37°C with shaking until the OD₆₀₀ reaches 0.4, then culture was placed on ice for 30 minutes. The cooled culture was centrifuged at 2,000 x g and resuspended in 10 ml cold CaCl₂ solution and incubated on ice for another 30 minutes. Cells were collected by centrifugation at 2,000 x g and resuspended in 2.5 ml cold CaCl₂, aliquoted in 100 μ l volume, and stored at -80°C.

5.7.2 Plasmid transformation

The plasmid transformation onto bacteria was done by heat shock method. A total of 2 ng vector was added to 100 μ l competent cells. The mixture was incubated on ice for 20 min, then heated at 42°C for 2 min and incubated again on ice for 2 min. A total of 900 μ l of prewarmed LB medium was added and the mixture was grown at 37°C with shaking for 1-2 h. A total of 100 μ l culture was spread in kanamycin agar plates and incubated overnight at 37°C.

5.7.3 Plasmid isolation

Plasmid extraction was done from overnight culture using either High Pure Plasmid Isolation Kit (#11754777001, Roche, Mannheim, Germany), or NucleoSpin Plasmid (NoLid), Mini kit (#740499.50, Macherey-Nagel, Düren, Germany), according to the manufacturer's instructions. Plasmid DNA concentration was measured at 260 nm and purity was controlled by 260/280 ratio of with the Thermo Scientific® NanoDrop Lite Spectrophotometer (Wilmington, DE, USA).

5.8 Protein purification

5.8.1 IMP2 expression

Histidine-tagged full-length IMP2 was expressed using a pET-28a vector in BL-21 *E. coli* at 18° C; expression was induced with 0.4 mM IPTG. Cells were harvested by centrifugation at $6,733 \times g$ and resuspended in binding buffer (20 mM Tris-HCl, pH 7.4, 2 mM MgCl₂, 150 mM NaCl, 10 % glycerol (v/v), 2 mM mercaptoethanol, 40 mM imidazole). EDTA-free protease inhibitor cocktail (cOmplete®, #11836170001, Sigma-Aldrich, Darmstadt, Germany) was added freshly to the binding buffer. Cells were lysed using a French press homogenizer (two passages) and cell debris were removed by centrifugation at $42,858 \times g$ at 4°C for 1 h.

5.8.2 Immobilized metal affinity chromatography

The supernatant was applied to a 5 ml HisTrap HP Nickel-Sepharose column (#17524701, GE Healthcare Life Sciences, Frankfurt, Germany) at 0.75 ml/min on an ÄKTExpress system (GE Healthcare). The column was equilibrated with binding buffer in 10 x column volume or until the UV signal was stable. The column was then washed with 15 x column volume with binding buffer and with 15 x column volumes of high salt at 3 ml/min. (Tris-HCl, pH 7.4, 2 mM MgCl₂, 1 M NaCl, 2.5% glycerol (v/v), 2 mM mercaptoethanol, 40 mM imidazole). Subsequently, the column was washed with 15 x column volumes of binding buffer containing 100 mM imidazole.

Then a gradient washing was done with a linear gradient to 100% of 500 mM imidazole buffer (Tris–HCl, pH 7.4, 2 mM MgCl₂, 150 mM NaCl, 2.5% glycerol (v/v), 2 mM mercaptoethanol, 500 mM imidazole) in 10 x column volumes at 3 ml/min.

The protein was eluted in 0.7–1 M imidazole buffer (Tris–HCl, pH 7.4, 2 mM MgCl₂, 150 mM NaCl, 2.5% glycerol (v/v), 2 mM mercaptoethanol, 700-1,000 mM imidazole), protein purity and identity were assessed by SDS-PAGE, Western blot, and circular dichroism spectrometry (CDS). The eluted IMP2 fractions were concentrated *via* centrifugal filtration using Vivaspin columns (30,000 MWCO, # VS0121, Sartorius, Gottingen, Germany). Buffer exchange into storage buffer (Tris–HCl, pH 7.4, 2 mM MgCl₂, 150 mM NaCl, 2 mM DTT, 10% glycerol (v/v), in DEPC treated H₂O) was performed using multi-step dilution inside Vivaspin columns. Protein concentrations were measured by both UV spectroscopy ($\epsilon=280$ nm) and Pierce assay (according to the manufacturer's instructions). Protein aliquots were stored at -80°C.

5.8.3 Recombinant IMP2 visualization

The collected protein fractions during IMP2 isolation were subjected into SDS-PAGE as mentioned in 2.3.1. A loading buffer (4 x Roti[®]-Load 1, #K929.1, Carl-Roth, Karlsruhe, Germany) was added to the recombinant protein samples before denaturation. The separated protein samples were incubated ON in InstantBlue[®] Ultrafast Protein Stain solution (# ISB1L, Sigma-Aldrich, Darmstadt, Germany). Gels were scanned using the Odyssey near-infrared imaging system from LI-COR Bioscience (Bad Homburg, Germany).

5.8.4 RNA electrophoresis

The absence of potential RNase contamination in the protein preparations was assessed by mixing 15 μ l of human RNA (470 ng/ μ l) isolated from MCF7 cells with either 15 μ l storage buffer or 15 μ l IMP2 protein (22.1 μ M) and incubated on ice or at RT for 1.5 h. RNA electrophoresis was performed in presence of 2.2M formaldehyde to achieve full RNA denaturation as described in Maniatis et al., (1982). A total of 1% agarose gel was prepared by melting 0.5 g agarose in 37 ml distilled water, cooled to approximately 55°C and mixed with 8.75 ml 40% formaldehyde and 5 ml 10 x

autoclaved MOPS (0.2M MOPS pH 7.0, 50 mM sodium acetate, 5mM EDTA). A total of 5 µl 10 mg/ml ethidium bromide was added for RNA visualization. RNA samples were mixed with 4 x denaturation buffer (10 ml 100% deionized formamide, 3.5 ml 40% formaldehyde, 1.5 ml 10 x MOPS buffer) before subjection into the agarose gel. RNA samples were separated at 100 V. A 1 kbp ladder (#11823963, Thermo Fisher Scientific, Darmstadt, Germany) was run parallel to the RNA samples for size determination. RNA visualization was performed using a UV transilluminator (Biostep Dark Hood DH-40/50) and the software ArgusX1 (Biostep, Jahnsdorf, Germany).

5.8.5 Liquid chromatography – tandem mass spectrometry

The liquid chromatography– tandem mass spectrometry was done by Dr. David Aurabach (Department of Microbial Natural Products, Helmholtz Institute for Pharmaceutical Research Saarland (HIPS), Saarland University, 66123 Saarbrücken, Germany).

5.9 Fluorescence polarization-based screening assay

5.9.1 Probe design

Fluorescein (FLC) labeled or non-labeled HPLC-purified single-stranded RNA oligomers were purchased from Sigma-Aldrich (Darmstadt, Germany). Based on published IMP2 target sequences, two different RNA oligonucleotides were designed as IMP2 binding partners. The sequence of RNA_A was based on the published motifs CAUC, ACACA, and CCCC (Conway et al., 2016; Hafner et al., 2010; Jia et al., 2018) and contained a 3' nucleotide extension after the FLC label: FLC-AUGCAUCCCCGCAGCUACACACACAACA. RNA_B was designed based on the binding motif UUCACGUUCAC described by (Nielsen et al., 1999) and contained the motif as a tandem repeat with a 7-nucleotide extension before FLC: CCCCCUUCACGUUCACUCUGUCU-FLC. A third RNA_C sequence (FLC-GAAAAAAGAUUUUUUAUUUAAGA) was reported to bind to AU rich elements (ARE) binding proteins and was used to detect the specificity of the fluorescent probe binding to the target (Wu et al., 2015).

5.9.2 Compound libraries

A total number of 1,428 compounds from four different libraries was screened ; (838 compounds were from a synthetic in house library from the Helmholtz Institute for Pharmaceutical Research Saarland (HIPS), 253 compounds from in the house natural products library from HIPS, 192 compounds from ASINEX (Winston-Salem, NC, USA; <https://www.asinex.com/>), and 145 compounds from the Maybridge library (small molecular weight chemical fragments, Thermo Fischer Scientific®: https://www.maybridge.com/portal/alias_Rainbow/lang_en/tabID_177/DesktopDefault.aspx). Compounds were dissolved in DMSO to a concentration of 5 or 10 mM stocks depending on their solubility.

5.9.3 FP assay optimization and validation

FP and fluorescence intensity (FI) were measured using a CLARIOstar® Plus microplate reader (BMG LABTECH, Ortenberg, Germany) with an excitation at 485-495 nm and an emission at 520-530 nm. In general, focal height and gain adjustments were done before starting each measurement to reach the maximum sensitivity (Rossi and Taylor, 2011). The FI values of any compound deviating more than $\pm 20\%$ from values of the controls were excluded from further procedure (Nakayama et al., 2006). Each sample was tested in duplicate, and FP values are reported in milli polarization units (mP). Lyophilized RNA oligomers were dissolved in FP assay buffer (Tris-HCl, pH 7.4, 2 mM MgCl₂, 150 mM NaCl, 10% glycerol, 2 mM DTT, 10% glycerol (v/v), in DEPC treated H₂O), to have 100 μ M stock solutions of RNAs, further diluted into 100 nM aliquots, and stored at -80°C. Saturation experiments were performed to detect direct binding of different RNA oligomers to either IMP2 or BSA. Thereby, a constant concentration (1 nM final) of each FLC-labeled RNA with a constant concentration (1 nM) were titrated with serial dilutions in a range of 0.15 nM to 3 μ M final concentration in FP assay buffer. In the competitive FP experiments, IMP2 was used in excess (2-3 folds above the EC₅₀ values). Based on the saturation experiments, a final IMP2 concentration of 200 nM was selected to be used in subsequent competition assays with RNA_A and RNA_B.

All competitive experiments included a 1-hour incubation of IMP2 with nonlabelled RNA oligo or compounds in black 384 well microplates before the addition of the labeled RNAs. Competition experiments were done at constant concentrations of RNA_A and RNA_B (1 nM) and a fixed IMP2 concentration (200 nM) by titration against serial dilutions of unlabeled RNAs (0.32 nM-100 μ M final). DMSO tolerance was evaluated by incubating different DMSO concentrations (0 –10% v/v) and RNA_A or RNA_B at 1 nM, either with or without IMP2. The stability of FP values was assessed over time by measuring the FP at different time points (every 30 min until 4 h). The assay robustness was verified by assaying low controls (LCs) in 192 samples with RNA_A or RNA_B (1 nM final concentration) in 5% DMSO in FP assay buffer and a high control (LC) plate containing the 192 samples in the same plate in addition to IMP2. Z' value was calculated according to the formula $Z' = 1 - [(3SD * HC) + (3SD * LC)] / |(\text{HC mean} - \text{LC mean})|$ (Zhang et al., 1999).

5.9.4 FP-based screening

Compounds were diluted in FP assay buffer to concentrations of 450 μ M. A total of 10 μ l in duplicates (15% DMSO) from each compound was added into 384 well microtiter plates using an electronic Eppendorf Xplorer[®] 12-channel pipette (Eppendorf, Germany). In addition, 10 μ l of 600 nM IMP2 in FP assay buffer was added into the same plate, and the samples were incubated for 1 h shaking at room temperature. Afterward, 10 μ l of a 3 nM RNA_A/B solution in FP assay buffer was added to the mixture and incubated for an additional 1.5 h at room temperature in the dark. Accordingly, the final assay concentrations were 1 nM of RNA_A/B, 200 nM of IMP2, and 150 μ M for compounds, in 5% DMSO. Any compound that enhanced or quenched the total FI more than 20% of the FI of the controls was excluded. The percentage of binding inhibition was calculated as: % inhibition = (mean of HC – read compound value) / (mean of HCs – mean of LC) \times 100%. In addition, Pluronic[®] was added to the FP buffer to a final concentration of 0.01% in the competitive assay to rule out any false-positive results from aggregation.

5.9.5 FP-based dose-response measurement

Different dilutions of a 333 μM starting concentration of hit compounds were prepared in FP buffer in 5% DMSO and titrated in the presence or absence of IMP2. The experiments were performed in two independent experiments using duplicates.

5.9.5.1 Compound solubility test

The solubility limit of hit compounds was tested qualitatively by sight inside a transparent glass vial and quantitatively by measuring the absorbance at 620 nm. The cut limit was determined by the up surging of absorbance value compared to the control.

5.10 Thermal shift assay

The shift of the melting point of IMP2 in the presence or absence of hit compounds was recorded in 96 well plates using an Applied Biosystems® StepOnePlus® Real-Time PCR System from Thermo Fisher Scientific (Darmstadt, Germany). Thermal shift experiments were performed at fixed concentrations of IMP2 (4.5 μM), and 100 μM hit compound. Sypro Orange dye (Sigma Aldrich, Darmstadt, Germany) was used in 2.5-fold concentration (stock 5,000-fold) in a total volume of 20 μl . The heating gradient started at 25°C, and the temperature was increased by 0.5°C/ min to 95°C, detecting the fluorescence of Sypro Orange. Melting curve plots of fluorescence versus temperature were converted into melting peaks and melting temperatures were calculated subsequently by Protein Thermal Shift Software v1.3-Thermo Fisher Scientific (Darmstadt, Germany).

5.11 Microscale thermophoresis technique

His6-IMP2 protein was diluted to 600 nM in MST buffer (20 mM Tris-HCl, pH 7.4, 150mM NaCl, 0.01% Pluronic®, 0.5% Tween-20, 10% glycerol). Monolith His-Tag Labeling Kit purchased from NanoTemper Technologies GmbH® (Munich, Germany), RED-tris-NTA dye was diluted in MST buffer to a final concentration of 100 nM. 100 μl

of IMP2 was mixed with 100 μ l of NTA dye and the mixtures were incubated for 30-60 min at room temperature in the dark. 12-step serial dilutions (500 μ M to 15 nM) of hit compound # 9 were prepared in MST buffer with 5% DMSO, with a final volume of 10 μ l in each 1.5 ml tube of the dilution series. 10 μ l of 600 nM His6-labeled IMP2 protein was added to each sample and mixed by pipetting up and down. Reaction mixtures were incubated for 1 h at room temperature in the dark and then were loaded into Monolith NT.115 capillaries. MST was measured using the Monolith NT.115 Microscale Thermophoresis Instrument from NanoTemper Technologies (Munich, Germany).

5.12 Saturation transfer difference – NMR

^1H -STD-NMR experiments were conducted using a Bruker Fourier spectrometer (500 MHz), (Massachusetts, USA), and the probe temperature was kept at 283 K.

The final compound concentration was 250 or 500 μ M based on the solubility limit in 10% DMSO D6. A volume of 25 μ l from each compound solution was diluted with 25 μ l of Tris buffer pH 7.4, 150 mM NaCl in D2O. IMP2 protein/ligand was used in 1:100 ratio with a final concentration of 2.5 or 5 μ M, respectively. A control spectrum was recorded under the same conditions without a protein to test for artifacts.

The STD-NMR experiments were carried out with a carrier set at -1 ppm for the on-resonance and -40 ppm for the off-resonance irradiation. Selective IMP2 protein pre-saturation was carried out at 0.5 s by using a train of 50 ms Gauss-shaped pulses. The mentioned NMR conditions were established and optimized by Dr. Josef Zapp.

The STD effect resulting from the difference in signal intensity after saturation transfer was quantified using formula $\text{STD}_{\text{effect}} = (I_0 - I_{\text{sat}})/I_0$. This provides insights into the relative proximity of the respective protons to the protein surface. I_0 represents the intensity of one signal in the off-resonance or reference spectrum, and I_{sat} represents the intensity of a signal in the on-resonance spectrum.

The STD-NMR spectrum of the IMP2 : ligand sample was subtracted from the respective STD spectrum of the ligand alone using the same NMR conditions to eliminate any artefacts arising from the ligand. Protons of the residual imidazole contamination from the elution step appear at 7.2 and 8.1 ppm.

5.13 Molecular docking

The homology modelling and molecular docking experiments were performed with MOE 2019.01 (Molecular Operating Environment). A homology model for IMP2 RRM1 was generated using a reported NMR structure of IMP2 (RRM1, pdb ID: 2CQH) (Suzuki et al., 2005) and an X-ray structure of IMP3 in complex with RNAs (ACAC and CCCC) (IMP3 RRM12, pdb ID: 6GX6 and 6FQR) (Jia et al., 2018). Another homology model for IMP2 KH34 was generated using a reported X-ray structure for IMP2 (KH34, pdb: 6ROL) (Biswas et al., 2019) and an X-ray structure for IMP1 in complex with RNAs (CAC/CCC, and CGGA) , (KH34, pdb ID: 2N8L and 2N8M, respectively) (Nicastro et al., 2017).

The sequence of IMP2 RRM1 and KH34 as well as the co-crystallized RNA structures atom coordinates were loaded into MOE and the homology model was generated using the built-in homology model function with standard parameters, AMBER10:EHT force field, and the RNA atoms as environment. Dr. Martin Empting was participated in docking of compound 4 with RNAs (ACAC).

5.14 Biological activity of hit compounds on cell viability and proliferation

Cells were seeded in 96-well plates at a density of 2,500 -10,000 cells/well based on cells type (95-100% confluency at time of measurement). Cell viability was measured 96 h after treatment of hit compounds at the indicated concentrations (80, 70, 60, 50, 40, 30, 25, 20, 15, 12.5, 10, 5, and 1 μ M) using MTT. For each compound, the inhibition of cell proliferation was calculated for each concentration relatively to their respective DMSO control or non-treated control for the viability above 90%. IC₅₀ values were calculated with Origin pro version 19 software. The IC₅₀ values are shown as a dot plot figure generated by Python 3.8.1 software.

5.15 Electric cell-substrate impedance sensing

ECIS represents a powerful tool to assess cell proliferation in real-time, but cell impedance is also responsive towards changes in cell adhesion (Stolwijk and

Wegener, 2019), which has been shown to be affected by IMP2 (Xing et al., 2019). HCT116 parental and IMP2 CRISPR knockout cells were seeded (7,000 cells/well in 150 μ l) into 96 (96W10E+) well plates coated with rat tail collagen (30 μ g/ml in 0.2% acetic acid). The cells were seeded directly after the compounds were added into the plate to reduce cell stress. Cells were treated with 25 μ M of hit compounds in triplicate. Effects of hit compounds on proliferation were normalized to (0.25%) DMSO controls. Cell impedance was assessed in an ECIS[®] Z θ (theta) instrument (Applied BioPhysics Inc., New York, USA). Measurements were started immediately after cell seeding and were taken every 450-900 s for each well.

5.16 Proliferation of primary human umbilical vein endothelial cell

HUVEC cells (50,000 cells in 100 μ l medium per well) were cultured on 96 well plate and were treated with different hit compounds in final concentration of 25 μ M and 50 μ M in 200 μ l total volume. Cell viability was measured with MTT 72 h after incubation with hit compounds.

5.17 Differentiation of Huh7 cells

Huh7 cells were seeded into 96 well plates (3,000 cells/well) in full RPMI growth medium containing 10% FBS. After 24 h medium was aspirated and changed to RPMI medium containing 2% human serum (HS) in order to induce cell differentiation as described (Steenbergen et al., 2018). Fresh medium was added twice a week for 21 days. Differentiated cells were treated with hit compounds, and cell viability was assessed with MTT assay 96 h after treatment.

5.18 *In vivo* xenograft zebrafish embryo model

The *in vivo* assessment of hit compounds 4, 6, and 9 on zebrafish was performed by Charlotte Dahlem as reported in (Dahlem et al., 2020).

5.19 Statistics

Data analysis was done by Microsoft Excel, and statistics were performed using OriginPro 2019 b (OriginLab Corporation, USA). IC₅₀ and EC₅₀ values were calculated using non-linear regression analysis with Origin pro version 2019 software. Values are expressed as mean ± SD/SEM. Shapiro-Wilk test was performed to analyze data distribution. Depending on whether the data were normally distributed and on group size, statistical differences were calculated using a one-way ANOVA, Student`s t-test, Mann-Whitney U test, or Kolmogorov-Smirnov test. * p<0.05; ** p<0.01; *** p<0.001.

Summary and conclusion

IMP2 protein is a promising target in cancer therapy. In this study, we showed that IMP2 knockdown/knockout slow down the proliferation rate of cancer cells. IMP1 and IMP3 expression are suggested to be targeted by IMP2 in cell dependent pattern.

We showed for the first time that IMP2 is druggable, and IMP2 binding to its targets can be inhibited by small molecule compounds. For this purpose, a competitive FP assay was established. In the same context, TSA and MST were established as a secondary confirmation of FP assay findings.

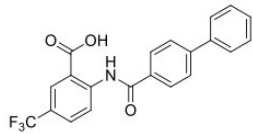
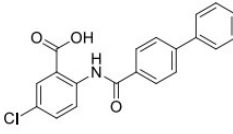
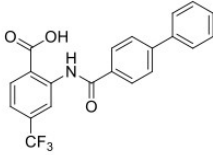
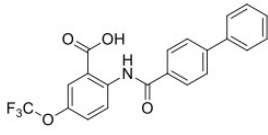
Furthermore, this study provides first insight into the mode-of-action of these inhibitors *via* STD-NMR orthogonal method and molecular modeling.

The biological activity of hit compounds was assessed in different cancer cell lines and most of hit compounds were biologically actives. Further assessments showed hit compounds led to a target-specific reduction of cellular proliferation. Also, the toxicity studies showed class B compounds are nontoxic to normally proliferating cells.

Furthermore, this study provides for the first-time an *in vivo* inhibition of tumor growth in xenograft zebrafish model *via* IMP2 inhibitors.

This study serves as a promising starting point for further structure optimization *via* establishing structure activity relationship studies and pharmacophore modeling in order to identify more potent, and target-specific compounds.

supplementary data

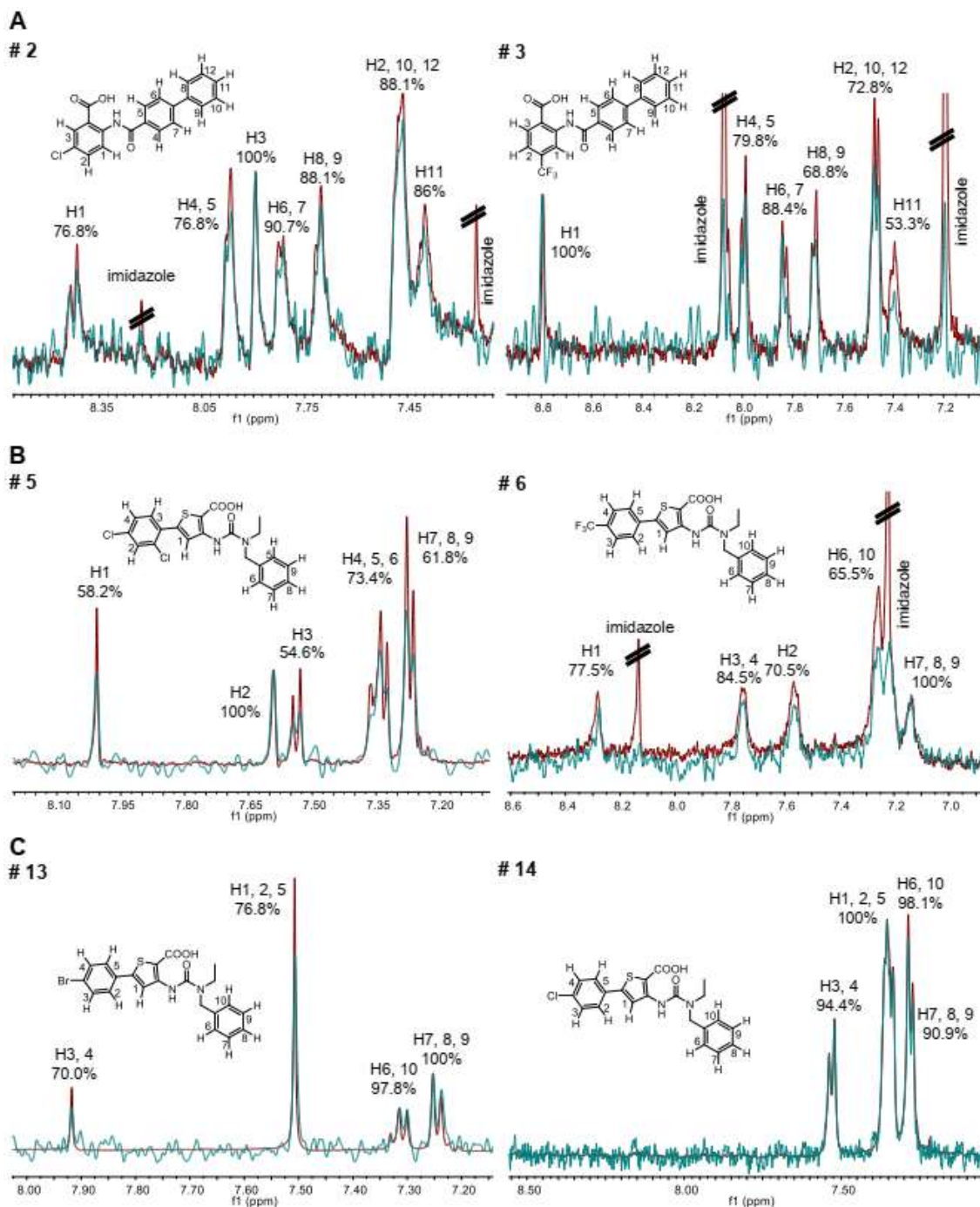
#	HIPS code	MW	Structure	Analytical Data
1	403	385.34		¹ H NMR (500 MHz, DMSO- <i>d</i> ₆) δ ppm 12.41 (s, 1H) 8.93 (d, <i>J</i> = 8.8 Hz, 1H) 8.28 (d, <i>J</i> = 1.9 Hz, 1H) 8.03 - 8.06 (m, 2H) 8.01 (dd, <i>J</i> = 8.8, 1.9 Hz, 1H) 7.87 - 7.92 (m, 2H) 7.73 - 7.78 (m, 2H) 7.47 - 7.54 (m, 2H) 7.40 - 7.46 (m, 1H). ¹³ C NMR (126 MHz, DMSO- <i>d</i> ₆) δ ppm 168.90, 164.66, 144.27, 144.01, 138.75, 132.65, 130.85 (q, <i>J</i> _{CF} = 3.7 Hz) 129.06, 128.35, 127.94 (q, <i>J</i> _{CF} = 3.7 Hz), 127.84, 127.20, 126.95, 123.80 (q, <i>J</i> _{CF} = 271.3 Hz), 122.76 (q, <i>J</i> _{CF} = 33.0 Hz) 120.36, 116.81. LC/MS: <i>m/z</i> = 386, 771; <i>t</i> _R = 14.60 min; 99.76% pure (UV). White solid; mp. 264.8-266.0°C.
2	434	351.78		¹ H NMR (500 MHz, DMSO- <i>d</i> ₆) δ ppm 12.14 (s, 1H) 8.74 (d, <i>J</i> = 9.1 Hz, 1H) 8.02 - 8.05 (m, 2H) 8.00 (d, <i>J</i> = 2.8 Hz, 1H) 7.86 - 7.91 (m, 2H) 7.75 - 7.79 (m, 2H) 7.73 (dd, <i>J</i> = 9.0, 2.7 Hz, 1H) 7.48 - 7.54 (m, 2H) 7.41 - 7.47 (m, 1H). ¹³ C NMR (126 MHz, DMSO- <i>d</i> ₆) δ ppm 168.77, 164.38, 143.80, 139.88, 138.82, 133.87, 132.92, 130.39, 129.08, 128.32, 127.75, 127.18, 126.96, 126.53, 121.81, 118.55. LC/MS: <i>m/z</i> = 352, 354; <i>t</i> _R = 14.32 min; 99.33% pure (UV). White solid; mp. 273.8-278.9°C.
3	468	385.34		¹ H NMR (500 MHz, DMSO- <i>d</i> ₆): δ ppm 12.35 (s, 1H) 9.10 (d, <i>J</i> = 1.6 Hz, 1H) 8.26 (d, <i>J</i> = 8.2 Hz, 1H) 8.04 - 8.08 (m, 2H) 7.89 - 7.95 (m, 2H) 7.75 - 7.81 (m, 2H) 7.57 (dd, <i>J</i> = 8.2, 1.6 Hz, 1H) 7.49 - 7.55 (m, 2H) 7.41 - 7.47 (m, 1H). ¹³ C NMR (126 MHz, DMSO- <i>d</i> ₆) δ ppm 169.00, 164.78, 143.98, 141.41, 138.79, 133.38 (q, <i>J</i> _{CF} = 32.0 Hz), 132.67, 132.45, 129.08, 128.35, 127.80, 127.23, 126.97, 122.88 (q, <i>J</i> _{CF} = 273.1 Hz), 119.15 (q, <i>J</i> _{CF} = 3.7 Hz), 116.25 (q, <i>J</i> _{CF} = 3.7 Hz). LC/MS: <i>m/z</i> = 386, 427, 771; <i>t</i> _R = 14.11 min; 100.00% pure (UV). White solid; mp. 244.9-245.8°C.
4	471	401.34		¹ H NMR (500 MHz, DMSO- <i>d</i> ₆) δ ppm 12.17 (s, 1H) 8.81 (d, <i>J</i> = 9.1 Hz, 1H) 8.03 - 8.06 (m, 2H) 7.92 (dd, <i>J</i> = 3.0, 0.8 Hz, 1H) 7.88 - 7.91 (m, 2H) 7.74 - 7.78 (m, 2H) 7.68 - 7.74 (m, 1H) 7.49 - 7.53 (m, 2H) 7.41 - 7.46 (m, 1H). ¹³ C NMR (126 MHz, DMSO- <i>d</i> ₆): δ ppm 168.61, 164.48, 143.86, 142.66 (q, <i>J</i> _{CF} = 1.8 Hz), 140.12, 138.82, 132.88, 129.08, 128.33, 127.80, 127.20, 127.04, 126.96, 123.31, 121.90, 118.55, 120.04 (q, <i>J</i> _{CF} = 256.0 Hz). LC/MS: <i>m/z</i> = 402, 803; <i>t</i> _R = 14.58 min; 100.00% pure (UV). White solid; mp. 244.6-245.9°C.

Supplementary data: Table 1. Descriptive data of class A. Table 1 shows the molecular weights, chemical structures, and analytical data of class A compounds. Abbreviations: carbonNMR (¹³C NMR); coupling constant (*J*); deuterated dimethyl sulfoxide (DMSO-*d*₆); doublet peak (d); liquid chromatography–mass spectrometry (LC/MS); melting point (mp); multiplet peak (m); parts per million (ppm); proton NMR (¹H NMR); quartet peak (q); retention time (*t*_R); singlet peak (s); triplet peak (t).

Supplementary Data

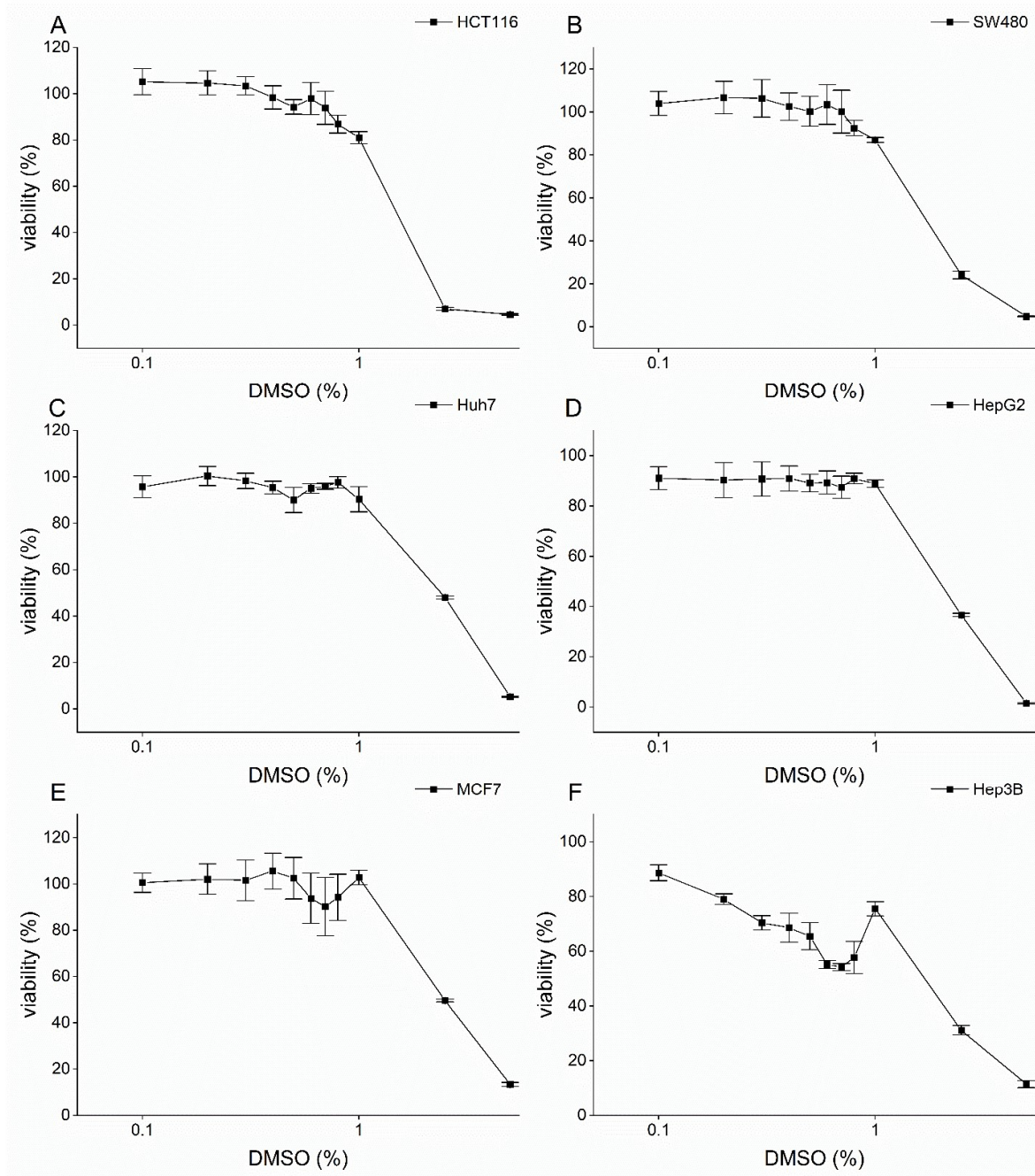
#	HIPS code	MW	Structure	Analytical Data
5	386	449.35		¹ H-NMR (300 MHz, DMSO- <i>d</i> ₆): δ ppm 1.15 (t, <i>J</i> = 7.1, 3H), 3.39 (q, <i>J</i> = 7.1, 2H), 4.58 (s, 2H), 7.23 – 7.37 (m, 5H), 7.53 (dd, <i>J</i> = 8.5, 2.1, 1H), 7.68 (d, <i>J</i> = 8.5, 1H), 7.79 (d, <i>J</i> = 2.1, 1H), 8.27 (s, 1H), 10.04 (s, 1H), 13.51 (br. s., 1H). ¹³ C NMR (75 MHz, DMSO- <i>d</i> ₆) δ ppm 13.1, 41.8, 49.3, 108.8, 122.1, 127.1, 128.1, 128.5, 130.1, 130.5, 132.1, 132.4, 134.3, 138.0, 142.3145.6, 153.0, 165.6. LC/MS: <i>m/z</i> = [M+H ⁺] 448.55, [2M+H ⁺] 898.57 <i>t</i> _R = 15.14 min, 99.3% pure (UV). mp: 212 – 214°C.
6	423	448.46		¹ H-NMR (300 MHz, DMSO- <i>d</i> ₆): δ ppm 1.16 (t, <i>J</i> = 7.1, 3H), 3.40 (q, <i>J</i> = 7.1, 2H), 4.59 (s, 2H), 7.24 – 7.38 (m, 5H), 7.79 (d, <i>J</i> = 8.4, 2H), 7.91 (d, <i>J</i> = 8.1, 2H), 8.41 (s, 1H), 10.05 (s, 1H), 13.47 (br. s., 1H). ¹³ C NMR (75 MHz, DMSO- <i>d</i> ₆) δ ppm 13.1, 41.8, 49.3, 108.2, 124.0 (q, ¹ <i>J</i> _{CF} = 272.0 Hz), 126.2 (q, ³ <i>J</i> _{CF} = 3.7 Hz), 126.4, 127.2, 128.4, 128.5, 129.3 (q, ² <i>J</i> _{CF} = 32.0 Hz) 136.5, 138.1, 145.3, 146.7, 153.0, 165.6. LC/MS: <i>m/z</i> = [M+H ⁺] 448.68, [2M+H ⁺] 896.93 <i>t</i> _R = 14.59 min, 98.02% pure (UV). mp: 193 – 194°C.
7	429	510.96		¹ H-NMR (300 MHz, DMSO- <i>d</i> ₆): δ ppm 0.88 (t, <i>J</i> = 7.5, 3H), 1.25 – 1.37 (m, 2H), 1.52 – 1.63 (m, 2H), 3.32 (t, <i>J</i> = 7.5, 2H), 4.59 (s, 2H), 7.23 – 7.38 (m, 5H), 7.77 – 7.80 (s, 1H), 7.98 – 8.00 (m, 2H), 8.38 (s, 1H), 10.08 (s, 1H), 13.56 (br. s, 1H). LC/MS: <i>m/z</i> = [M+H ⁺] 510.85; <i>t</i> _R = 16.16 min, 100% pure (UV).
8	431	511.42		¹ H-NMR (300 MHz, DMSO- <i>d</i> ₆): δ ppm 4.64 (s, 4H), 7.26 – 7.38 (m, 10H), 7.65 – 7.71 (m, 2H), 7.94 (s, 1H), 8.35 (s, 1H), 10.08 (s, 1H), 12.66 (br. s, 1H). ¹³ C NMR (75 MHz, DMSO- <i>d</i> ₆) δ ppm 49.9, 50.1, 118.8, 128.9, 127.1, 127.3, 127.3, 128.6, 128.6, 128.9, 130.0, 131.4, 131.6, 131.8, 132.1, 133.3, 137.2, 144.2, 146.2, 153.5, 165.4. LC/MS: <i>m/z</i> = [M+H ⁺] 511.35; <i>t</i> _R = 16.36 min, 95.70% pure (UV). mp: 190 – 191°C.
9	432	477.40		¹ H-NMR (300 MHz, DMSO- <i>d</i> ₆): δ ppm 0.88 (t, <i>J</i> = 7.4, 3H), 1.60 (q, <i>J</i> = 7.4, 2H), 2.89 (t, <i>J</i> = 7.4, 2H), 3.25 (t, <i>J</i> = 7.4, 2H), 3.50, <i>J</i> = 7.4, 2H), 7.19 – 7.32 (m, 5H), 7.65 – 7.71 (m, 2H), 7.93 (d, <i>J</i> = (dd, <i>J</i> = 1.1, 1H), 8.33 (s, 1H), 10.03 (s, 1H), 13.56 (br. s, 1H). ¹³ C NMR (75 MHz, DMSO- <i>d</i> ₆) δ ppm 11.0, 21.2, 34.1, 49.0, 49.1, 197.7, 118.7, 125.9, 126.2, 127.3, 128.4, 128.8, 131.4, 131.6, 132.1, 133.3, 138.7, 144.4, 146.7, 152.6, 165.8. LC/MS: <i>m/z</i> = [M+H ⁺] 476.89, [2M+H ⁺] 954.65 <i>t</i> _R = 16.58 min, 98.83% pure (UV). mp: 178 – 179°C.
10	433	524.98		¹ H-NMR (300 MHz, DMSO- <i>d</i> ₆): δ ppm 0.88 (t, <i>J</i> = 7.3, 3H), 1.25 – 1.37 (m, 2H), 1.50 – 1.60 (m, 2H), 2.89 (t, <i>J</i> = 7.8, 2H), 3.29 (t, <i>J</i> = 8.1, 2H), 3.50 (t, <i>J</i> = 8.2, 2H), 7.18 – 7.37 (m, 5H), 7.78 – 7.81 (m, 1H), 7.99 – 8.01 (m, 2H), 8.38 (s, 1H), 10.04 (s, 1H), 13.61 (br. s., 1H). LC/MS: <i>m/z</i> = [M+H ⁺] 524.86 <i>t</i> _R = 16.85 min, 96.95% pure (UV).

Supplementary data: Table 2. Descriptive data of class B. Table 1 shows the molecular weights, chemical structures, and analytical data of class B compounds. Abbreviations: carbonNMR (¹³C NMR); coupling constant (*J*); deuterated dimethyl sulfoxide (DMSO.*d*₆); doublet peak (d); liquid chromatography–mass spectrometry (LC/MS); melting point (mp); multiplet peak (m); parts per million (ppm); proton NMR (¹H NMR); quartet peak (q); retention time (*t*_R); singlet peak (s); triplet peak (t).



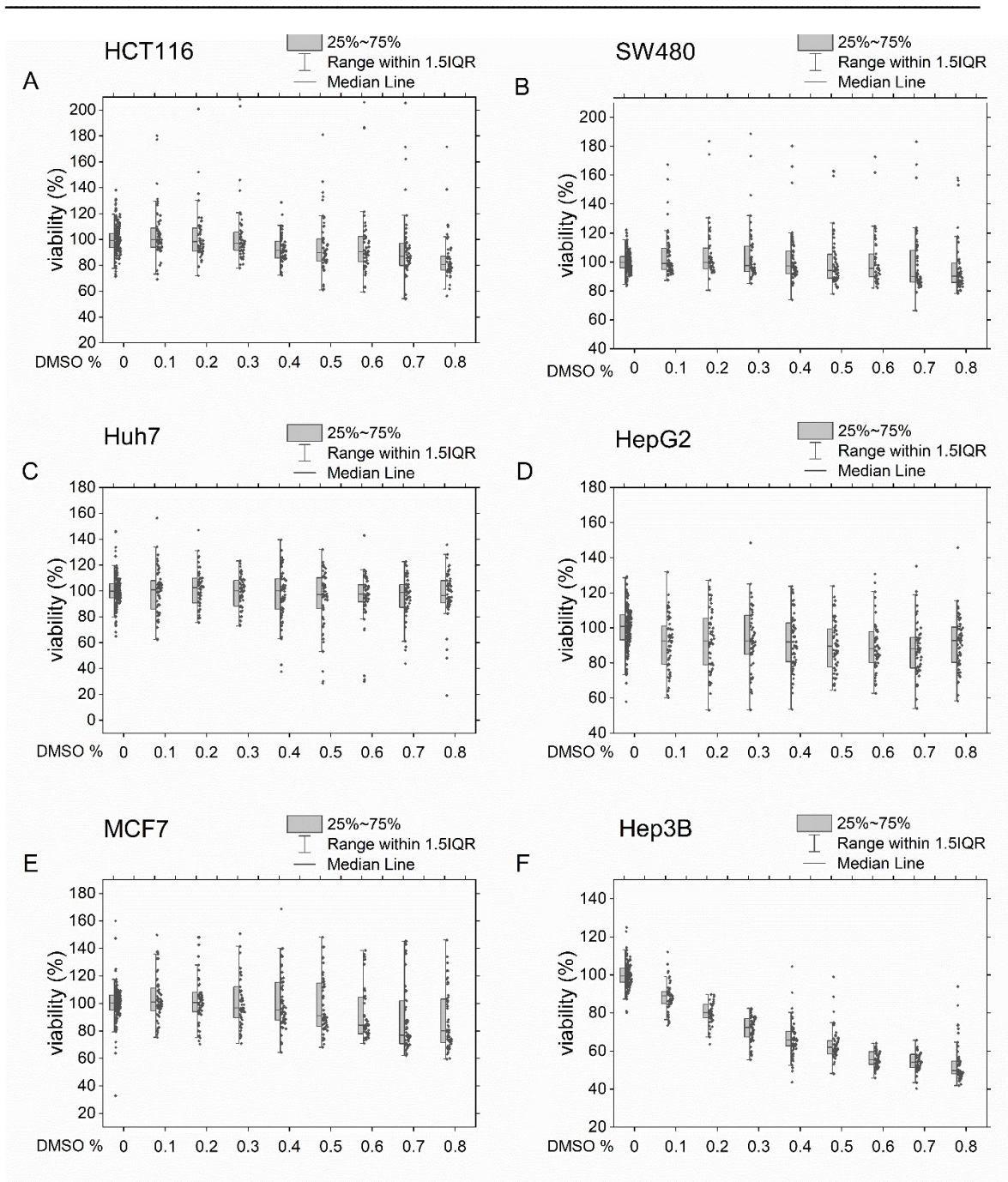
Supplementary data: Figure 1. STD-NMR IMP2 complex analysis. Further confirmation and characterization of IMP2-hit compound interactions was done using STD-NMR. The STD-NMR experiments were performed at fixed concentrations of 2.5-5 μM IMP2 and either 250 μM for compound 2 and 3 or 500 μM for compounds 5-6 and 13-14 based on the solubility limit in 10% DMSO D6 (molar ratio of protein to ligand was 1:100). Compounds 2 and 3 represent class A hit compounds (A), compounds 5 and 6 class B compounds (B), and compounds 13 and 14, selective RNA_A inhibitors (C). The reference spectrum without protein is shown in red, and the STD difference spectrum of the IMP2/compound complexes is shown in green. Overlaid STD off-resonance and STD effect spectra were normalized to the signal of the highest proton signal.

Supplementary Data



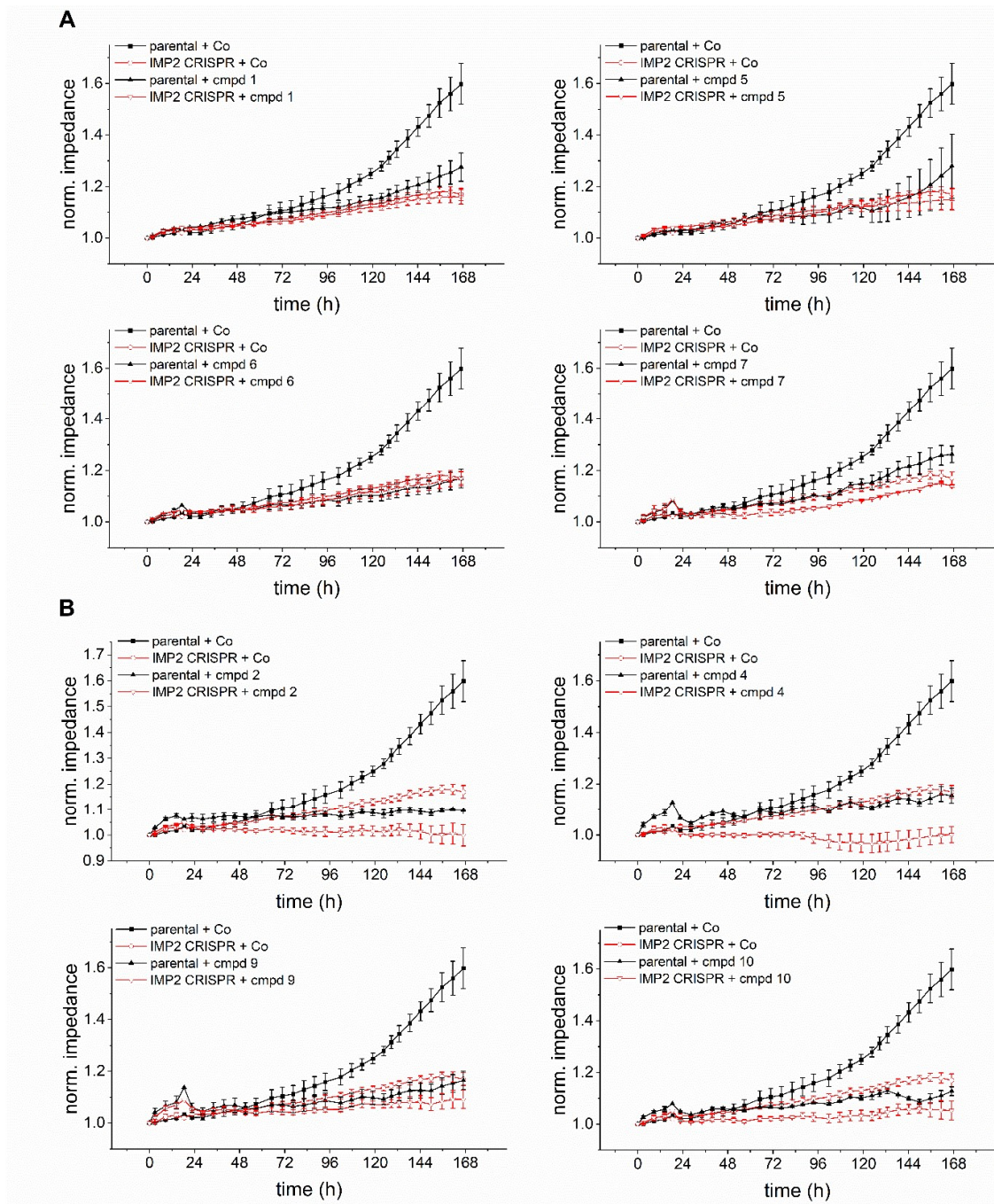
Supplementary data: Figure 2. DMSO concentration vs mean cell viability. Cell tolerance to different DMSO% was assessed in different cell lines used in the evaluation of the biological activity of hit compounds. Cell viability was tested with MTT 96 h after treatment with different DMSO concentrations (0, 0.1, 0.2, 0.3, 0.4, 0.5, 0.6, 0.7, 0.8, 1, 2.5, 5%). Viability was normalized to non-treated controls. Data represent means \pm SEM; n = 5 (at least in triplicates).

Supplementary Data



Supplementary data: Figure 3. DMSO concentration vs median cell viability. Cell tolerance to different DMSO% was assessed in different cell lines used in the evaluation of the biological activity of hit compounds. Cell viability was tested with MTT 96 h after treatment with different DMSO concentrations (0, 0.1, 0.2, 0.3, 0.4, 0.5, 0.6, 0.7, 0.8, 1, 2.5, 5%). Viability was normalized to non-treated controls. N = 5 (at least in triplicates).

Supplementary Data



Supplementary data: Figure 4. Effect of hit compounds on cell proliferation in the absence of the target. Cell impedance was assessed as readout parameter for cell density and adhesion. HCT116 parental and IMP2 CRISPR/Cas9 knockout cells were seeded in equal numbers and treated with 25 μM of the respective compound or DMSO solvent control (Co). Hit compounds demonstrated effective anti-proliferative effects in HCT116 parental cells but (A) no or (B) lower effects in IMP2 CRISPR cells. Data are represented as means \pm SEM; n = 2 (triplicates).

References

Akash, M. S., and Rehman, K. (2015). Recent progress in biomedical applications of pluronic (PF127): pharmaceutical perspectives. *J Control Release* 209, 120-138.

Alajez, N. M., Shi, W., Wong, D., Lenarduzzi, M., Waldron, J., Weinreb, I., and Liu, F. F. (2012). Lin28b promotes head and neck cancer progression *via* modulation of the insulin-like growth factor survival pathway. *Oncotarget* 3, 1641-1652.

Alimbetov, D., Askarova, S., Umbayev, B., Davis, T., and Kipling, D. (2018). Pharmacological targeting of cell cycle, apoptotic and cell adhesion signaling pathways implicated in chemoresistance of cancer cells. *Int J Mol Sci* 19, 1690.

Alkhatib, A., Werner, M., Hug, E., Herzog, S., Eschbach, C., Faraidun, H., Köhler, F., Wossning, T., and Jumaa, H. (2012). FoxO1 induces Ikaros splicing to promote immunoglobulin gene recombination. *J Exp Med* 209, 395-406.

Amarasinghe, A., Macdiarmid, R., Adams, M., and Rio, D. (2001). An *in vitro*-selected RNA-binding site for the KH domain protein PSI acts as a splicing inhibitor element. *RNA* 7, 1239-1253.

Armer, J. M., Cormier, J. N., and Stewart, B. R. (2013). The global economic impact of cancer and related premature death and disability (including those caused by treatment effects) in 2008 are reported to exceed \$895 billion. Introduction. *Semin Oncol Nurs* 29, 1-3.

Ascher, D. B., Wielens, J., Nero, T. L., Doughty, L., Morton, C. J., and Parker, M. W. (2014). Potent hepatitis C inhibitors bind directly to NS5A and reduce its affinity for RNA. *Sci Rep* 4, 4765.

Bai, N., Roder, H., Dickson, A., and Karanicolas, J. (2019). Isothermal analysis of thermofluor data can readily provide quantitative binding affinities. *Sci Rep* 9, 2650-2650.

Bailey, D., and Brown, D. (2001). High-throughput chemistry and structure-based design: survival of the smartest. *Drug Discov Today* 6, 57-59.

Barghash, A., Golob-Schwarzl, N., Helms, V., Haybaeck, J., and Kessler, S. M. (2016). Elevated expression of the IGF2 mRNA binding protein 2 (IGF2BP2/IMP2) is linked to short survival and metastasis in esophageal adenocarcinoma. *Oncotarget* 7, 49743-49750.

Barile, E., and Pellecchia, M. (2014). NMR-based approaches for the identification and optimization of inhibitors of protein-protein interactions. *Chem Rev* 114, 4749-4763.

Becker, W., Bhattiprolu, K. C., Gubensäk, N., and Zangger, K. (2018). Investigating protein-ligand interactions by solution nuclear magnetic resonance spectroscopy. *Chemphyschem* 19, 895-906.

Bell, A. M., Wagner, J. L., Barber, K. E., and Stover, K. R. (2016). Elbasvir/grazoprevir: a review of the latest agent in the fight against hepatitis C. *Int J Hepatol* 2016, 3852126.

References

Bell, J. L., Wachter, K., Muhleck, B., Pazaitis, N., Kohn, M., Lederer, M., and Huttelmaier, S. (2013). Insulin-like growth factor 2 mRNA-binding proteins (IGF2BPs): post-transcriptional drivers of cancer progression? *Cell Mol Life Sci* **70**, 2657-2675.

Berger, N. A. (1986). Cancer chemotherapy: new strategies for success. *J Clin Invest* **78**, 1131-1135.

Bernetti, M., Cavalli, A., and Mollica, L. (2017). Protein-ligand (un)binding kinetics as a new paradigm for drug discovery at the crossroad between experiments and modelling. *MedChemComm* **8**, 534-550.

Bhullar, K. S., Lagarón, N. O., McGowan, E. M., Parmar, I., Jha, A., Hubbard, B. P., and Rupasinghe, H. P. V. (2018). Kinase-targeted cancer therapies: progress, challenges and future directions. *Mol Cancer* **17**, 48-48.

Bibette, J. (2012). Gaining confidence in high-throughput screening. *Proc Natl Acad Sci U S A* **109**, 649-650.

Biswas, J., Patel, V. L., Bhaskar, V., Chao, J. A., Singer, R. H., and Eliscovich, C. (2019). The structural basis for RNA selectivity by the IMP family of RNA-binding proteins. *Nat Commun* **10**, 4440.

Booser, D. J., and Hortobagyi, G. N. (1994). Anthracycline antibiotics in cancer therapy. Focus on drug resistance. *Drugs* **47**, 223-258.

Boudoukha, S., Cuvellier, S., and Poleskaya, A. (2010). Role of the RNA-binding protein IMP-2 in muscle cell motility. *Mol Cell Biol* **30**, 5710-5725.

Bray, F., Ferlay, J., Soerjomataram, I., Siegel, R. L., Torre, L. A., and Jemal, A. (2018). Global cancer statistics 2018: GLOBOCAN estimates of incidence and mortality worldwide for 36 cancers in 185 countries. *CA Cancer J Clin* **68**, 394-424.

Bridges, R. R., and Jennison, T. A. (1984). Spurious phenobarbital levels by fluorescence polarization immunoassay using TDx analyzer in patients with renal disease. *Ther Drug Monit* **6**, 368-370.

Bruce, D., Cardew, E., Freitag-Pohl, S., and Pohl, E. (2019). How to stabilize protein: stability screens for thermal shift assays and nano differential scanning fluorimetry in the virus-X project. *J Vis Exp* **144**.

Burke, T., Loniello, K., Beebe, J. A., and Ervin, K. (2003). Development and application of fluorescence polarization assays in drug discovery. *Comb Chem High Throughput Screen* **6**, 183-194.

Cao, J., Mu, Q., and Huang, H. (2018). The roles of insulin-like growth factor 2 mRNA-binding protein 2 in cancer and cancer stem cells. *Stem Cells Int* **2018**, 15.

Chakraborty, C., Hsu, C. H., Wen, Z. H., Lin, C. S., and Agoramoorthy, G. (2009). Zebrafish: a complete animal model for *in vivo* drug discovery and development. *Curr Drug Metab* **10**, 116-124.

Cheng, Y., and Prusoff, W. H. (1973). Relationship between the inhibition constant (K₁) and the concentration of inhibitor which causes 50 per cent inhibition (I₅₀) of an enzymatic reaction. *Biochem Pharmacol* **22**, 3099-3108.

References

Cheow, L., Viswanathan, R., Chin, C.-S., Jennifer, N., Jones, R., Guccione, E., Quake, S., and Burkholder, W. (2014). Multiplexed analysis of protein-ligand interactions by fluorescence anisotropy in a microfluidic platform. *Anal Chem* **86**.

Christiansen, J., Kolte, A. M., Hansen, T. v. O., and Nielsen, F. C. (2009). IGF2 mRNA-binding protein 2: biological function and putative role in type 2 diabetes. *J Mol Endocrinol* **43**, 187.

Cimpmperman, P., Baranauskiene, L., Jachimovičiūtė, S., Jachno, J., Torresan, J., Michailoviene, V., Matuliene, J., Sereikaite, J., Bumelis, V., and Matulis, D. (2008). A quantitative model of thermal stabilization and destabilization of proteins by ligands. *Biophys J* **95**, 3222-3231.

Ciulli, A. (2013). Biophysical screening for the discovery of small-molecule ligands. *Methods Mol Biol* **1008**, 357-388.

Cleyen, I., Brants, J. R., Peeters, K., Deckers, R., Debiec-Rychter, M., Sciôt, R., Van de Ven, W. J. M., and Petit, M. M. R. (2007). HMGA2 Regulates Transcription of the *Imp2* Gene via an Intronic Regulatory Element in Cooperation with Nuclear Factor- κ B. *Mol Cancer Res* **5**, 363-372.

Conway, A. E., Van Nostrand, E. L., Pratt, G. A., Aigner, S., Wilbert, M. L., Sundararaman, B., Freese, P., Lambert, N. J., Sathe, S., Liang, T. Y., *et al.* (2016). Enhanced CLIP uncovers IMP protein-RNA targets in human pluripotent stem cells important for cell adhesion and survival. *Cell Rep* **15**, 666-679.

Crowther, G. J., Napuli, A. J., Thomas, A. P., Chung, D. J., Kovzun, K. V., Leibly, D. J., Castaneda, L. J., Bhandari, J., Damman, C. J., Hui, R., *et al.* (2009). Buffer optimization of thermal melt assays of Plasmodium proteins for detection of small-molecule ligands. *J Biomol Screen* **14**, 700-707.

Czepukojc, B., Abuhaliema, A., Barghash, A., Tierling, S., Naß, N., Simon, Y., Körbel, C., Cadenas, C., van Hul, N., Sachinidis, A., *et al.* (2019). IGF2 mRNA binding protein 2 transgenic mice are more prone to develop a ductular reaction and to progress toward cirrhosis. *Front Med* **6**.

Dahlem, C., Barghash, A., Puchas, P., Haybaeck, J., and Kessler, S. M. (2019). The insulin-like growth factor 2 mRNA binding protein IMP2/IGF2BP2 is overexpressed and correlates with poor survival in pancreatic cancer. *Int J Mol Sci* **20**.

Dahlem, C., Siow, W. X., Lopatniuk, M., Tse, W. K. F., Kessler, S. M., Kirsch, S. H., Hoppstädter, J., Vollmar, A. M., Müller, R., Luzhetskyy, A., *et al.* (2020). Thiohologamide A, a New Anti-Proliferative Anti-Tumor Agent, Modulates Macrophage Polarization and Metabolism. *Cancers* **12**, 1288.

Dai, N., Christiansen, J., Nielsen, F. C., and Avruch, J. (2013). mTOR complex 2 phosphorylates IMP1 cotranslationally to promote IGF2 production and the proliferation of mouse embryonic fibroblasts. *Genes Dev* **27**, 301-312.

Dai, N., Ji, F., Wright, J., Minichiello, L., Sadreyev, R., and Avruch, J. (2017). IGF2 mRNA binding protein-2 is a tumor promoter that drives cancer proliferation through its client mRNAs IGF2 and HMGA1. *Elife* **6**.

Dai, N., Rapley, J., Angel, M., Yanik, M. F., Blower, M. D., and Avruch, J. (2011). mTOR phosphorylates IMP2 to promote IGF2 mRNA translation by internal ribosomal entry. *Genes Dev* **25**, 1159-1172.

References

Dai, N., Zhao, L., Wrighting, D., Kramer, D., Majithia, A., Wang, Y., Cracan, V., Borges-Rivera, D., Mootha, V. K., Nahrendorf, M., *et al.* (2015). IGF2BP2/IMP2-deficient mice resist obesity through enhanced translation of Ucp1 mRNA and Other mRNAs encoding mitochondrial proteins. *Cell Metab* 21, 609-621.

Davidson, B., Rosenfeld, Y. B., Holth, A., Hellesylt, E., Trope, C. G., Reich, R., and Yisraeli, J. K. (2014). VICKZ2 protein expression in ovarian serous carcinoma effusions is associated with poor survival. *Hum Pathol* 45, 1520-1528.

Degrauwe, N., Suvà, M.-L., Janiszewska, M., Riggi, N., and Stamenkovic, I. (2016). IMPs: an RNA-binding protein family that provides a link between stem cell maintenance in normal development and cancer. *Genes Dev* 30, 2459-2474.

Della Volpe, S., Nasti, R., Queirolo, M., Ünver, M., Jumde, D. V., Dömling, A., Vasile, F., Potenza, D., Ambrosio, F., Costa, G., *et al.* (2019). Towards the modulation of RNA-binding proteins: new compounds targeting protein HuR. *Proceedings* 22, 65.

DeMicco, A., Naradikian, M. S., Sindhava, V. J., Yoon, J.-H., Gorospe, M., Wertheim, G. B., Cancro, M. P., and Bassing, C. H. (2015). B Cell–Intrinsic Expression of the HuR RNA-Binding Protein Is Required for the T Cell–Dependent Immune Response *in vivo*. *J Immunol* 195, 3449-3462.

Dimitriadis, E., Trangas, T., Milatos, S., Foukas, P. G., Gioulbasanis, I., Curtis, N., Nielsen, F. C., Pandis, N., Dafni, U., Bardi, G., and Ioannidis, P. (2007). Expression of oncofetal RNA-binding protein CRD-BP/IMP1 predicts clinical outcome in colon cancer. *Int J Cancer* 121, 486-494.

Ergun, A., Doran, G., Costello, J. C., Paik, H. H., Collins, J. J., Mathis, D., and Benoist, C. (2013). Differential splicing across immune system lineages. *110*, 14324-14329.

Fan, J. L., Wei, X. Z., Wan, L. C., Zhang, L. Y., Zhao, X. Q., Liu, W. Z., Hao, H. Q., and Zhang, H. Y. (2011). Disarrangement of actin filaments and Ca²⁺(+) gradient by CdCl₂ alters cell wall construction in *Arabidopsis thaliana* root hairs by inhibiting vesicular trafficking. *J Plant Physiol* 168, 1157-1167.

Farina, K. L., Huttelmaier, S., Musunuru, K., Darnell, R., and Singer, R. H. (2003). Two ZBP1 KH domains facilitate beta-actin mRNA localization, granule formation, and cytoskeletal attachment. *J Cell Biol* 160, 77-87.

Ghandi, M., Huang, F. W., Jané-Valbuena, J., Kryukov, G. V., Lo, C. C., McDonald, E. R., Barretina, J., Gelfand, E. T., Bielski, C. M., Li, H., *et al.* (2019). Next-generation characterization of the Cancer Cell Line Encyclopedia. *Nature* 569, 503-508.

Glisovic, T., Bachorik, J. L., Yong, J., and Dreyfuss, G. (2008). RNA-binding proteins and post-transcriptional gene regulation. *FEBS Lett* 582, 1977-1986.

Gohlke, H., and Klebe, G. (2002). Approaches to the description and prediction of the binding affinity of small-molecule ligands to macromolecular receptors. *Angew Chem Int Ed Engl* 41, 2644-2676.

References

Hafner, M., Landthaler, M., Burger, L., Khorshid, M., Hausser, J., Berninger, P., Rothballer, A., Ascano, M., Jr., Jungkamp, A. C., Munschauer, M., *et al.* (2010). Transcriptome-wide identification of RNA-binding protein and microRNA target sites by PAR-CLIP. *Cell* **141**, 129-141.

Hagner, N., and Joerger, M. (2010). Cancer chemotherapy: targeting folic acid synthesis. *Cancer Manag Res* **2**, 293-301.

Hall, M. D., Yasgar, A., Peryea, T., Braisted, J. C., Jadhav, A., Simeonov, A., and Coussens, N. P. (2016). Fluorescence polarization assays in high-throughput screening and drug discovery: a review. *Methods Appl Fluoresc* **4**, 022001.

Harris, K. A., Shekhtman, A., and Agris, P. F. (2013). Specific RNA-protein interactions detected with saturation transfer difference NMR. *RNA Biol* **10**, 1307-1311.

Haselhorst, T., Lamerz, A. C., and Itzstein, M. (2009). Saturation transfer difference NMR spectroscopy as a technique to investigate protein-carbohydrate interactions in solution. *Methods Mol Biol* **534**, 375-386.

Henriksen, J., Stabell, M., Meza-Zepeda, L. A., Lauvrak, S. A., Kassem, M., and Myklebost, O. (2010). Identification of target genes for wild type and truncated HMGA2 in mesenchymal stem-like cells. *BMC Cancer* **10**, 329.

Hentze, M. W., Castello, A., Schwarzl, T., and Preiss, T. (2018). A brave new world of RNA-binding proteins. *Nat Rev Mol Cell Biol* **19**, 327-341.

Hinsberger, S., de Jong, J. C., Groh, M., Haupenthal, J., and Hartmann, R. W. (2014). Benzamidobenzoic acids as potent PqsD inhibitors for the treatment of *Pseudomonas aeruginosa* infections. *Eur J Med Chem* **76**, 343-351.

Hinsberger, S., Hüsecken, K., Groh, M., Negri, M., Haupenthal, J., and Hartmann, R. W. (2013). Discovery of novel bacterial RNA polymerase inhibitors: pharmacophore-based virtual screening and hit optimization. *J Med Chem* **56**, 8332-8338.

Hoelder, S., Clarke, P. A., and Workman, P. (2012). Discovery of small molecule cancer drugs: successes, challenges and opportunities. *Mol Oncol* **6**, 155-176.

Hoffman, B., Schorge, J., Schaffer, J., Halvorson, L., Bradshaw, K., and Cunningham, F. (2012). *Williams gynecology*, 2 edn (New York, NY: McGraw-Hill Medical).

Hong, S. (2017). RNA binding protein as an emerging therapeutic target for cancer prevention and treatment. *J Cancer Prev* **22**, 203-210.

Hsieh, Y. T., Chou, M. M., Chen, H. C., and Tseng, J. J. (2013). IMP1 promotes choriocarcinoma cell migration and invasion through the novel effectors RSK2 and PPME1. *Gynecol Oncol* **131**, 182-190.

Hughes, J. P., Rees, S., Kalindjian, S. B., and Philpott, K. L. (2011). Principles of early drug discovery. *Br J Pharmacol* **162**, 1239-1249.

References

Huynh, K., and Partch, C. L. (2015). Analysis of protein stability and ligand interactions by thermal shift assay. *Curr Protoc Protein Sci* 79, 28.29.21-28.29.14.

Idler, R. K., and Yan, W. (2012). Control of messenger RNA fate by RNA-binding proteins: an emphasis on mammalian spermatogenesis. *J Androl* 33, 309-337.

Jain, C. K., Majumder, H. K., and Roychoudhury, S. (2017). Natural compounds as anticancer agents targeting DNA topoisomerases. *Curr Genomics* 18, 75-92.

Janiszewska, M., Suvà, M. L., Riggi, N., Houtkooper, R. H., Auwerx, J., Clément-Schatlo, V., Radovanovic, I., Rheinbay, E., Provero, P., and Stamenkovic, I. (2012). Imp2 controls oxidative phosphorylation and is crucial for preservin glioblastoma cancer stem cells. *Genes Dev* 26, 1926-1944.

Jerabek-Willemsen, M., Wienken, C. J., Braun, D., Baaske, P., and Duhr, S. (2011). Molecular interaction studies using microscale thermophoresis. *Assay Drug Dev Technol* 9, 342-353.

Jia, M., Gut, H., and Chao, J. A. (2018). Structural basis of IMP3 RRM12 recognition of RNA. *RNA* 24, 1659-1666.

Kelley, L. A., Mezulis, S., Yates, C. M., Wass, M. N., and Sternberg, M. J. E. (2015). The Phyre2 web portal for protein modeling, prediction and analysis. *Nat Protoc* 10, 845-858.

Kessler, S. M., Haybaeck, J., and Kiemer, A. K. (2016). Insulin-like growth factor 2 - the oncogene and its accomplices. *Curr Pharm Des* 22, 5948-5961.

Kessler, S. M., Laggai, S., Barghash, A., Schultheiss, C. S., Lederer, E., Artl, M., Helms, V., Haybaeck, J., and Kiemer, A. K. (2015). IMP2/p62 induces genomic instability and an aggressive hepatocellular carcinoma phenotype. *Cell Death Dis* 6, e1894.

Kessler, S. M., Lederer, E., Laggai, S., Golob-Schwarzl, N., Hosseini, K., Petzold, J., Schweiger, C., Reihls, R., Keil, M., Hoffmann, J., *et al.* (2017). IMP2/IGF2BP2 expression, but not IMP1 and IMP3, predicts poor outcome in patients and high tumor growth rate in xenograft models of gallbladder cancer. *Oncotarget* 8, 89736-89745.

Kirsch, P., Jakob, V., Oberhausen, K., Stein, S. C., Cucarro, I., Schulz, T. F., and Empting, M. (2019). Fragment-based discovery of a qualified hit targeting the latency-associated nuclear antigen of the oncogenic kaposi's sarcoma-associated herpesvirus/human herpesvirus 8. *J Med Chem* 62, 3924-3939.

Kovalchuk, A., and Kolb, B. (2017). Chemo brain: from discerning mechanisms to lifting the brain fog- an aging connection. *Cell Cycle* 16, 1345-1349.

Lan, L., Appelman, C., Smith, A. R., Yu, J., Larsen, S., Marquez, R. T., Liu, H., Wu, X., Gao, P., Roy, A., *et al.* (2015). Natural product (-)-gossypol inhibits colon cancer cell growth by targeting RNA-binding protein Musashi-1. *Mol Oncol* 9, 1406-1420.

Lea, W. A., and Simeonov, A. (2011). Fluorescence polarization assays in small molecule screening. *Expert Opin Drug Discov* 6, 17-32.

References

-
- Liu, Y., Liu, N., Ma, X., Li, X., Ma, J., Li, Y., Zhou, Z., and Gao, Z. (2015). Highly specific detection of thrombin using an aptamer-based suspension array and the interaction analysis *via* microscale thermophoresis. *Analyst* *140*, 2762-2770.
- Lu, M., Nakamura, R. M., Dent, E. D., Zhang, J. Y., Nielsen, F. C., Christiansen, J., Chan, E. K., and Tan, E. M. (2001). Aberrant expression of fetal RNA-binding protein p62 in liver cancer and liver cirrhosis. *Am J Pathol* *159*, 945-953.
- Mahapatra, L., Andruska, N., Mao, C., Le, J., and Shapiro, D. J. (2017). A novel IMP1 inhibitor, BTYNB, targets c-Myc and inhibits melanoma and ovarian cancer cell proliferation. *Transl Oncol* *10*, 818-827.
- Mahapatra, L., Mao, C., Andruska, N., Zhang, C., and Shapiro, D. J. (2014). High-throughput fluorescence anisotropy screen for inhibitors of the oncogenic mRNA binding protein, IMP-1. *J Biomol Screen* *19*, 427-436.
- Manieri, N. A., Drylewicz, M. R., Miyoshi, H., and Stappenbeck, T. S. (2012). Igfbp1 is required for full induction of Ptg2 mRNA in colonic mesenchymal stem cells in mice. *Gastroenterology* *143*, 110-121.e110.
- Maruyama, I., Hasegawa, T., Yamamoto, T., and Momose, K. (1989). Effects of pluronic F-127 on loading of fura 2/AM into single smooth muscle cells isolated from guinea pig taenia coli. *J Toxicol Sci* *14*, 153-163.
- Mayer, M., and James, T. (2004). NMR-based characterization of phenothiazines as a RNA binding scaffold. *J Am Chem Soc* *126*, 4453-4460.
- Meng, X.-Y., Zhang, H.-X., Mezei, M., and Cui, M. (2011). Molecular docking: a powerful approach for structure-based drug discovery. *Curr Comput Aided Drug Des* *7*, 146-157.
- Mills, C. C., Kolb, E. A., and Sampson, V. B. (2018). Development of chemotherapy with cell-cycle inhibitors for adult and pediatric cancer therapy. *Cancer Res* *78*, 320-325.
- Moerke, N. J. (2009). Fluorescence polarization (FP) assays for monitoring peptide-protein or nucleic acid-protein binding. *Curr Protoc Chem Biol* *1*, 1-15.
- Moitessier, N., Englebienne, P., Lee, D., Lawandi, J., and Corbeil, C. R. (2008). Towards the development of universal, fast and highly accurate docking/scoring methods: a long way to go. *Br J Pharmacol* *153 Suppl 1*, S7-26.
- Monteiro, C. R. d. A., Schoueri, J. H. M., Cardial, D. T., Linhares, L. d. C., Turke, K. C., Steuer, L. V., Menezes, L. W. d. A., Argani, I. L., Sette, C., Cubero, D. d. I. G., and Giglio, A. d. (2019). Evaluation of the systemic and therapeutic repercussions caused by drug interactions in oncology patients. *Rev Assoc Med Bras* (1992) *65*, 611-617.
- Mu, Q., Wang, L., Yu, F., Gao, H., Lei, T., Li, P., Liu, P., Zheng, X., Hu, X., Chen, Y., *et al.* (2015). Imp2 regulates GBM progression by activating IGF2/PI3K/Akt pathway. *Cancer Biol Ther* *16*, 623-633.

References

Nakayama, G. R., Bingham, P., Tan, D., and Maegley, K. A. (2006). A fluorescence polarization assay for screening inhibitors against the ribonuclease H activity of HIV-1 reverse transcriptase. *Anal Biochem* 351, 260-265.

Neugut, A. I., and Prigerson, H. G. (2017). Curative, life-extending, and palliative chemotherapy: new outcomes need new names. *Oncologist* 22, 883-885.

Newman, M. A., Thomson, J. M., and Hammond, S. M. (2008). Lin-28 interaction with the Let-7 precursor loop mediates regulated microRNA processing. *RNA* 14, 1539-1549.

Nicastro, G., Candel, A. M., Ramos, A., and Hollingworth, D. (2017). Zipcode-binding-protein-1 KH3KH4(DD) domains in complex with the RNA target GCACACCC. In, (<http://www.rcsb.org/structure/2N8L>).

Nielsen, F. C., Nielsen, J., Kristensen, M. A., Koch, G., and Christiansen, J. (2002). Cytoplasmic trafficking of IGF-II mRNA-binding protein by conserved KH domains. *J Cell Sci* 115, 2087.

Nielsen, J., Christiansen, J., Lykke-Andersen, J., Johnsen, A. H., Wewer, U. M., and Nielsen, F. C. (1999). A family of insulin-like growth factor II mRNA-binding proteins represses translation in late development. *Mol Cell Biol* 19, 1262-1270.

Nielsen, J., Kristensen, M. A., Willemoes, M., Nielsen, F. C., and Christiansen, J. (2004). Sequential dimerization of human zipcode-binding protein IMP1 on RNA: a cooperative mechanism providing RNP stability. *Nucleic Acids Res* 32, 4368-4376.

Nikolovska-Coleska, Z., Wang, R., Fang, X., Pan, H., Tomita, Y., Li, P., Roller, P. P., Krajewski, K., Saito, N. G., Stuckey, J. A., and Wang, S. (2004). Development and optimization of a binding assay for the XIAP BIR3 domain using fluorescence polarization. *Anal Biochem* 332, 261-273.

Nurgali, K., Jagoe, R. T., and Abalo, R. (2018). Editorial: adverse effects of cancer chemotherapy: anything new to improve tolerance and reduce sequelae? *Front Pharmacol* 9, 245-245.

Pearce, A., Haas, M., Viney, R., Pearson, S.-A., Haywood, P., Brown, C., and Ward, R. (2017). Incidence and severity of self-reported chemotherapy side effects in routine care: a prospective cohort study. *PLoS one* 12, e0184360-e0184360.

Petersen, M. C., Vatner, D. F., and Shulman, G. I. (2017). Regulation of hepatic glucose metabolism in health and disease. *Nat Rev Endocrinol* 13, 572-587.

Pommier, Y. (2013). Drugging topoisomerases: lessons and challenges. *ACS Chem Biol* 8, 82-95.

Popova, V. V., Kurshakova, M. M., and Kopytova, D. V. (2015). Methods to study the RNA-protein interactions. *Mol Biol* 49, 418-426.

Qu, H., Xing, W., Wu, F., and Wang, Y. (2016). Rapid and inexpensive method of loading fluorescent dye into pollen tubes and root hairs. *PLoS one* 11, e0152320-e0152320.

References

Rai, Y., Pathak, R., Kumari, N., Sah, D. K., Pandey, S., Kalra, N., Soni, R., Dwarakanath, B. S., and Bhatt, A. N. (2018). Mitochondrial biogenesis and metabolic hyperactivation limits the application of MTT assay in the estimation of radiation induced growth inhibition. *Sci Rep* **8**, 1531-1531.

Rainard, J. M., Pandarakalam, G. C., and McElroy, S. P. (2018). Using microscale thermophoresis to characterize hits from high-throughput screening: a european lead factory perspective. *SLAS Discov* **23**, 225-241.

Ralhan, R., and Kaur, J. (2007). Alkylating agents and cancer therapy. *Expert Opin Ther Pat* **17**, 1061-1075.

Ren, F., Shu, G., Liu, G., Liu, D., Zhou, J., Yuan, L., and Zhou, J. (2014). Knockdown of p62/sequestosome 1 attenuates autophagy and inhibits colorectal cancer cell growth. *Mol Cell Biochem* **385**, 95-102.

Renaud, J.-P., Chung, C.-w., Danielson, U. H., Egner, U., Hennig, M., Hubbard, R. E., and Nar, H. (2016). Biophysics in drug discovery: impact, challenges and opportunities. *Nat Rev Drug Discov* **15**, 679-698.

Roos, M., Pradere, U., Ngondo, R. P., Behera, A., Allegrini, S., Civenni, G., Zagalak, J. A., Marchand, J. R., Menzi, M., Towbin, H., *et al.* (2016). A Small-Molecule Inhibitor of Lin28. *ACS Chem Biol* **11**, 2773-2781.

Rossi, A. M., and Taylor, C. W. (2011). Analysis of protein-ligand interactions by fluorescence polarization. *Nat Protoc* **6**, 365-387.

Sahner, J. H., Groh, M., Negri, M., Hauptenthal, J., and Hartmann, R. W. (2013). Novel small molecule inhibitors targeting the "switch region" of bacterial RNAP: structure-based optimization of a virtual screening hit. *Eur J Med Chem* **65**, 223-231.

Schaeffer, V., Hansen, K. M., Morris, D. R., LeBoeuf, R. C., and Abrass, C. K. (2012). RNA-binding protein IGF2BP2/IMP2 is required for laminin-beta2 mRNA translation and is modulated by glucose concentration. *Am J Physiol Renal Physiol* **303**, F75-82.

Seidel, S. A. I., Dijkman, P. M., Lea, W. A., van den Bogaart, G., Jerabek-Willemsen, M., Lazic, A., Joseph, J. S., Srinivasan, P., Baaske, P., Simeonov, A., *et al.* (2013). Microscale thermophoresis quantifies biomolecular interactions under previously challenging conditions. *Methods* **59**, 301-315.

Seidler, J., McGovern, S. L., Doman, T. N., and Shoichet, B. K. (2003). Identification and prediction of promiscuous aggregating inhibitors among known drugs. *J Med Chem* **46**, 4477-4486.

Senisterra, G., Chau, I., and Vedadi, M. (2012). Thermal denaturation assays in chemical biology. *Assay Drug Dev Technol* **10**, 128-136.

Shoichet, B. K. (2006). Screening in a spirit haunted world. *Drug Discov Today* **11**, 607-615.

Sink, R., Gobec, S., Pecar, S., and Zega, A. (2010). False positives in the early stages of drug discovery. *Curr Med Chem* **17**, 4231-4255.

References

Sliwoski, G., Kothiwale, S., Meiler, J., and Lowe, E. W., Jr. (2013). Computational methods in drug discovery. *Pharmacol Rev* 66, 334-395.

Smith, C. (2003). Drug target validation: hitting the target. *Nature* 422, 342-345.

Steenbergen, R., Oti, M., Ter Horst, R., Tat, W., Neufeldt, C., Belovodskiy, A., Chua, T. T., Cho, W. J., Joyce, M., Dutilh, B. E., and Tyrrell, D. L. (2018). Establishing normal metabolism and differentiation in hepatocellular carcinoma cells by culturing in adult human serum. *Sci Rep* 8, 11685-11685.

Stolwijk, J. A., and Wegener, J. (2019). Impedance-based assays along the life span of adherent mammalian cells *in vitro*: from initial adhesion to cell death. In *Label-Free Monitoring of Cells in vitro*, J. Wegener, ed. (Cham: Springer International Publishing), pp. 1-75.

Streiff, J. H., Juranic, N. O., Macura, S. I., Warner, D. O., Jones, K. A., and Perkins, W. J. (2004). Saturation transfer difference nuclear magnetic resonance spectroscopy as a method for screening proteins for anesthetic binding. *Mol Pharmacol* 66, 929-935.

Suzuki, S., Muto, Y., Inoue, M., Kigawa, T., Terada, T., Shirouzu, M., Yokoyama, S., and RIKEN Structural Genomics/Proteomics Initiative (RSGI) (2005). Solution structure of the RNA binding domain of Nucleolysin TIAR (Solution structure of the RNA binding domain of IGF-II mRNA-binding protein 2). In, (<http://www.rcsb.org/structure/2CQI>).

Szulcek, R., Bogaard, H. J., and van Nieuw Amerongen, G. P. (2014). Electric cell-substrate impedance sensing for the quantification of endothelial proliferation, barrier function, and motility. *J Vis Exp*, 51300.

Taylor, D., Ma, E., Shigematsu, H., Cianfrocco, M., Noland, C., Nagayama, K., Nogales, E., Doudna, J., and Wang, H.-W. (2013). Substrate-specific structural rearrangements of human Dicer. *Nat Struct Mol Biol* 20.

Uhlen, M., Zhang, C., Lee, S., Sjöstedt, E., Fagerberg, L., Bidkhori, G., Benfeitas, R., Arif, M., Liu, Z., Edfors, F., *et al.* (2017). A pathology atlas of the human cancer transcriptome. *Science* 357.

Vasile, F., Della Volpe, S., Ambrosio, F. A., Costa, G., Unver, M. Y., Zucal, C., Rossi, D., Martino, E., Provenzani, A., Hirsch, A. K. H., *et al.* (2018). Exploration of ligand binding modes towards the identification of compounds targeting HuR: a combined STD-NMR and Molecular Modelling approach. *Sci Rep* 8, 13780.

Viegas, A., Manso, J., Nobrega, F. L., and Cabrita, E. J. (2011). Saturation-transfer difference (STD) nmr: a simple and fast method for ligand screening and characterization of protein binding. *J Chem Educ* 88, 990-994.

Volkova, M., and Russell, R. (2011). Anthracycline cardiotoxicity: prevalence, pathogenesis and treatment. *Curr Cardiol Rev* 7, 214-220.

Waly, A. A., El-Ekiaby, N., Assal, R. A., Abdelrahman, M. M., Hosny, K. A., El Tayebi, H. M., Esmat, G., Breuhahn, K., and Abdelaziz, A. I. (2019). Methylation in mirlet7a3 gene induces the expression of IGF-II and its mRNA binding proteins IGF2BP-2 and 3 in hepatocellular carcinoma. *Front Physiol* 9.

References

World Health Organization (2020). WHO report on cancer: setting priorities, investing wisely and providing care for all. Geneva : World Health Organization: Licence: CC BY-NC-SA 3.0 IGO.

Wu, X., Lan, L., Wilson, D. M., Marquez, R. T., Tsao, W. C., Gao, P., Roy, A., Turner, B. A., McDonald, P., Tunge, J. A., *et al.* (2015). Identification and validation of novel small molecule disruptors of HuR-mRNA interaction. *ACS Chem Biol* *10*, 1476-1484.

Wyatt, P. G., Gilbert, I. H., Read, K. D., and Fairlamb, A. H. (2011). Target validation: linking target and chemical properties to desired product profile. *Curr Top Med Chem* *11*, 1275-1283.

Xing, M., Li, P., Wang, X., Li, J., Shi, J., Qin, J., Zhang, X., Ma, Y., Francia, G., and Zhang, J.-Y. (2019). Overexpression of p62/IMP2 can promote cell migration in hepatocellular carcinoma *via* activation of the wnt/ β -catenin pathway. *Cancers* *12*, 7.

Zhang, J. H., Chung, T. D., and Oldenburg, K. R. (1999). A simple statistical parameter for use in evaluation and validation of high throughput screening assays. *J Biomol Screen* *4*, 67-73.

Zhang, L., Liu, Y., Hao, S., Woda, B., and Lu, D. (2011). IMP2 expression distinguishes endometrioid From Serous Endometrial Adenocarcinomas. *Am J Surg Pathol* *35*, 868-872.

Zhou, R.-B., Lu, X., Zhang, C., and Yin, D.-C. (2015). RNA binding motif protein 3: a potential biomarker in cancer and therapeutic target in neuroprotection. *Oncotarget* *8*.

Zudaire, E., Cuesta, N., Murty, V., Woodson, K., Adams, L., Gonzalez, N., Martinez, A., Narayan, G., Kirsch, I., Franklin, W., *et al.* (2008). The aryl hydrocarbon receptor repressor is a putative tumor suppressor gene in multiple human cancers. *J Clin Invest* *118*, 640-650.

Publications

Ali Abuhaliema, Sonja M. Kessler, Charlotte Dahlem, Tarek Kröhler, Ben G. E. Zoller, Susanne H. Kirsch, Stephan Laggai, Rolf Müller, Martin Empting, Alexandra K. Kiemer. **“Discovery of the first small molecules targeting the mRNA binding protein IGF2BP2/IMP2 as potential target in cancer therapy”**, submitted.

Czepukojc, B., **Abuhaliema, A.**, Barghash, A., Tierling, S., Naß, N., Simon, Y., Körbel, C., Cadenas, C., van Hul, N., Sachinidis, A., *et al.* (2019). **IGF2 mRNA Binding Protein 2 Transgenic Mice Are More Prone to Develop a Ductular Reaction and to Progress Toward Cirrhosis**. *Frontiers in Medicine* 6.

Conferences

Poster presentation at the Helmholtz-Institut für Pharmazeutische Forschung Saarland (HIPS) Symposium 2019

Ali Abuhaliema, Sonja M. Kessler, Tarek Kröhler, Charlotte Dahlem, Martin Empting, Alexandra K. Kiemer. **“Discovery of the first small molecules targeting the mRNA binding protein IGF2BP2/IMP2 as potential target in cancer therapy”**. Poster session presented at the HIPS Symposium 2019. June 27-28, 2019, Saarbrücken, Germany.

Acknowledgment

I would like to express my gratitude and appreciation to Prof. Dr. Alexandra Kiemer for supervising me to pursue my Ph.D. as member in her research team. I appreciate her guidance, continues support, and her contribution of time.

Also, I would like to thank Prof. Dr. Christin Ducho for being the second examiner of my Ph.D. dissertation.

I would like to extend a special acknowledgment to Prof. Dr. Sonja Kessler for her assistance, scientific discussions, and encouragement over my Ph.D. journey.

I thank Dr. Martin Empting for supervising and guiding me during my work in HIPS.

I would like to thank all my colleges in the Pharmaceutical Biology research group for the nice time I spent with them. Special thank for Tarek kröhler for passing me the IMP2 knockout cells, and to Charlotte Dahlen for performing the Zebrafish experiment.

Furthermore, I would like to thank all my colleges in the Drug Design and Optimization research group in HIPS for the technical assistance, scientific exchange, and nice time. A special thanks for Dr. Ghamdan Beshar for his scientific advice in protein isolation and screening, and for Dr. Josef Zapp for his contribution in establishing the STD-NMR protocol, and for Dr. David Auerbach for performing the LC-MS/MS experiment.

I would like to thank Dr. Mostafa Hamed, Dr. Mohammed Salah, and Dr. Ahmed Saad for the good-company and nice time I spent with them in HIPS, can't forget sharing the daily coffee breaks.

At this occasion, I would extend my appreciation and thankful to Prof. Dr. Al-Motassem Yousef for his motivational speech and memorable words.

I appreciate and thank the Deutsche Akademischer Austauschdienst (DAAD) for financing me during Ph.D. time, endless support, and being ready to help whenever I needed.

Acknowledgment

I would like to show my deep grateful to my lovely mother and father for their endless support and encouragement along the road. I won't forget your words and favor as I am living.

Also, I thank my sisters and brothers for their trust and support since I left our sweet home.

I would like to thank my lovely wife for being my source of continues support, motivation, inspiration and encouragement, I appreciate her patience and time.

This work was done only with God willing and assistance, I thank you Allah for giving me the patience and well to overcome all my problems, sickness and hardships to achieve my long-term dream.

اللَّهُمَّ إِنِّي أَسْأَلُكَ بِرَحْمَتِكَ
وَجَدِّكَ وَعَظِيمِ سُلْطَانِكَ